Developing Low Fouling Peptides and Zwitterionic Materials for Biomedical Applications

Ann K. Nowinski

A dissertation

submitted in partial fulfillment of the

requirements for the degree of

Doctor of Philosophy

University of Washington

2015

Reading Committee:

Prof. Shaoyi Jiang, Chair

Prof. François Baneyx

Prof. Suzie H. Pun

Program Authorized to Offer Degree:

Chemical Engineering

University of Washington

Abstract

Developing Low Fouling Peptides and Zwitterionic Materials for Biomedical Applications

Ann K. Nowinski

Chair of the Supervisory Committee:
Prof. Shaoyi Jiang
Chemical Engineering

This dissertation is a compilation of efforts aimed at developing mixed charge and zwitterionic materials to prevent biofouling in biomedical applications. Peptides are considered for use as natural low fouling materials due to their biocompatibility, diverse chemical properties, well-defined sequence, and biodegradability. Low fouling peptide sequences were rationally designed from known zwitterionic principles and biomimetically designed from the examination of human protein surfaces found in nature. The peptide sequences glutamic acid/lysine (EK) and asparagine (N) were identified as displaying resistance to nonspecific protein adsorption. The low fouling sequence EK was further applied to several biomedical applications including multifunctional self-assembled monolayers on a gold surface, stealth coatings on gold nanoparticles, and biodegradable EK-poly(lactic-*co*-glycolic) acid (EK-PLGA) drug delivery nanocarriers. Importantly, the EK sequence can be extended with functional peptide sequences (such as RGD for specific cell targeting) without the need for complex chemical conjugation. In addition to rational and biomimetic peptide design, a combinatorial

screening method was explored to facilitate the testing of thousands of peptide sequences for low protein adsorption. Finally, zwitterionic polymers were explored to form particles for mucus-penetrating applications.

Table of Contents

List of Tables

List of Schemes

List of Figures

Acknowledgements

For all the work presented here, I would like to thank my advisor, Prof. Shaoyi Jiang for support and guidance throughout the 5.5 years I spent working with him at the University of Washington. I also wish to thank my Ph.D. committee members Prof. François Baneyx, Prof. Suzie Pun, and Prof. Lih-Yuan Lin for their time and assistance with my research direction. Thank you to current and former members of the Jiang lab, especially Prof. Andrew White and Dr. Andrew Keefe for useful discussion related to projects.

The work presented in Chapter 2 has been financially supported by the National Science Foundation (CBET-0854298) and the Office of Naval Research (N00014-10-1-0600). XPS samples were analyzed by the NESAC/BIO facility at the University of Washington (NIH Grant EB-002027). I would like to thank Fang Sun for assistance with cell seeding experiments and Prof. Andrew White for simulation studies. I would also like to thank Dr. Lara Gamble and Dr. Jeanette Stein for useful discussion relating to this project. The work presented in Chapter 3 has been financially supported by the National Science Foundation (CBET-0854298), the Office of Naval Research (N00014-10-1-0600), and the Army Research Office (63926-LS-II). Thank you to Leize Zhu for assistance with TEM analysis and J. Sean Yeung for assistance with ICP-MS analysis. The work presented in Chapter 4 is financially supported by the Army Research Office (63926-LS-II). I would like to thank Andy Sinclair for assistance with SEM analysis and Dr. Priyesh Jain for help with peptide synthesis. The work presented in Chapter 5 has been financially supported by the Office of Naval Research (N00014-10-1-0600 and N00014-12-1-0441) and the National Science Foundation (CBET-0854298). Confocal microscopy was performed at the University of Washington NanoTech User Facility, a member of the NSF National Nanotechnology Infrastructure Network (NNIN). The work presented in Chapter 5 is a

continuation of Dr. Andrew Keefe's research and would not be possible without him. The work presented in Chapter 6 has been financially supported by the Army Research Office (63926-LS-II). I would like to thank Dr. Greg Newbloom for assistance with rheology measurements, Dr. Jean-René Ella-Menyé for synthesis of initiator and monomers, Susan Liu for help with polymer synthesis, Caroline Tsao for help with particle tracking data analysis, and Prof. Andrew White for help with coding a python script to analyze particle tracking data. I would also like to acknowledge financial support from a National Science Foundation Graduate Fellowship.

Lastly, I would like to acknowledge my family and friends for continual support in my endeavors. A special mention is included for my parents, Danuta La Rance and Piotr Nowinski, who have instilled a love of science in me and have always been extremely supportive of my ambitions. I would also like to particularly thank my sister Magda Nowinski who has dedicated countless hours of her time throughout the years in helping me edit papers and prepare for presentations.

Chapter 1: Introduction

Biofouling of surfaces caused by the nonspecific adsorption of biomolecules, bacteria, and microorganisms is encountered in a wide spectrum of technical systems, ranging from the pharmaceutical, water purification, shipping, power, automobile, food, and microelectronics industries. Biofouling also creates challenges in the development of products which will be used in complex environments such as the human body. The development of low fouling materials that can resist protein adsorption, bacterial adhesion, and biofilm formation can have many applications in the biomedical field including *ex vivo* biosensor coatings, *in vivo* drug delivery carriers, wound dressings, contact lenses, and implant coatings. The goal for developing ultra-low fouling materials is to attain less than 5 ng/cm^2 of adsorbed fibrinogen on surfaces, which is the threshold for platelet adhesion[1].

The unwanted accumulation of proteins and cells onto surfaces leads to the detriment of function of equipment and devices. For example, biofilm formation on indwelling urinary catheters accounts for over 40% of all hospital-acquired infections, with more than one million cases diagnosed annually in the United States[2]. These infections increase hospital stays, affect patient health, and generate an extra $600 million in medical expenditures every year[3,4]. In addition to infection, the surgical implantation of medical devices can lead to a foreign body reaction, beginning with blood protein adsorption and eventually leading to formation of a tough fibrous capsule around the device. This foreign body reaction is known to lead to degradation of biomaterials with subsequent device failure such as in the case of degradation of polyether polyurethane pacemaker leads[5]. The fibrous capsule can also block mass transport and/or electric communication between the implant and the body. Nonspecific protein adsorption also plays a significant role in the design of drug delivery nanocarriers. Surface protein deposition upon

introduction into the blood stream may induce nanoparticle aggregation and can trigger rapid recognition and clearance from the blood by circulating phagocytes[6]. Finally, biosensor surface fouling can lead to problems with sensor stability and calibration, malfunction of devices, reduced lifespan, and increased power consumption[7].

Low fouling materials include poly(ethylene glycol) (PEG)[8], polysaccharides[9], poly(2-methyl-2-oxazoline) polymers[10], mixed charge polymers[11,12], peptides[13,14] and zwitterionic polymers[15]. Currently, the most commonly used low fouling material in the biomedical field is poly(ethylene glycol) (PEG) (Scheme 1-1). The concept of adding PEG to products (PEGylation) was first introduced in the late 1970s; however, it only reached widespread application in the 1990s[16]. PEG obtains it low fouling properties by bonding water to its surface via hydrogen bonding. The precise positioning of ether groups along the backbone of PEG acts as an ideal hydrogen bond acceptor for water[17]. Although PEG binds water to its surface, it is considered an amphiphilic polymer because it can also dissolve in organic solvents such as toluene, dichloromethane, and acetone. Its dual solubility makes end-group modifications relatively easy, but its hydrophobic nature can also have negative consequences by undesirably interfering with hydrophobic regions in many applications[18]. The use of PEG can also be hampered by its autoxidation, especially in the presence of oxygen and transition metal ions[19,20]. Finally, PEG has been shown to induce specific as well as nonspecific recognition by the immune system, thereby leading to a response of the body to intravenously administered PEG formulations such as liposomal and micellar carrier systems or conjugates[16].

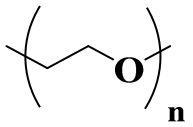

PEG

Scheme 1-1. Chemical structure of poly(ethylene glycol) (PEG).

More recently, zwitterionic polymers such as sulfobetaine methacrylate (SBMA)[21], carboxybetaine methacrylate (CBMA)[15], and 2-methacryloyloxylethyl phosphorylcholine (MPC)[22] have been shown to be excellent low fouling materials (Scheme 1-2). Zwitterionic polymers possess a negatively and positively charged moiety on the same side chain while maintaining an overall net neutral charge. Mixed charge polymers which possess alternating negatively and positively charged moieties have also been shown to exhibit low fouling properties[11]. Water molecules bind more strongly and stably to zwitterionic and mixed charged polymers compared to other hydrophilic polymers such as PEG via electrostatically induced hydration making it even more difficult for proteins to adsorb to the surface[23]. Zwitterionic polymers have been shown to resist nonspecific protein adsorption from undiluted human blood plasma and serum, cell adhesion, and bacterial biofilm formation[24]. In addition, the utility of zwitterionic polymers has been demonstrated in a number of applications including gene delivery[25], cell encapsulation[26], marine surface coatings[27], biosensing[28], protein conjugation[18], and imaging magnetic nanoparticles[29].

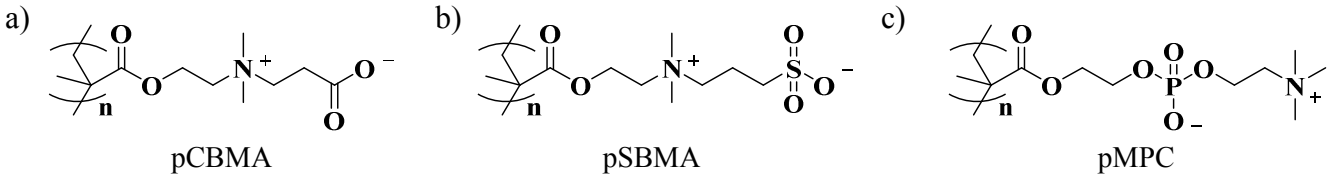

pCBMA pSBMA pMPC

Scheme 1-2. Chemical structure of zwitterionic polymers.
Chemical structures of zwitterionic polymers (a) poly(carboxybetaine methacrylate) (pCBMA) (b) poly(sulfobetaine methacrylate) (pSBMA) (c) poly(2-methacryloyloxyethyl phosphorylcholine) (pMPC).

There are many applications where the use of low fouling materials can be further developed and prove beneficial. This work examines the rational, biomimetic, and combinatorial design of peptides as a new class of low fouling materials. In addition, zwitterionic polymers are applied in the development of mucus-penetrating particles.

1.1 Designing Peptides as Low Fouling Materials

Peptides are advantageous as biomaterials since they are biocompatible. In addition, the twenty naturally occurring amino acids offer nearly infinite possible sequence combinations resulting in access to varying chemistries and functionalities. Peptides are chemically well-defined since they are commonly produced using solid phase peptide synthesis or genetic engineering[30,31]. Importantly, peptide-based materials can incorporate specific function without the need for chemical conjugation, which can involve complex chemistries and additional synthesis steps[32]. Functionalities such as specific cell recognition, antimicrobial properties, surface-binding, or protease cleavage sites can be incorporated by simply extending the peptide sequence[33]. Finally, peptides are biodegradable breaking down to non-toxic components that can be readily metabolized or excreted from the body[34].

Low fouling peptides were designed based on the principle of zwitterionic polymers possessing equal amounts of positive and negative charges. The peptide sequences were rationally hypothesized to consist of alternating negatively and positively charged residues, while maintaining an overall net neutral charge. From the twenty naturally occurring amino acids there are two options for negatively charged side chains (glutamic acid (E) and aspartic acid (D)) and two options for positively charged side chains (arginine (R) and lysine (K)) at neutral pH (Scheme 1-3). All four possible combinations were evaluated for nonspecific protein adsorption

(ER, DR, EK, DK). Only peptide sequences containing lysine as the positively charged residue (EK, DK) were low fouling, whereas peptide sequences containing arginine as the positively charged residue (ER, DR) were high fouling[13]. Arginine is thought to be fouling due to its propensity for specific interactions, whereas lysine appears to be suited for weak nonspecific interactions[35]. In addition, the guanidinium group in arginine can form multiple hydrogen bonds since its positive charge is de-localized[36]. Furthermore, guanidinium is one of the most weakly hydrated cations[37], and favorably interacts with the majority of amino acid side chains[38].

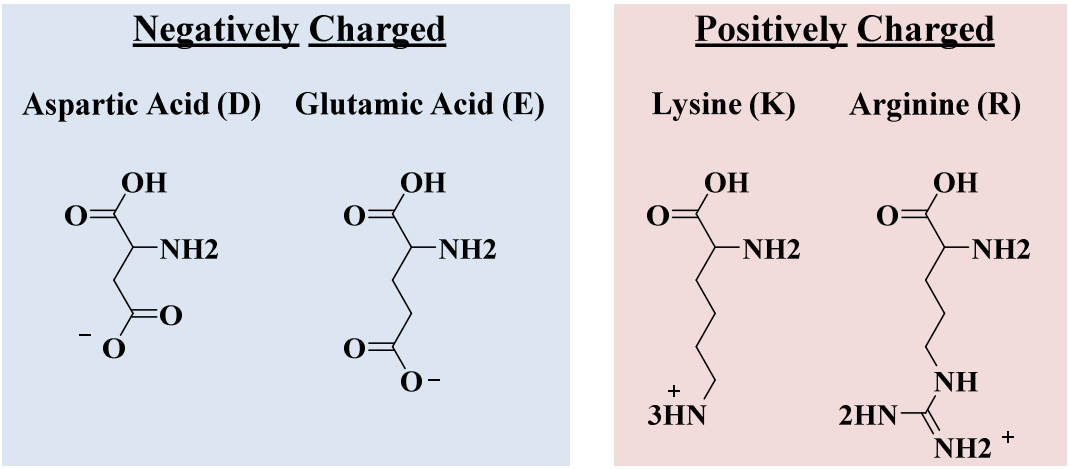

Scheme 1-3. Positively and negatively charged naturally occurring amino acids at pH 7.4. Chemical structures of negatively charged amino acids aspartic acid (D) and glutamic acid (E) (left) and positively charged amino acids lysine (K) and arginine (R) (right).

As a supplement to rational design, examining existing low fouling systems in nature can lead to further insights in the development of stealth materials. Proteins in the human body interact with thousands of other proteins without aggregating and can circulate for extended periods of time up to 20 days[39]. By examining human protein surfaces their surface chemistry can be probed. The analysis of 1,162 human protein surfaces determined that charged residues make up 37.5% of extracellular proteins and 43.8% of intracellular proteins, with glutamic acid and lysine having the highest prevalence on the surfaces of proteins[40]. The percentage of charged

residues present on the surfaces of proteins increases as the environment becomes more complex: 44% for proteins found in the crowded cytoplasm, 56% for proteins that have close contact with other proteins such as the interior of molecular chaperone proteins, and 70% for the interior of molecular chaperone proteins found in thermophilic bacteria[40,41]. The high occurrence of glutamic acid and lysine on the surfaces of proteins confirmed that they are prime candidates for low fouling materials. In addition to examining the frequency of amino acids on the surface, we also examined which residues have high hydration and which residues have disfavored interactions with the protein core. This led to the identification of the amino acid asparagine (N) as another potential low fouling sequence[40]. The low fouling EK peptide sequence identified through rational and biomimetic design was chosen for the development of several biomedical applications presented in this work including self-assembled monolayers, gold nanoparticle coatings, and controlled drug delivery carriers.

Rational design guided by known zwitterionic principles and biomimetics can successfully identify new low fouling peptide sequences, but is limited to easily testing tens of sequences. Combinatorial screening methods can offer a complimentary approach to designing low fouling peptide materials by increasing the number of sequences tested from tens to thousands of sequences[42]. Traditional combinatorial screening platforms seek to identify specific targeting via the use of phage[43], yeast[44], bacterial[45] or polymer resin display[46]. Although effective for identifying sequences with a high binding affinity to a specific target, these systems cannot be used for screening of low binding compounds due to nonspecific background binding. New screening platforms must be developed to successfully utilize combinatorial screening in the identification of low fouling peptide sequences[47]. A novel high throughput combinatorial

screening platform for the identification of low fouling peptide sequences is explored in this work.

1.2 Application of Zwitterionic Polymers to Mucus-Penetrating Particles

In addition to the development of peptide-based low fouling materials, zwitterionic polymers were considered for mucus penetration applications. Polymers containing zwitterionic moieties such as carboxybetaine and sulfobetaine have already been shown to resist interactions in complex environments such as whole blood, tissue, and marine environments[15]. Mucosal barriers in the human body are challenging to penetrate due to the sticky, viscoelastic nature of the mucus layer and its continual clearance and renewal from the body[48]. Delivery through mucosal surfaces can have many biomedical applications such as drug delivery[49], gene therapy[50], and vaccination[51]. A method that could provide more uniform and longer lasting delivery to mucosal surfaces can greatly improve therapeutic approaches for a number of diseases including sexually transmitted infections, cystic fibrosis, chronic rhinosinusitis, inflammatory bowel disease, and glaucoma[48]. Traditional methods for mucosal drug delivery include the development of mucoadhesive particles. Recently, the strategy has shifted to the development of mucus-penetrating particles, such as particles coated with low molecular weight PEG. The ability of zwitterionic materials to resist nonspecific adsorption of proteins and cells can impart stealth behavior, which translates directly to improving current mucus penetration strategies.

1.3 Organization of the Dissertation

The dissertation is organized into seven chapters. Chapter 1 provides an introduction to the importance of developing low fouling materials, a summary of designing low fouling peptides, and an overview of using zwitterionic polymers as mucus-penetrating particles.

Chapter 2 describes the impact of sequence, structure, and function on the development of ultra-low fouling peptide self-assembled monolayers. Results from this work have been published in the *Journal of the American Chemical Society* 2012, 134 (13), p. 6000-6005 and in *Chemical Science* 2012, 3, p. 3488-3494. Chapter 3 describes the application of the low fouling EK peptide sequence as a biologically inspired stealth coating for gold nanoparticles. Results from this work have been published in *Langmuir* 2014, 30, p. 1864-1870. Chapter 4 introduces the development of a controlled biodegradable drug delivery nanocarrier composed of a peptide-polymer conjugate (EK-PLGA) consisiting of the peptide sequence EK and the polymer poly(lactic-co-glycolic) acid (PLGA). Chapter 5 explores the use of combinatorial techniques to discover novel low fouling peptide sequences. A novel platform is considered for high throughput screening of peptide sequences. Chapter 6 introduces the use of zwitterionic-coated particles as candidates for mucus penetration. Finally, Chapter 7 provides concluding remarks for these projects.

Chapter 2: Design of Low Fouling Peptide Self-Assembled Monolayers

Cysteine is commonly used to attach peptides onto gold surfaces. In this work, we show that the inclusion of an additional linker of four residues in length (-PPPPC) of a rigid, hydrophobic nature, is a better choice for forming peptide self-assembled monolayers (SAMs) with well-ordered structure and high surface density. We compare the structure and function of the nonfouling peptide EKEKEKE-PPPPC-Am with EKEKEKE-C-Am. Circular dichroism (CD), attenuated total internal reflection Fourier transform infrared spectroscopy (ATR-FTIR), and molecular dynamics (MD) results show that EKEKEKE-PPPPC-Am forms a secondary structure while EKEKEKE-C-Am has a random structure. Surface plasmon resonance (SPR) sensor results show that protein adsorption on EKEKEKE-PPPPC-Am/gold is very low with small variation while protein adsorption on EKEKEKE-C-Am/gold is high with large variation. X-ray photoelectron spectroscopy (XPS) results show that both peptides have strong gold-thiol binding onto a gold surface, indicating that their difference in protein adsorption is due to their assembled structures. Further experimental and simulation studies were performed to show that -PPPPC is a more robust linker than -PC, -PPC, and -PPPC. We extend EKEKEKE-PPPPC-Am with the cell-binding sequence RGD and demonstrate control over specific vs. non-specific cell adhesion without using poly(ethylene) glycol (PEG). Extending the low fouling EK sequence with a functional peptide avoids complex chemistries that are commonly used for connection to low fouling synthetic materials. Finally, we evaluate the importance of ordering in the EK peptide sequence and the use of asparagine (N) as a neutrally charged, low fouling peptide sequence inspired by natural protein surfaces.

2.1 Introduction

A low fouling peptide was rationally designed by alternating negatively charged glutamic acid (E) and positively charged lysine (K) amino acid residues[13]. This corresponds with our recent analysis of 1,162 protein surfaces that indicates E and K are the two most prevalent amino acids on the surface. The EK sequence forms a strong hydration layer similar to zwitterionic materials[52]. Natural materials based on low fouling peptides have many biomedical applications. A non-peptide synthetic thiol anchor[13,14,53] is often used to attach functional peptides to gold surfaces. Polypeptide mimics have also been used as water-resistant anchors to surfaces and display fouling resistance.[54] EK peptide-based SAMs containing synthetic butanethiol anchors have been previously shown to have high surface packing densities and ultra-low fouling properties on gold surfaces.[13] It is, however, highly desirable to replace these synthetic linkers with a natural peptide for surface attachment to form an all-peptide based material. The amino acid cysteine (C), which contains a thiol side chain,[55] has been commonly used to attach peptides onto gold surfaces. Although cysteine binds strongly to gold, unlike synthetic thiol anchors, a peptide using cysteine alone as its surface anchoring group was not able to achieve well-ordered structure and high surface density necessary for ultra-low fouling surfaces[19].

In addition to low fouling properties, it is beneficial to achieve specific interactions for biomedical applications. One such application is mimicking extracellular matrix proteins using the well-established arginine-glycine-aspartate (RGD) sequence, which can mimic fibronectin, vitronectin, fibrinogen, osteopontin, and bone sialoprotein[56]. This and other functional sequences are commonly conjugated onto a low fouling synthetic polymer, such as PEG[57], to prevent nonspecific protein adsorption which can undermine sequence specificity. Such conjugation processes are complex[32]. Polydispersity of polymers, identification of appropriate conjugation

sites, non-uniformly distributed functional groups, and difficult post conjugation evaluation[58,59] are all drawbacks to various conjugation methods. Integrating the low fouling EK peptide sequence with RGD allows replacement of nonfouling synthetic materials and avoids complex chemistries used in bioconjugation.

In this work, we investigate the impact of the length and the nature of a short linker to form a well-packed, ultra-low fouling peptide SAM, specifically the additional inclusion of one to four proline linker residues which provide hydrophobicity and helical secondary structure. We compare structures of the low fouling sequence EKEKEKE-PPPPC-Am and EKEKEKE-C-Am in solution and on a gold surface. The low fouling segment of the peptide contains four negatively charged glutamic acid residues (E) and three positively charged lysine residues (K). Overall charge neutrality of the peptide is maintained by leaving the N-terminus as a free amine, which contributes an extra positive charge to the peptide. To prevent a negative charge near the gold binding thiol which could impede packing of the SAM through electrostatic repulsion, the C-terminus of all peptides was amidated.

The secondary structures of these two sequences (EKEKEKE-PPPPC-Am and EKEKEKE-C-Am) were characterized using circular dichroism (CD) and attenuated total internal reflection Fourier transform infrared spectroscopy (ATR-FTIR) in a solution and on a surface, respectively. Molecular dynamics simulations were also performed to further elucidate secondary structure differences. X-ray photoelectron spectroscopy (XPS) was used to evaluate surface attachment. Nonspecific protein adsorption was measured via surface plasmon resonance (SPR) sensors. Furthermore, RGD was added to the N-terminus of the EKEKEKE-PPPPC-Am sequence to gain specific cell adhesion while maintaining the ultra-low fouling background of the EK peptide. Extending the EK peptide sequence with RGD eliminates the need for

conjugation of biomolecular recognition peptides to nonfouling synthetic polymers, such as PEG. The peptide sequence RGD-EKEKEKE-PPPPC-Am used in this work is illustrated in Figure 2-1. This all-in-one peptide contains biomolecular recognition, ultra-low fouling, and surface anchoring functions.

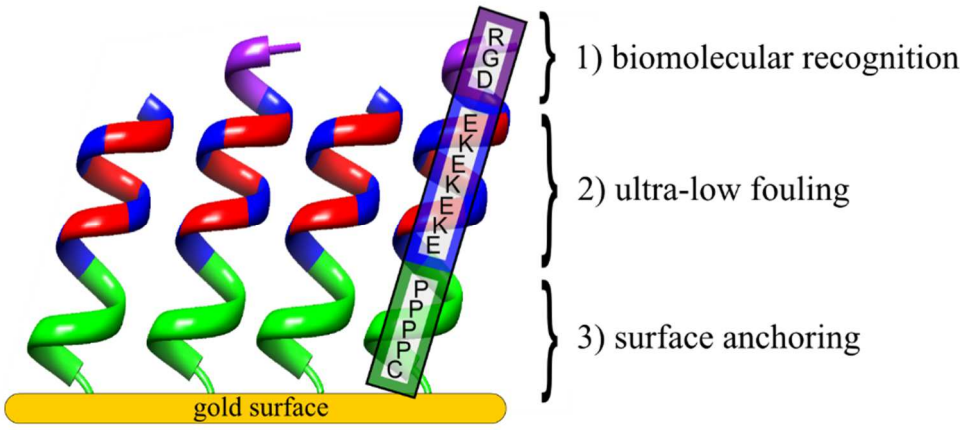

Figure 2-1. Multifunctional all-in-one natural peptide SAM on gold.
All-in-one natural peptide SAM on gold with three distinct functions incorporated into the peptide sequence: 1) biomolecular recognition via RGD (purple) 2) ultra-low fouling via EKEKEKE (blue and red) 3) surface anchoring composed of four rigid, hydrophobic proline (P) residues and a cysteine (C) residue via PPPPC (green).

Finally, we examine the surfaces of human proteins to gain inspiration for the biomimetic design of additional low fouling sequences. Proteins have adapted to avoid nonspecific adsorption and display stability in complex media. The analysis of 1,162 human proteins surfaces, confirmed that glutamic acid and lysine are likely candidates for low fouling materials since they are the most prevalent amino acids on the surfaces of proteins. In addition, asparagine (N) was identified as a neutrally charged potential low fouling peptide sequence. The robust surface anchoring linker developed in this work, -PPPPC, was used to evaluate the low fouling properties of a random EK sequence and an asparagine (N) sequence. Peptide self-assembled monolayers were formed from Ac-$[EK]_7$-PPPPC-Am and Ac-CPPPP-NNNNNNN-Am and evaluated by SPR for protein fouling.

2.2 Experimental Methods

2.2.1. Materials

N-Fluorenylmethoxycarbonyl (Fmoc)-protected amino acids with the amine and side chain protected (Fmoc–Asn(Trt)–OH, Fmoc–Cys(Trt)–OH, Fmoc–Glu(OtBu)–OH, Fmoc–Gly–OH, Fmoc–Lys(Boc)–OH, Fmoc–Pro–OH), Rink amide AM resin, O-benzotriazole-N,N,N',N'-tetramethyluronium hexafluorophosphate (HBTU), N-hydroxybenzotriazole (HOBt), and N,N-dimethylformamide (DMF) were bought from AAPPTec (Louisville, KY). N,N-Diisopropylethylamine (DIPEA) was bought from TCI America (Portland, OR). Trifluoroacetic acid (TFA), pyridine, acetic anhydride, and sodium sulfate were bought from EMD (Darmstadt, Germany). Piperidine, dichloromethane (DCM), triisopropylsilane (TIS), 1,3-dimethoxybenzene (DMB), 1,2-ethanedithiol (EDT), 1,1,1,3,3,3-hexafluoro-2-propanol (HFIP), phosphate buffered saline (PBS), fibrinogen from bovine plasma, and lysozyme from chicken egg white were purchased from Sigma Aldrich (St. Louis, MO). Ethanol was purchased from Decon Labs, Inc. (King of Prussia, PA). Tris(2-carboxyethyl)phosphine hydrochloride (TCEP) was purchased from Pierce (Rockford, IL). Potassium phosphate was purchased from JT Baker (Austin, TX). NIH-3T3 fibroblast cells were purchased from ATCC (Manassas, VA). Dulbecco's Modified Eagle Medium (DMEM), fetal bovine serum (FBS), and penicillin-streptomycin (PS) were purchased from Invitrogen (Carlsbad, CA). Water used in experiments was purified using a Millipore water purification system (Darmstadt, Germany) with a minimum resistivity of 18.0 MΩ•cm.

2.2.2. Peptide Synthesis and Characterization

EKEKEKE-C-Am, EKEKEKE-PC-Am, EKEKEKE-PPPC-Am, EKEKEKE-PPPPC-Am, RGD-EKEKEKE-PPPPC-Am, RDG-EKEKEKE-PPPPC-Am, and EKEKEKE-GGGGC-Am peptides were ordered from Synthetic Biomolecules (San Diego, CA) at a purity of >95%. Peptides

were synthesized using Fmoc chemistry and purified by reverse phase high performance liquid chromatography (RP-HPLC). The sequences Ac-[EK]$_7$-PPPPC-Am (random EK), Ac-GGGGGGG-PPPPC-Am, and Ac-CPPPP-NNNNNNN-Am were synthesized using the AAPPTec Titan 357 automated synthesizer (Louisville, KY) by a solid-phase technique, starting from a polystyrene Rink amide AM resin (0.58 mmol/g loading capacity). Coupling was performed using amino acid monomer, HBTU, HOBt, and DIPEA prepared in DMF in a molar ratio of 1.1:1:1:2 in four times excess of the loading capacity of the resin. Deprotection of Fmoc groups was achieved using 20% piperidine in DMF. N-terminal acetylation was achieved with a solution of pyridine (5%), acetic anhydride (5%) and DMF (90%) (v/v/v). Random peptide sequences were created using the mix and split capability of the AAPPTec Titan 357. The cleavage of the final peptide product was performed using a TFA (75%), DCM (15%), DMB (4%), water (2%), TIS (2%), and EDT (2%) (v/v/v/v/v/v) cleavage cocktail. The peptide purity was evaluated by RP-HPLC for known sequences and purified as needed. The purity of the glycine peptide sequence was 92% and the asparagine peptide sequence was 97%. Peptides were analyzed by matrix-assisted laser desorption/ionization time-of-flight mass spectrometry (MALDI-TOF) to confirm molecular weight values.

2.2.3. Preparation of Peptide SAMs

Gold coated chips were cleaned by rinsing with Millipore water, ethanol, and then drying with filtered air. They were placed in a UV cleaner for 20 minutes. Cleaned gold chips were incubated in a PBS solution (pH 7.4 and ionic strength of 150 mM) containing 0.14 mM peptide for 24 hours. Peptide sequences containing asparagine (Ac-CPPPP-NNNNNNN-Am) were first dissolved in HFIP (4 mg/mL) and then diluted to a final concentration of 0.2 mg/mL PBS containing 0.5 mM TCEP. Once removed, the gold chips were rinsed with Millipore water and dried by filtered

air. This procedure was followed for all peptide SAM surfaces prepared for SPR, ATR-FTIR, XPS, and cell adhesion experiments.

2.2.4 Protein Adsorption by SPR Sensor

A four-channel SPR sensor was used to measure protein adsorption. Samples were rinsed with Millipore water, dried by filtered air, and mounted to the device. The temperature controller was set to 25 ± 0.01˚C. Protein adsorption was measured by flowing PBS over the SAM at 40 μL/min for 10 minutes, followed by 1 mg/mL protein solutions of fibrinogen (from bovine plasma) or lysozyme (from chicken egg white) for 10 minutes, and finally a PBS rinse for 10 minutes. The wavelength shift between baselines before protein injection and after rinsing was used to quantify the total amount of protein adsorbed. A reference channel containing PBS was flown for each chip and used to correct for baseline drift. A 1 nm wavelength shift from 750 nm corresponds to 17 ng/cm^2 adsorbed proteins[60]. The detection limit for the SPR is 0.3 ng/cm^2.

2.2.5 CD of Peptide Solutions

CD spectra were recorded between 190 and 270 nm (step resolution of 0.2 nm) of 0.1 mg/mL peptide in 10 mM potassium phosphate, 50 mM sodium sulfate buffer (pH 7.4) at 25˚C with a JASCO J-720 CD spectropolarimeter using an optical cell of 1.0 mm path length. Each experiment was repeated three times. Buffer spectra were recorded and subtracted from the sample spectra.

2.2.6 Secondary Structure Simulations for Proline Linker Addition

The study of addition of proline to the peptides was done using the Rosetta protein structure prediction package[61]. It has had excellent performance in the past with *de novo* structure prediction[61]. The goal of our simulations was not to determine the structure of the peptides, but to

instead see if the peptides have a more extended conformation. The peptides were first built to have their ideal rotamers with ideal α-helix rotamers and ideal β-sheet (non-proline residues only), thus giving two starting structures for each sequence. Next, their bonds, angles, and dihedrals were optimized according to the Rosetta scoring function using the "idealize" module of Rosetta. Then, a Monte Carlo optimization of the structures was done for 400,000 steps. The Monte Carlo moves are backbone dihedral changes. The top 12 structures for the α-helix and β-sheet were chosen for continuation, resulting in 24 structures for each sequence. Next, the "relax" module of Rosetta was used to minimize side-chain clashes by changing χ-rotamers of the side chains of the top 24 structures. This was followed by another backbone Monte Carlo optimization on each of the 24 structures 300,000 steps and the structures were relaxed. Finally, the 10 structures with the lowest scores among the 24 candidates were aligned and are shown in Figure 2-4a.

2.2.7 Molecular Simulations for Determination of Secondary Structure Mode and the Probability Distribution of the Cα-Cα Distance

Molecular dynamics were conducted using the GROMACS 4.5.3 simulation engine[62] and the AMBER99sb-ildn force field[63]. Single peptides were built using the α-helical Dunbrack rotamers[64]. They were then energy minimized using 10,000 steps of steepest descent. The minimized system was solvated in a box such that the peptide had 1 nm of solvent in all directions. Ions were added to charge equilibrate the system. Annealing was then done for 200 ps with a schedule from 100 K to 500 K in the NPT ensemble. Finally, an equilibration for 100 ps again in the NPT ensemble was conducted. The resulting system was then used for the production simulation.

Replica exchange with 100 replicas, exchange attempts every 50 fs, and a time step of 2 fs in the NVT ensemble was used for the simulations. The temperature distribution for replica exchange

was: 300.0, 301.2, 302.5, 303.7, 305.0, 306.2, 307.5, 308.7, 310.0, 311.3, 312.5, 313.8, 315.1, 316.4, 317.7, 319.0, 320.3, 321.6, 323.0, 324.3, 325.6, 326.9, 328.3, 329.6, 331.0, 332.3, 333.7, 335.1, 336.5, 337.8, 339.2, 340.6, 342.0, 343.4, 344.8, 346.2, 347.7, 349.1, 350.5, 352.0, 353.4, 354.9, 356.3, 357.8, 359.2, 360.7, 362.2, 363.7, 365.2, 366.7, 368.2, 369.7, 371.2, 372.7, 374.3, 375.8, 377.3, 378.9, 380.4, 382.0, 383.6, 385.1, 386.7, 388.3, 389.9, 391.5, 393.1, 394.7, 396.3, 398.0, 399.6, 401.2, 402.9, 404.5, 406.2, 407.9, 409.5, 411.2, 412.9, 414.6, 416.3, 418.0, 419.7, 421.5, 423.2, 424.9, 426.7, 428.4, 430.2, 431.9, 433.7, 435.5, 437.3, 439.1, 440.9, 442.7, 444.5, 446.3, 448.2, 450.0. Particle-mesh Ewald sums was used to treat electrostatics[65]. The Van der Walls cut-off was 1 nm with an appropriate shifting function. The "v-rescale" thermostat[66] was used, a stochastic thermostat not to be confused with velocity rescaling. The thermostat time constant was 0.5 ps. The simulations were run for 20 ns and the secondary structure was characterized at the 300 K replica using the DSSP program[67] and the per-residue modes are shown in Figure 2-6a. The "crystallographers' intuition" codes were used from the DSSP calculations to visually represent the mode of the secondary structure. The mode corresponds to the free energy minimum when canonically sampling from an NVT ensemble. Figure 2-6b was plotted using a kernel density estimator with a bandwidth of 2Å. The choice of a kernel density estimator, as opposed to a histogram, was to allow plotting of the three sequences simultaneously. The horizontal lines are the raw data medians.

2.2.8 ATR-FTIR of Peptide SAMs

Peptide SAMs were assembled on gold coated mica substrates as described previously. After incubation the chips were dried in a desiccator overnight before evaluation by ATR-FTIR. The ATR-FTIR spectra were acquired using Harrick's GATR single-angle reflection accessory in conjunction

with a Bruker Tensor spectrometer (Bruker, Billerica, MA). Each spectrum was collected with a minimum of 80 scans, at 4 cm^{-1} resolution, and 65˚ incident angle. Optimum contact between the germanium crystal and the sample were maintained throughout measurements. Bare gold on mica was recorded as the background spectra and subtracted from the sample spectra. Three replicates of each SAM were analyzed.

2.2.9 XPS of Peptide SAMs

Peptide SAMs were assembled on gold coated mica substrates. XPS experiments were performed on a Kratos Axis Ultra DLD (Kratos Analytical, Manchester, United Kingdom) spectrometer using a monochromatic Al K α x-ray source (hν = 1486.6 eV) operated at 10 mA at 15 kV. The analysis area was approximately 300 x 700 μm. Survey spectra were acquired with an analyzer pass energy of 80 eV. The high resolution S_{2p} and C_{1s} spectra were acquired with an analyzer pass energy of 20 eV. All XPS data were acquired at a nominal photoelectron takeoff angle of 0˚, where the takeoff angle is defined as the angle between the surface normal and the axis of the analyzer lens. Three spots on two replicates of each SAM were examined. The compositional data are averages of the values determined at each analysis spot.

2.2.10 Cell Seeding of Peptide SAMs

Prior to cell adhesion experiments, samples were sterilized by soaking and rinsing with copious amounts of sterilized PBS. NIH-3T3 fibroblasts were plated at 4 x 10^4 cells/mL in 3 mL DMEM with 10% (v/v) FBS and 1% (v/v) PS and incubated for 24 hours at 37 ˚C in 5% CO_2 and 100% relative humidity. Cell seeding density was determined using a hemocytometer. Cell adhesion and morphology was observed using a Nikon Eclipse TE2000-U phase contrast microscope (Nikon,

Tokyo, Japan). The number of cells adhered was determined by visually counting cells present in at least three microscope images (100x objective magnification).

2.3 Results and Discussion

2.3.1 Peptide Synthesis Characterization

All synthesized peptides were characterized by reverse phase high performance liquid chromatography (RP-HPLC) for known sequences and purified as needed (Figure 2-2). The purity of the glycine peptide sequence (Ac-GGGGGGG-PPPPC-Am) was 92% and the purity of the asparagine peptide sequence (Ac-CPPPP-NNNNNNN-Am) was 97%. Peptides were also analyzed by matrix-assisted laser desorption/ionization time-of-flight mass spectrometry (MALDI-TOF-MS) to confirm molecular weight values.

a) random Ac-$[EK]_7$-PPPPC-Am

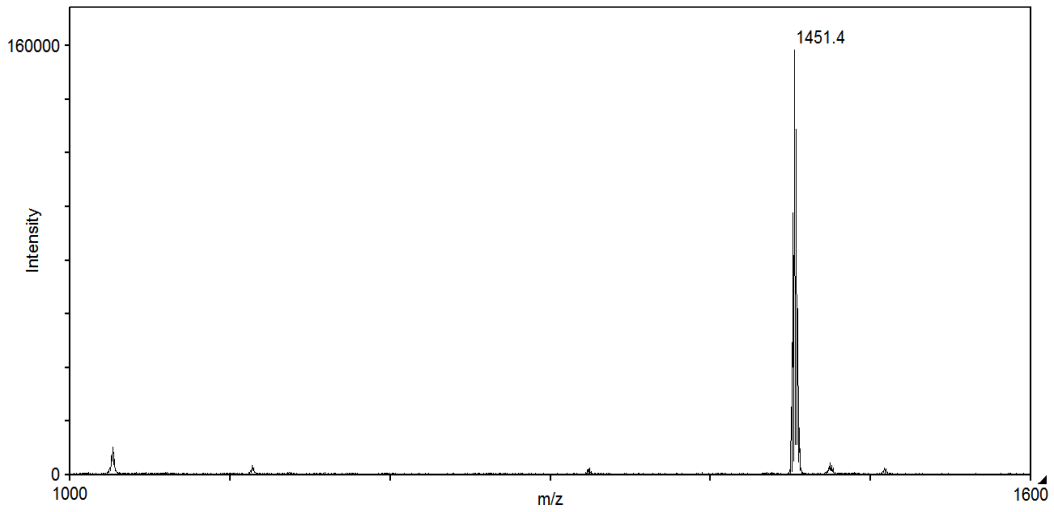

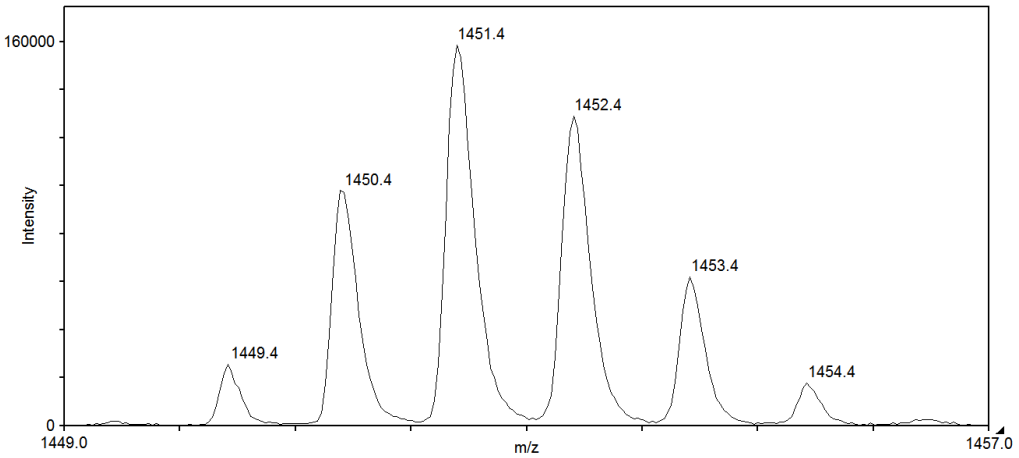

b) Ac-GGGGGGG-PPPPC-Am

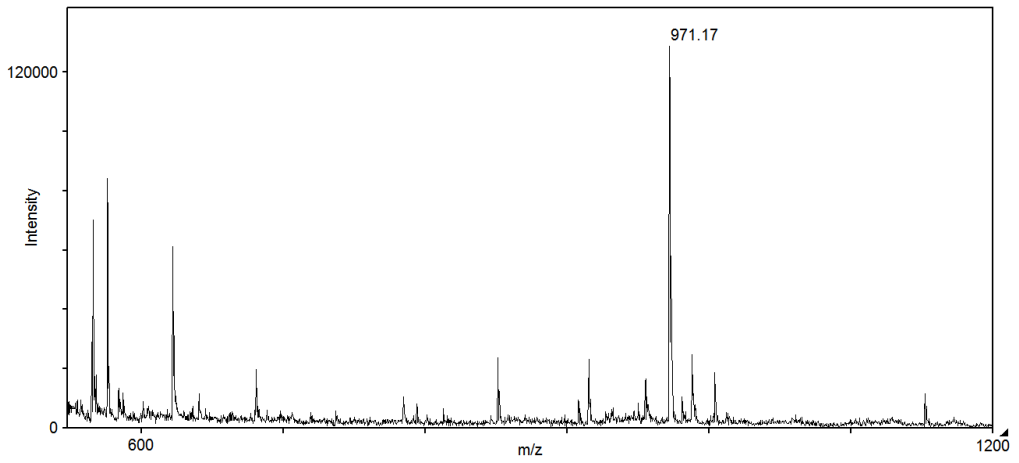

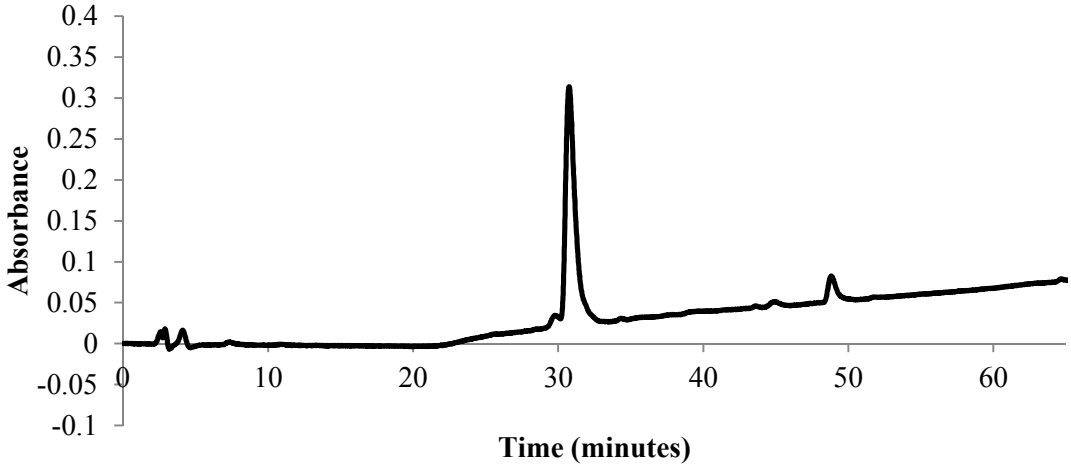

c) Ac-CPPPP-NNNNNNN-Am

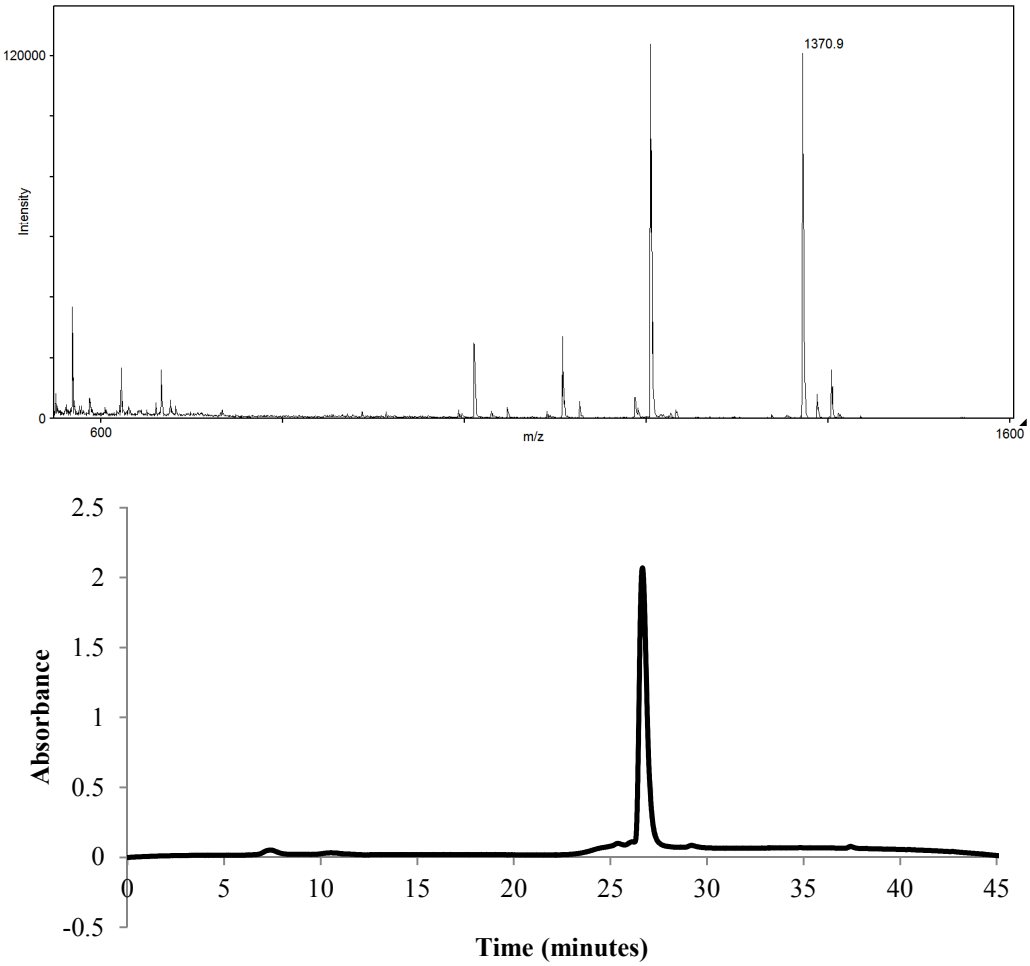

Figure 2-2. RP-HPLC and MALDI peptide synthesis characterization.
(a) MALDI-TOF mass spectra of Ac-XXXXXXXPPPPC-Am, where X is K or E randomly (top). The expected molecular weight of Ac-XXXXXXXPPPPC-Am is approximately 1451. A distribution of molecular weights around this value can be seen in the MALDI spectra (bottom). (b) RP-HPLC (top) and MALDI (bottom) data for Ac-GGGGGGGPPPPC-Am. The expected molecular weight of Ac-GGGGGGGPPPPC-Am is 950.03. (c) RP-HPLC (top) and MALDI (bottom) data for Ac-CPPPP-NNNNNNN-Am. The expected molecular weight of Ac-CPPPP-NNNNNNN-Am is 1349.4. The molecular weight of Ac-GGGGGGGPPPPC-Am and Ac-CPPPP-NNNNNNN-Am are higher by 21.14, which corresponds to a positive sodium ion conjugated to the peptide and the loss of a proton.

2.3.2 Impact of Nature and Length of Linker on SAM Formation

Surface plasmon resonance (SPR) shows that simply using a cysteine residue containing a thiol side chain for surface anchoring is insufficient to form a low fouling peptide SAM (Figure 2-3a). The fouling to fibrinogen and lysozyme for the linker-free peptide SAM (EKEKEKE-C-Am)

is 38.3 ± 29.0 ng/cm^2 and 5.3 ± 4.4 ng/cm^2, respectively. In addition to high fouling, there is a large distribution in the fibrinogen protein adsorption values (Figure 2-3b).

Here, we consider the effect of including a proline (P) linker and a glycine (G) linker in the EKEKEKE-C-Am peptide studied. Proline was selected based on its hydrophobicity, its ability to act as an α-helix destabilizing residue[68], and its rigid structure which all should promote high density packing for SAM formation. Additionally, the covalently constrained backbone of proline reduces the entropy loss upon adsorption of the peptide to the surface, whereas other amino acids lose mobility upon adsorption[69]. Glycine was selected based on its hydrophilicity and its flexibility for comparison with proline.

The additional inclusion of four prolines as a linker resulted in an ultra-low fouling SAM, defined as having an adsorption of less than 5 ng/cm^2 of fibrinogen[1]. The fouling to fibrinogen and lysozyme for the proline linker peptide SAM (EKEKEKE-PPPPC-Am) is 4.4 ± 2.9 ng/cm^2 and 3.5 ± 2.6 ng/cm^2, respectively, which is comparable to the previously studied butanethiol containing peptide SAM[13]. Furthermore, the proline linker peptide has a narrow distribution for fibrinogen protein adsorption, as opposed to the large distribution seen for the linker-free peptide (Figure 2-3d).

As a comparison to the rigid, hydrophobic proline residue, the flexible, hydrophilic glycine residue was also used as a linker. SPR indicates that the inclusion of a glycine linker (EKEKEKE-GGGGC-Am) results in a high fouling SAM, with fouling to fibrinogen and lysozyme of 17.9 ± 11.4 ng/cm^2 and 4.5 ± 3.8 ng/cm^2, respectively. It is not surprising that the flexible linker compromised the fouling properties of the SAM as this would disrupt close packing on the surface, just as in the linker-free peptide. The glycine linker peptide also has a large distribution for fibrinogen protein adsorption (Figure 2-3c). In contrast, the inclusion of the rigid, hydrophobic proline linker allows for

favorable hydrophobic interactions between chains, enabling better packing. These hydrophobic groups may be analogous to the role of the methyl groups found in synthetic butanethiol anchors.[13]

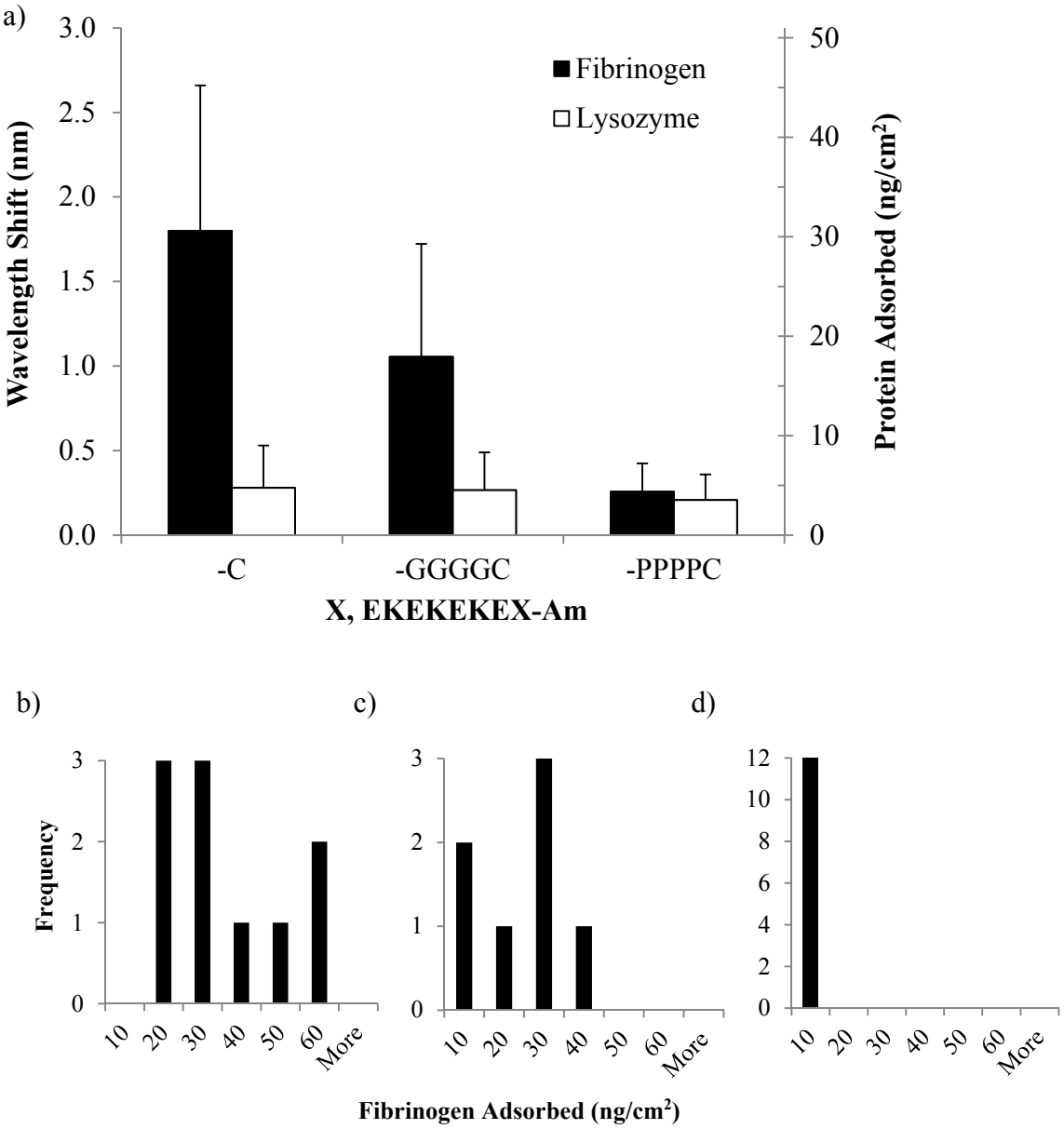

Figure 2-3. Effect of peptide linker type on protein adsorption.
(a) Protein adsorption on peptide SAMs composed of the linker-free peptide (EKEKEKE-C-Am), the glycine linker peptide (EKEKEKE-GGGGC-Am), and the proline linker peptide (EKEKEKE-PPPPC-Am). SPR results are in the unit of wavelength shift (nm) or converted protein surface concentration (ng/cm^2). (black: fibrinogen, white: lysozyme). Each data point represents an average value ± standard deviation from at least three independent measurements. Lower Panel: Histograms of adsorbed fibrinogen protein (ng/cm^2) for (b) linker-free peptide (c) glycine linker peptide and (d) proline linker peptide.

To determine how many linker residues are needed to promote close packing of the surface, the effect of linker length on the fouling properties of the SAMs was examined. Backbone and side-chain Monte Carlo simulations were performed using the Rosetta scoring function[61] on peptide sequences containing one to four prolines in the linker. These simulations predict peptide conformations in solution. Because these peptides contain so few residues, they lack a deep free energy minimum (fold) and are expected to shift between several low energy conformations. A sample of the lowest energy structures predicted by simulations for peptide sequences containing one to four prolines in the linker shows that the addition of proline favors an extended, rigid conformation for the peptide sequence (Figure 2-4a). The important feature to note is the increasing extended conformations as proline is added, due to the change from random coil to polyproline helix. The proline also makes the conformations more rigid, which should reduce the entropic penalty of peptide adsorption onto a gold surface. We hypothesize that the extended, rigid conformation allows for closer packing of peptide chains, thus enabling the formation of a uniform, low fouling surface. As expected, SPR indicates an increase in proline number corresponds to a decrease in the amount of adsorbed protein (Figure 2-4b).

a)

-PC -PPC -PPPC -PPPPC

X, EKEKEKE-X-Am

b)

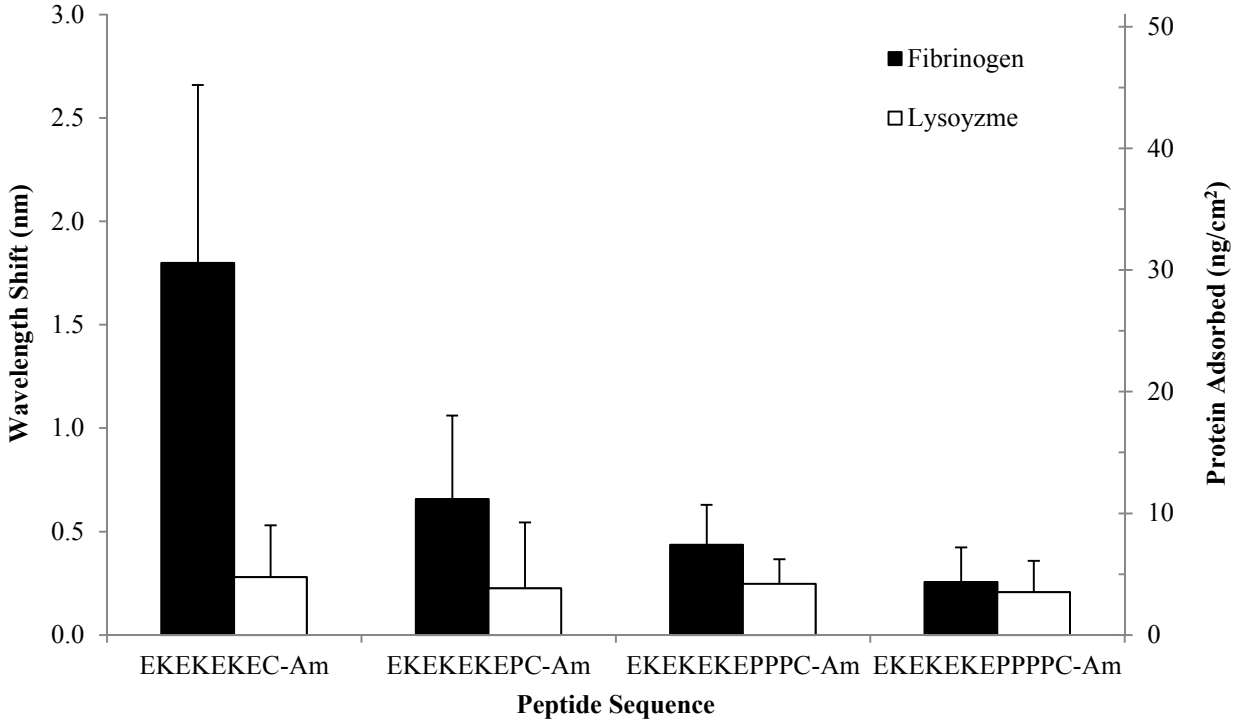

Figure 2-4. Effect of peptide linker length on protein adsorption.
(a) Ten lowest energy (score) conformations from 24 different starting structures as predicted using the Rosetta structure prediction package. They are aligned and oriented with the cysteine (C-terminus) at the bottom. Sequences from left to right are EKEKEKE-PC-Am, EKEKEKE-PPC-Am, EKEKEKE-PPPC-Am, and EKEKEKE-PPPPC-Am. (b) Adsorption of protein on peptide SAMs composed of proline linker series EKEKEKE-C-Am, EKEKEKE-PC-Am, EKEKEKE-PPPC-Am and EKEKEKE-PPPPC-Am determined from a surface plasmon resonance sensor (SPR) in the unit of wavelength shift (nm) or converted surface concentration (ng/cm^2). (black: fibrinogen, white: lysozyme). Each data point represents an average value ± standard deviation (SD) from at least three independent measurements.

The linker containing four prolines is the threshold for achieving an ultra-low fouling surface and thus four peptide residues was chosen as the linker length. Overall, simply using a cysteine residue for surface anchoring does not provide a peptide capable of self-assembly into an ultra-low fouling surface. Thus, selection of an appropriate peptide linker that will allow close-packing of chains is essential. Here, we have identified a linker of four residues in length and of a rigid, hydrophobic nature as one possible robust option. Other strategies have been considered using natural peptides to improve peptide self-assembly on surfaces[70], on nanoparticles[71], and for membrane formation[72].

2.3.3 Impact of Secondary Structure on SAM Formation

In order to further investigate the large differences in fouling between the linker-free peptide (EKEKEKE-C-Am) and the proline linker peptide (EKEKEKE-PPPPC-Am), we examined secondary structure in solution via CD and molecular simulations, and on the surface via ATR-FTIR. CD spectra were collected in 10 mM potassium phosphate, 50 mM sodium sulfate buffer, pH 7.4 (Figure 2-5a). The CD spectrum for the linker-free peptide is indicative of a disordered structure with very low ellipticity above 210 nm and negative bands near 195 nm[73]. In contrast, the CD spectrum for the proline linker peptide designates an extended polyproline helix conformation with a strong negative band near 200 nm and a weaker positive band around 225 nm[74].

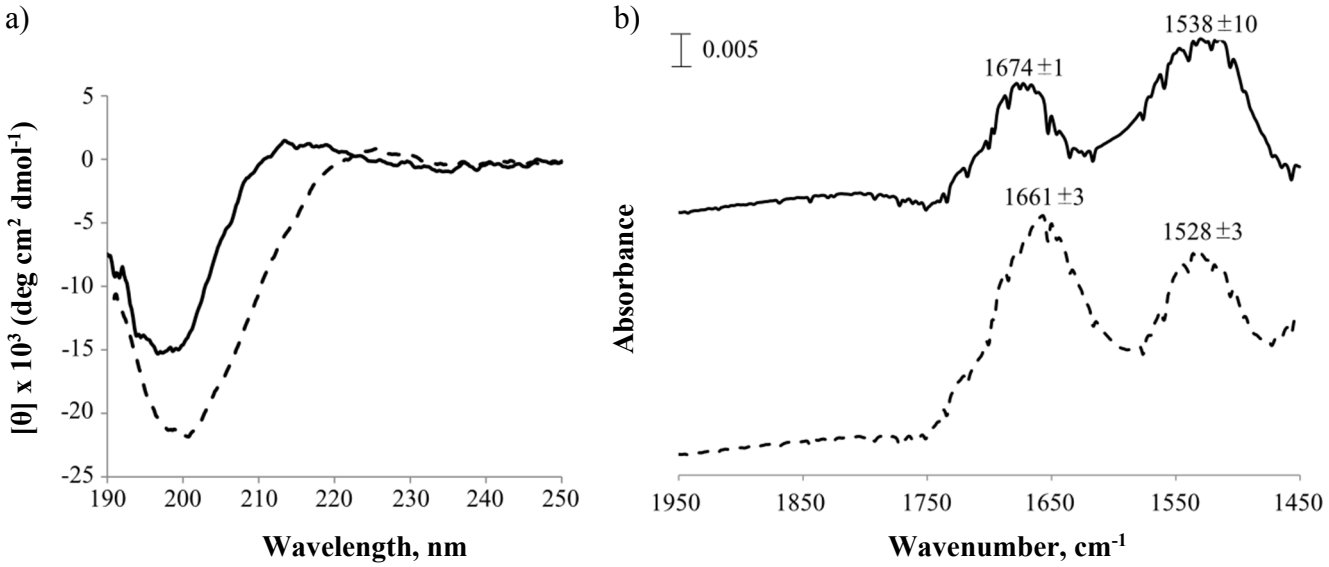

Figure 2-5. CD and ATR-FTIR secondary structure comparison.
Secondary structure comparison of the linker-free peptide (EKEKEKE-C-Am) and the proline linker peptide (EKEKEKE-PPPPC-Am). (a) CD spectra of peptide sequences EKEKEKE-C-Am (solid line) and EKEKEKE-PPPPC-Am (dashed line) in 10 mM potassium phosphate, 50 mM sodium sulfate buffer, pH 7.4. (b) Representative ATR-FTIR spectra for peptide SAMs EKEKEKE-C-Am (solid line) and EKEKEKE-PPPPC-Am (dashed line) on Au (111) coated mica substrate. Average maximum intensities for amide I (left) and amide II (right) bands are listed above peaks in the spectrum from at least three independent measurements.

Replica-exchange molecular dynamics simulations were performed in solution to supplement CD data for the linker-free peptide, the proline linker peptide, and the glycine linker peptide. Figure 2-6a shows the lowest energy secondary structure at each residue position for the three peptides. The linker-free and the glycine linker peptide lack secondary structure. The proline linker peptide displays helical structure most likely due to the rigidity imparted on the backbone from the proline linker. Figure 2-6b shows the C-α to C-α end to end distance as a probability distribution with the vertical lines indicating the median. The proline linker peptide is more extended than both the linker-free and the glycine linker control peptides.

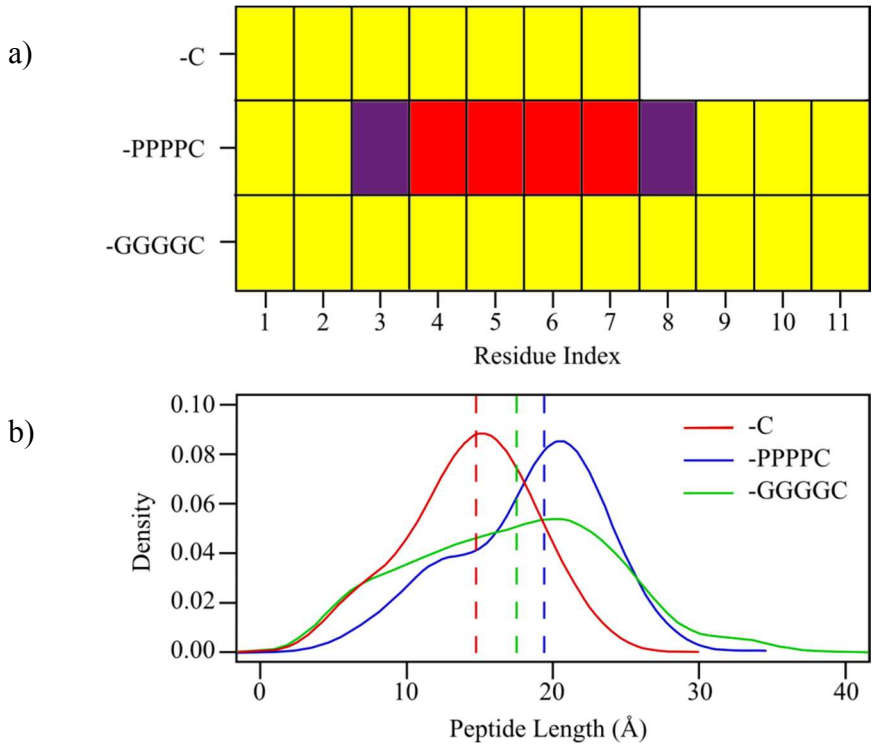

Figure 2-6. **Secondary structure molecular simulations.**
(a) Secondary structure mode for each residue on EKEKEKE-C-Am, EKEKEKE-PPPPC-Am, and EKEKEKE-GGGGC-Am. The secondary structure was determined using DSSP on the trajectories obtained from tempered annealing molecular dynamics simulations of dilute peptides. Yellow indicates no secondary structure, purple indicates a turn or bend with a hydrogen bond, and red indicates an alpha-helix. (b) Probability distribution of the Cα-Cα distance between the initial and final residues in the peptide EKEKEKE-C-Am (red line), EKEKEKE-PPPPC-Am (blue line), and EKEKEKE-GGGGC-Am (green line). The probability distribution is taken from a kernel density estimator with a bandwidth of 3. The vertical lines are the medians of the data. The proline linker peptide is the most extended among the three.

We examined the linker-free and proline linker peptide SAMs on a gold surface using ATR-FTIR. Evaluation of ATR-FTIR amide I bands provides surface sensitive information about the secondary structure of peptide monolayers. The ATR-FTIR spectrum for the linker-free peptide resulted in maximum intensities for amide I and amide II bands at 1674 ± 1 and 1538 ± 10 cm^{-1}, whereas the ATR-FTIR spectrum for the proline linker peptide resulted in maximum intensities for amide I and amide II bands at 1661 ± 3 and 1528 ± 3 cm^{-1} (Figure 2-5b). The higher shifted intensity of the amide I band for the linker-free peptide at 1674 cm^{-1} is not characteristic of an α-helix or a β-sheet, suggesting that the structure of this peptide is unordered [75,76]. The amide I band for the proline linker peptide at 1661 cm^{-1} is shifted slightly higher than regular alpha helical structures typically with amide I bands at 1650-1658 cm^{-1}. This most likely represents the presence of distorted and/or 3_{10} helices as expected for a peptide containing several proline residues[77]. Furthermore, the major amide I band is considerably broad, indicating a larger distribution of slightly different helical structures.

Results from CD, molecular simulations, and ATR-FTIR all support a disordered, random structure for the linker-free peptide and an extended, helical structure for the proline linker peptide. This secondary structure characterization provides a possible explanation for the differences in fouling between the two surfaces. The disordered structure of the peptide containing no linker (EKEKEKE-C-Am) could impede packing of the peptide SAM, resulting in non-uniform surface coverage leading to high fouling and large variations in the results. At the same time, the defined, extended conformation of the proline linker peptide (EKEKEKE-PPPPC-Am) allows for closer packing of the monolayer and a more uniform surface with consistent ultra-low fouling behavior. These results indicate that it is preferable to have a well-defined secondary structure to form a closely-packed, uniform monolayer.

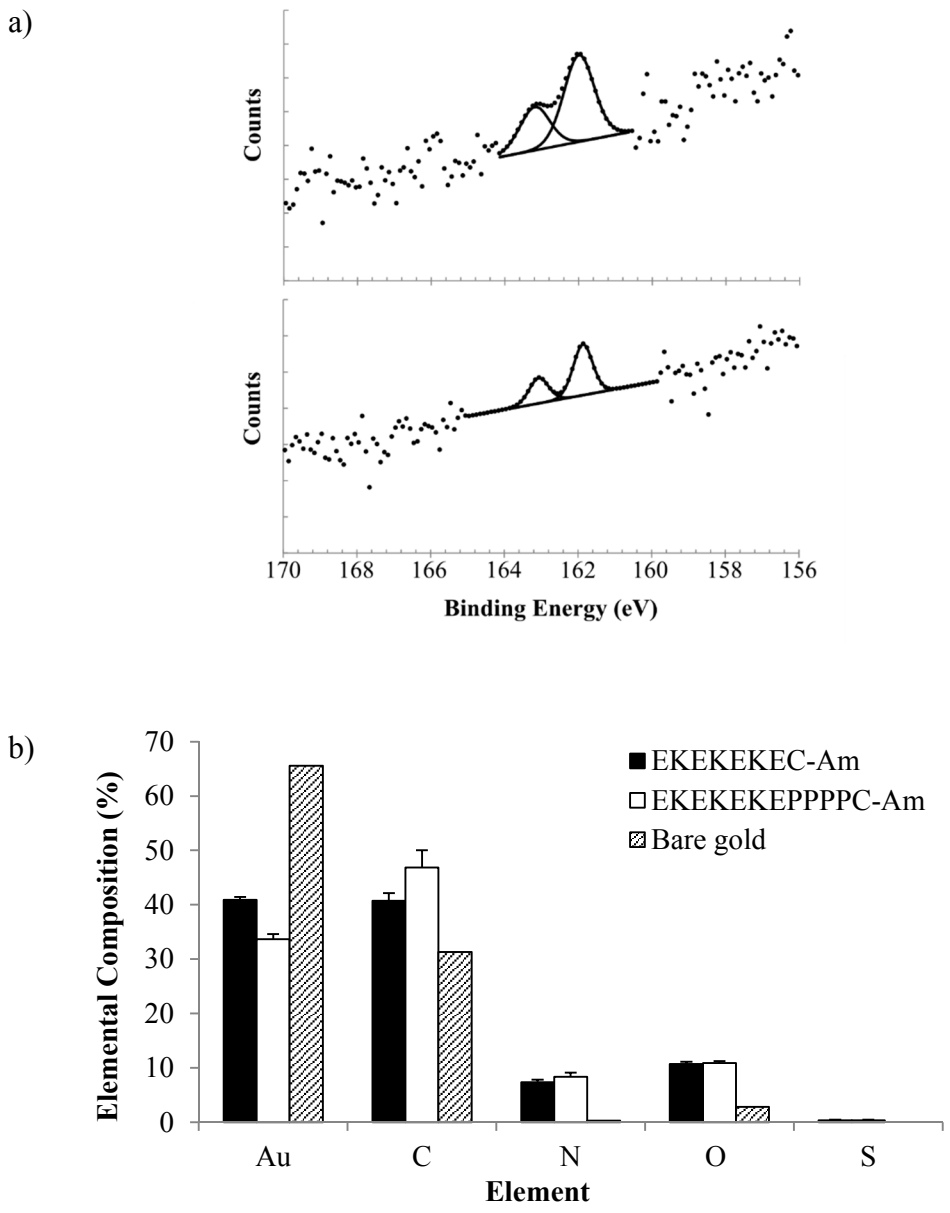

Figure 2-7. XPS surface characterization.
(a) XPS S_{2p} spectra for EKEKEKE-C-Am (top) and EKEKEKE-PPPPC-Am (bottom) peptide SAMs adsorbed on Au (111) coated mica substrate. To properly fit the experimental peptide SAM spectrum a S_{2p} doublet with 2:1 area ratio and splitting of 1.2 eV was used. (b) XPS surface compositions. Percent elemental surface compositions of Au, C, N, O, and S for EKEKEKE-C-Am (black) and EKEKEKE-PPPPC-Am (white) peptide SAMs and bare gold control (stripes).

Finally, XPS data were collected for the linker-free and proline linker peptide SAMs to confirm that their difference in performance is due to their secondary structure rather than their surface binding characteristics. The binding energy of the $S_{2p3/2}$ peak was 161.9 eV for both surfaces,

consistent with sulfur atoms bound to the gold surface as a thiolate species (Figure 2-7a)[78]. The presence of only bound thiolate species in the high resolution sulfur spectra indicate that the thiol side chain of the cysteine anchor is bound to the gold and is not simply physically adsorbed on the surface.

XPS data also provide information about the surface coverage and lateral packing density of a SAM, determined by measurement of the attenuation of the metal substrate photoelectrons (Au_{4f})[79]. The gold signal for the proline linker peptide is lower than the gold signal for the linker-free peptide, indicating that the proline linker peptide SAM surface is more densely packed (Figure 2-7b). However, the longer length of the proline linker peptide compared to the linker-free peptide may also partially account for the attenuation of the gold signal. XPS theoretical vs actual elemental percent compositions for C, N, O, and S are listed in Table 2-1. The higher surface coverage of the proline linker peptide SAM indicates improved packing of the peptide chains, corroborating the secondary structure data from CD, molecular simulations, and ATR-FTIR.

Table 2-1. **XPS theoretical vs actual elemental percent compositions.**
XPS calculated theoretical vs actual elemental percent compositions for carbon (C), nitrogen (N), oxygen (O), and sulfur (S) for peptide SAMs composed of EKEKEKE-C-Am and EKEKEKE-PPPPC-Am.

	EKEKEKE-C-Am		**EKEKEKE-PPPPC-Am**	
	Theoretical	Actual	Theoretical	Actual
C	58.6	68.8	62.2	70.6
N	17.1	12.5	16.3	12.5
O	22.9	18.1	20.4	16.4
S	1.4	0.6	1.0	0.5

Several parameters influence monolayer architecture and thus low fouling behavior, including chemical moieties, secondary structure formation, peptide length, and peptide packing density. The inclusion of the four proline residue linker introduced in this work induces helical structure at the base of the peptide as evidenced by ATR-FTIR and molecular simulations. The helical formation reduces the mobility of the chains. Thus, this rigid secondary structure results in

more uniform peptide molecular conformations, allowing chains to pack tighter, increasing packing density and reducing fouling. As seen in Figure 2-4, the number of proline residues in the linker has a profound effect on fouling, due to its importance in maintaining the rigid structure necessary for well-packed monolayers. The transition from three to four proline residues, however, shows that the effect of the peptide linker length lessens beyond three linker residues. Similarly, as seen in Figure 2-6, the EK residues more than four units beyond the linker are no longer influenced, adopting the random conformations seen in the linker-free and glycine linker sequences. Unlike mixed charge alkanethiol SAMs, where regular crystalline structures are observed[13], we expect that the solvent-exposed surface of peptide SAMs is a uniform display of mixed charge E and K residues. Our previous work on mixed E and K random copolymerization studies[13] show that even with amorphous conformations, low fouling is achieved.

2.3.4 Specific Biomolecular Recognition on an Ultra-Low Fouling Background

In this experiment, we extend EKEKEKE-PPPPC-Am with the cell-binding sequence RGD. Cell adhesion onto peptide SAMs composed of mixtures of RGD-EKEKEKE-PPPPC-Am and EKEKEKE-PPPPC-Am was evaluated to display the biomolecular recognition capabilities of our all-in-one peptide biomaterial. The molar percentage of RGD-EKEKEKE-PPPPC-Am was increased from 0 to 100%. Peptide SAMs were seeded with NIH-3T3 fibroblast cells and incubated in supplemented medium for a period of 24 hours. Cell adhesion was then evaluated by phase contrast microscopy. As expected, the number of adhered cells increases proportionally to the molar percentage of the RGD-EKEKEKE-PPPPC-Am peptide (Figure 2-8). The SAM composed entirely of EKEKEKE-PPPPC-Am had no cell attachment, corresponding with the ultra-low fouling results for protein adsorption.

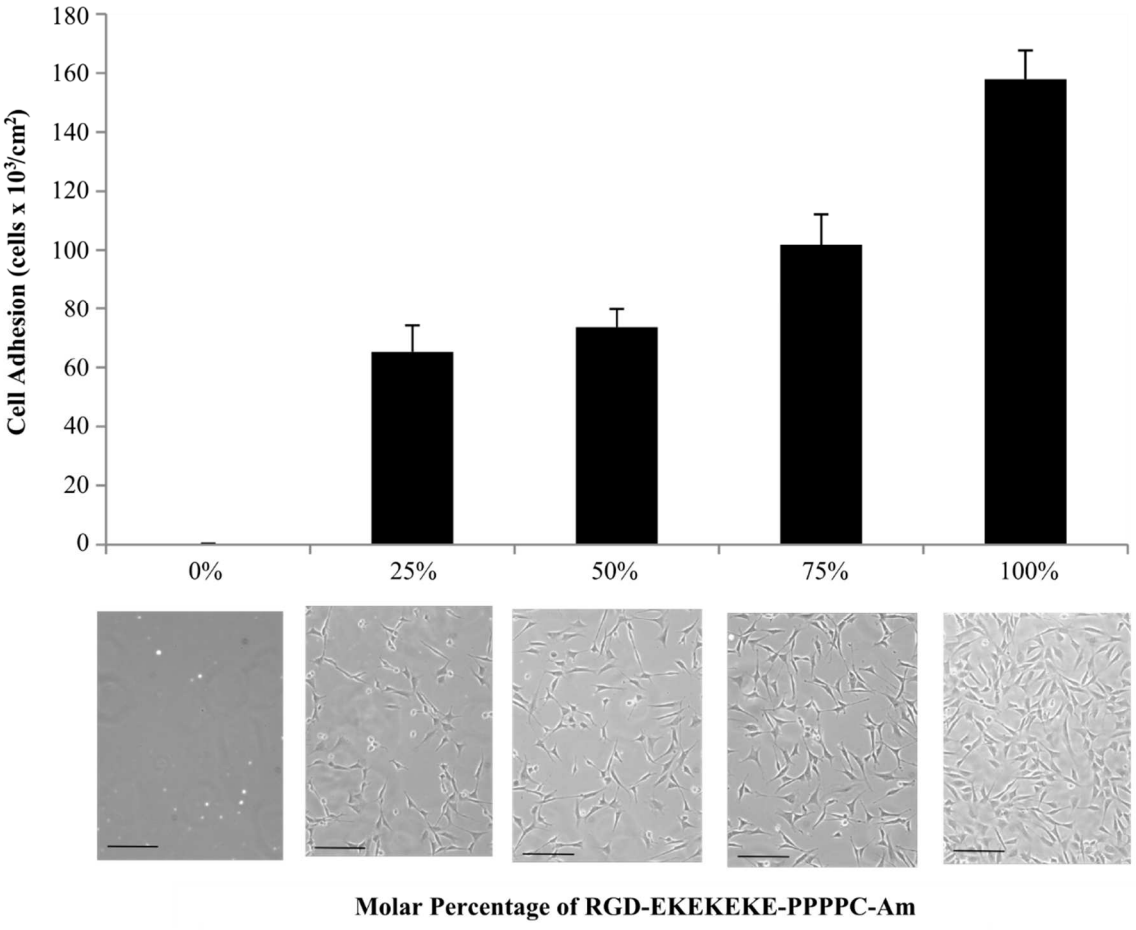

Figure 2-8. Specific recognition via cell adhesion.
NIH-3T3 fibroblast cell adhesion results after 24 hour incubation in supplemented medium for peptide SAMs composed of mixtures of RGD-EKEKEKE-PPPPC-Am and EKEKEKE-PPPPC-Am. The molar percentage of RGD-EKEKEKE-PPPPC-Am was increased from 0 to 100%. The scale bar represents 100μm.

The scrambled sequence RDG-EKEKEKE-PPPPC-Am was mixed with EKEKEKE-PPPPC-Am at molar percentages of 50% and 75% and evaluated for cell adhesion as a control. Surfaces containing scrambled RDG showed significantly less cell adhesion than peptide SAMs containing RGD (Figure 2-9). Furthermore, cells adhered to scrambled RDG surfaces displayed rounded morphology, whereas cells adhered to RGD surfaces were well spread out. These results show that interactions seen for the RGD sequence are specific and that the EK portion of the peptide maintains an ultra-low fouling background.

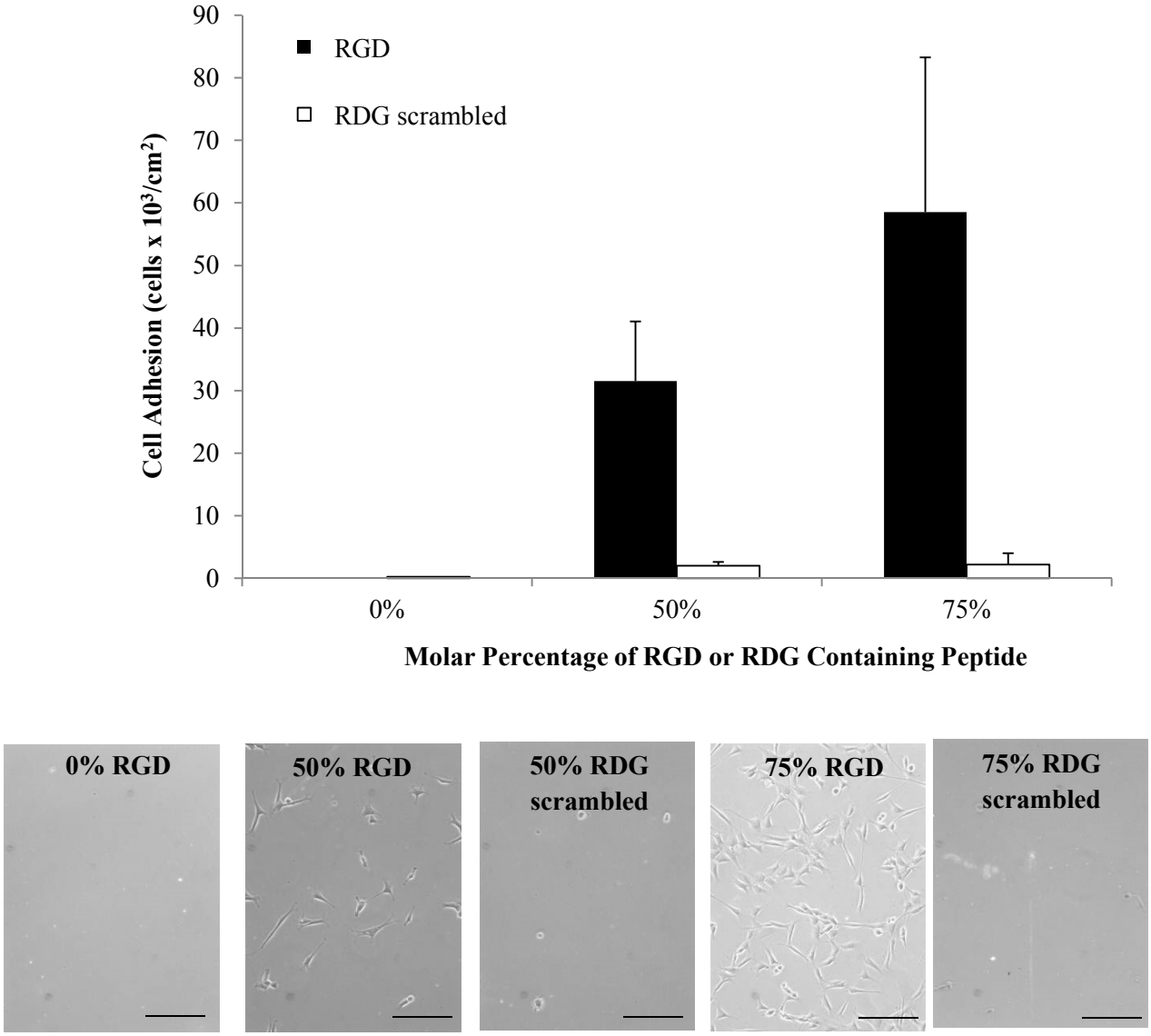

Figure 2-9. Control cell adhesion experiment with scrambled RDG sequence.
Cell adhesion results for peptide SAMs composed of mixtures of RGD-EKEKEKE-PPPPC-Am (black) and the scrambled sequence RDG-EKEKEKE-PPPPC-Am (white) with EKEKEKE-PPPPC-Am. The molar percentage of the RGD peptide and scrambled RDG peptide tested was 0%, 50%, and 75%. Scale bars represent 100 μm. The same cell seeding procedure of peptide SAMs was followed for the control experiment as listed in the paper, with the exception that the cell plating concentration was 3.3 x 10^4 cells/mL in 3 mL Dulbecco's Modified Eagle Medium (DMEM) with 10% (v/v) fetal bovine serum (FBS) and 1% (v/v) penicillin-streptomycin (PS).

2.3.5 Low Fouling Surfaces Based on Biomimicry of Human Protein Surfaces

Proteins resist nonspecific adsorption allowing them to be stable in complex environments such as the cytoplasm of a cell, which contains thousands of protein types[80]. 1,162 human protein surfaces were analyzed to gain insight into their surface chemistry[40]. It was found that the amino acids glutamic acid (E) and lysine (K) are the most prevalent amino acids on protein surfaces, and even more so on protein surfaces found in the crowded cytoplasm[40]. In addition, it was determined that the large fractions of E and K on the surface are not correlated with a frequently occurring surface motif and are instead nearly randomly distributed. In addition, asparagine (N) was selected as the best neutrally charged low fouling candidate based on its high hydration and disfavored interactions with the protein core[40].

In order to confirm the low fouling properties of random EK and N, the surface anchoring linker platform –PPPPC was used to create peptide self-assembled monolayers on gold. We evaluated surfaces containing the random glutamic acid/lysine sequence Ac-$[EK]_7$-PPPPC-Am and the sequence Ac-CPPPP-NNNNNNN-Am for fouling to single protein solutions using SPR. The sequence Ac-GGGGGGG-PPPPC-Am was evaluated as a general hydrophilic peptide for comparison. In addition, bare gold chips were evaluated as a control surface. Both the random EK sequence and the N sequence showed ultra-low fouling having less than 5 ng/cm^2 adsorbed fibrinogen on the surface (Figure 2-10). The fouling to fibrinogen and lysozyme for the random EK sequence (Ac-$[EK]_7$-PPPPC-Am) is 4.4 ± 3.1 ng/cm^2 and 1.7 ± 1.5 ng/cm^2 and for the N sequence (Ac-CPPPP-NNNNNNN-Am) is 5.2 ± 1.0 ng/cm^2 and 2.7 ± 0.4 ng/cm^2, respectively. The hydrophilic glycine peptide surface displayed moderate levels of fouling with 16.8 ± 7.1 ng/cm^2 of adsorbed fibrinogen and 3.2 ± 1.0 ng/cm^2 of adsorbed lysozyme on the surface. Finally, the bare gold

control surface displayed high levels of fouling with 352.6 ± 10.9 ng/cm^2 of adsorbed fibrinogen and 175.1 ± 7.5 ng/cm^2 of adsorbed lysozyme.

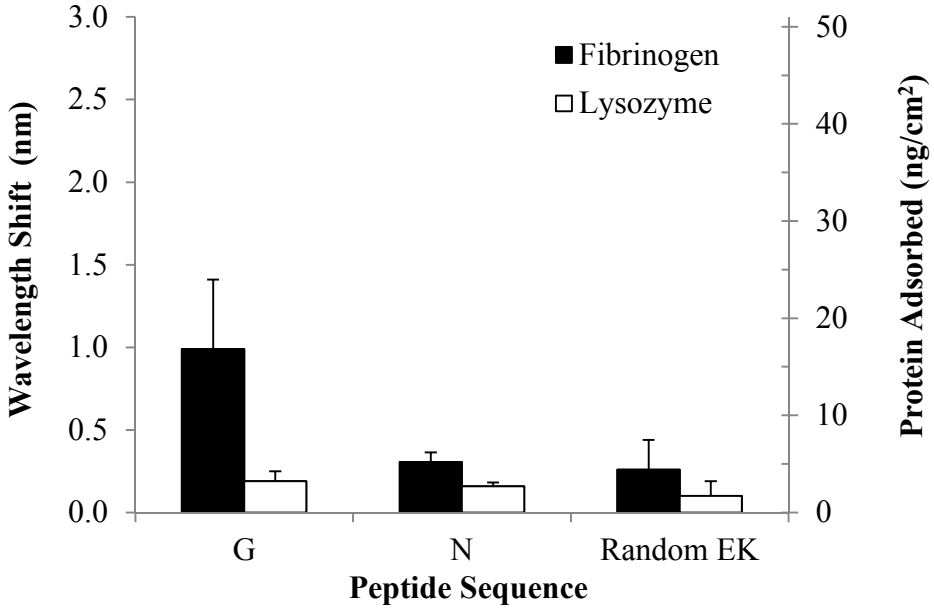

Figure 2-10. Protein adsorption on random EK and N surfaces.
Protein adsorption results as determined by SPR for Ac-GGGGGGG-PPPPC-Am (G), Ac-CPPPP-NNNNNNN-Am (N), and Ac-[EK]$_7$-PPPPC-Am (Random EK) to fibrinogen (black) and lysozyme (white).

2.4 Conclusions

Overall, simply using a cysteine residue for surface anchoring does not provide a peptide capable of self-assembly into an ultra-low fouling monolayer on gold surfaces. Selection of an appropriate peptide linker that will allow close-packing of chains is essential. Here, through rational design, we have identified a linker of four residues in length together with the amino acid cysteine and of a rigid, hydrophobic nature as one possible robust linker. This provides a well-defined secondary structure needed to promote closely packed monolayers with ultra-low fouling properties. The linker -PPPPC is an effective surface anchoring sequence for a wide range of applications beyond low fouling involving peptide assembly onto a gold surface. The tri-amino acid sequence RGD was added as an example for the inclusion of specific interactions on a low fouling

background, eliminating the need for chemical conjugation to synthetic materials such as PEG. This strategy is applicable to any other functional peptide beyond RGD. The concept of this all-in-one natural peptide can be easily adapted to introduce biomolecular recognition, ultra-low fouling and surface binding functions into all natural materials.

In addition, through biomimetic design, it was confirmed that EK is a robust choice for a low fouling material. The residues E and K are the most common amino acids on protein surfaces, and even more so on protein surfaces in crowded environments, such as the cytoplasm. Furthermore, structure and interaction results indicate that E and K rarely interact with other amino acids, are highly hydrated, and lack sequence patterns. SPR results of random EK peptide sequences show that EK does not need to be strictly alternating in order to display low fouling properties. In addition, it was shown that neutrally charged amino acids, such as asparagine (N), can also be used to form ultra-low fouling surfaces.

Chapter 3: Biologically Inspired Stealth Peptide-Capped Gold Nanoparticles

Introduction into the human body makes most nanoparticle systems susceptible to aggregation via nonspecific protein binding. Here, we developed a peptide-capped gold nanoparticle platform that withstands aggregation in undiluted human serum at 37˚C for 24 hours. This biocompatible and natural system is based on mimicking human proteins which are enriched in negatively charged glutamic acid and positively charged lysine residues on their surface. The multifunctional EKEKEKE-PPPPC-Am peptide sequence consists of a stealth glutamic acid/lysine portion combined with a surface anchoring linker containing four prolines and a cysteine. Particle stability was measured via optical spectroscopy and dynamic light scattering in single protein, high salt, and undiluted human serum solutions. *In vitro* cell experiments demonstrate EKEKEKE-PPPPC-Am capped gold nanoparticles effectively minimize nonspecific cell uptake by nonphagocytic bovine aortic endothelial cells and phagocytic murine macrophage RAW 264.7 cells. Cytotoxicity studies show that peptide-capped gold nanoparticles do not affect cell viability. Finally, the stealth peptide EKEKEKE-PPPPC-Am was extended with cyclic RGD to demonstrate specific cell targeting and stealth without using poly(ethylene glycol). Adding the functional peptide via peptide sequence extension avoids complex conjugation chemistries that are used for connection to synthetic materials. Inductively coupled plasma mass spectroscopy results indicate high aortic bovine endothelial cell uptake of c[RGDfE(SGG-KEKEKE-PPPPC-Am)] capped gold nanoparticles and low uptake of the control scrambled sequence c[RDGfE(SGG-KEKEKE-PPPPC-Am)] capped gold nanoparticles.

3.1 Introduction

Nanoparticle-based technology has many biomedical applications, including drug delivery, biosensing, diagnostics, and imaging[81–84]. These nanoparticle systems must be capped appropriately to render them biocompatible, functional, and stable against aggregation in biological systems. A current challenge is maintaining size and size distribution upon introduction into an *in vivo* environment. Ideally, the nanoparticle size should be larger than 10 nm to avoid renal clearance[85] and below 100 nm with a neutral or negative charge to avoid phagocytic uptake and hepatic filtration[86]. Most particles when introduced into the blood stream are susceptible to opsonization and are rapidly cleared from circulation by the reticuloendothelial system (RES) or the mononuclear phagocytic system (MPS)[87]. This process of nonspecific protein adsorption can drastically alter the physicochemical properties of nanoparticles and affect their circulation, biodistribution, cellular internalization, and trafficking *in vivo*[88]. In addition, opsonization can result in undesired cellular uptake, nanoparticle aggregation, or an immune system response.[89]

Current methods for creating "stealth" or "low fouling" nanoparticles that resist nonspecific protein adsorption include surface modification by poly(ethylene glycol) (PEG)[90], polysaccharides[91], mixed charge self-assembly[92], or zwitterionic polymers[93,94]. An attractive alternative for stealth coatings is to examine the use of natural materials such as peptides: they are biocompatible, well-characterized, nonimmunogenic, biodegradable, and multifunctional[33]. Peptide-coated gold nanoparticles have been reported to make stable systems in phosphate buffered saline (PBS)[95,96]. However, achieving stability in complex media such as undiluted human serum is even more challenging than in PBS due to the presence of thousands of proteins.

Peptide-coated gold nanoparticles have also been evaluated for *in vivo* applications[97,98]. The effect of interactions between peptide-capped gold nanoparticles and serum proteins were not fully

elucidated. It is essential to study particles in complex media solutions before performing *in vivo* experiments. Developing peptide-capped gold nanoparticles that are stable in complex environments, such as human serum, can broaden *in vivo* applications and provide additional low fouling materials.

In addition to possessing stealth properties, it is desirable to incorporate specific interactions for biomedical applications. Many peptide sequences possess specific molecular recognition for receptors on various cell types, including multiple cancer cells[99]. However, additional conjugation steps are required to add peptide targeting sequences onto stealth particles containing synthetic low fouling polymers such as PEG[100,101]. Peptide coatings offer an advantage because the targeting sequence can simply be extended off the existing peptide sequence[102,103] avoiding complex conjugation steps. Combining the stealth peptide sequence with a targeting moiety achieves specific interactions while maintaining a low fouling background leading to increased stability in complex media and improved functionality.

In this work, we have designed a low fouling peptide composed of alternating negatively charged glutamic acid (E) and positively charged lysine (K) amino acid residues. The EK sequence forms a strong hydration layer similar to zwitterionic materials providing resistance to nonspecific protein adsorption[13]. Furthermore, the EK sequence mimics the surfaces of human proteins which have adapted to avoid nonspecific adsorption and display stability in complex media (Figure 3-1a).

a)

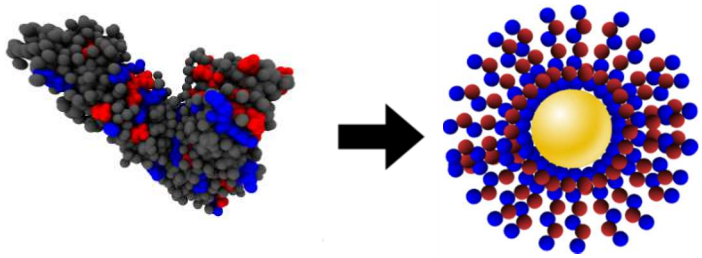

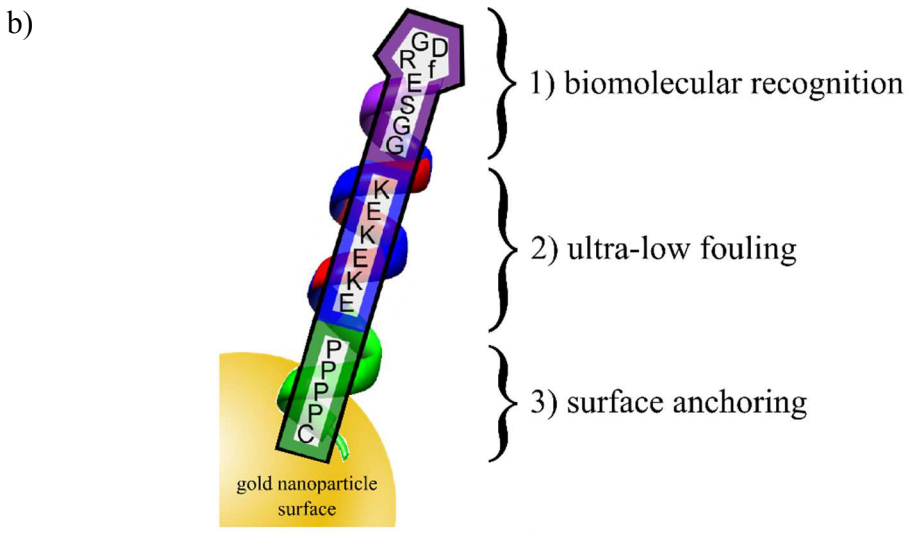

Figure 3-1. Design of stealth peptide sequence.
(a) Schematic depicting the design of the stealth peptide sequence inspired by the analysis of human protein surfaces, which contain E and K as the most prevalent amino acids on the surface (indicated by red and blue spheres). Structure of survivin-borealin-INCENP core complex (left). (b) All-in-one natural peptide sequence with three distinct functions: (1) biomolecular recognition via cyclic RGDfE (purple); (2) ultra-low fouling via KEKEKE (red and blue); and (3) surface anchoring via PPPPC (green).

We have previously shown from the analysis of 1,162 human proteins that E and K are the two most prevalent amino acids on the surfaces of proteins[40]. The percentage of charged residues present on the surfaces of proteins increases as the environment becomes more complex: 44% for proteins found in the crowded cytoplasm, 56% for proteins that have close contact with other proteins such as the interior of molecular chaperone proteins, and 70% for the interior of molecular chaperone proteins found in thermophilic bacteria[40,41]. On the basis of protein surfaces, the low fouling segment of our peptide contains four negatively charged glutamic acid residues and three positively charged lysine residues. Overall charge neutrality is maintained by leaving the N-terminus as a free amine, which contributes an extra positive charge to the peptide. The C-termini of all peptides were amidated to cap the negative charge of the carboxylic acid. The EK stealth peptide sequence was attached to gold nanoparticles via the inclusion of a surface anchoring linker containing four prolines and a cysteine (-PPPPC). Cysteine contains a thiol group allowing for covalent bonding to the gold

surface. The rigid, hydrophobic proline linker forms a well-ordered structure with a high surface density creating a robust self-assembled monolayer on the surface[104]. Optical spectroscopy (UV-vis) and dynamic light scattering (DLS) results indicate EKEKEKE-PPPPC-Am capped gold nanoparticles (EK-GNPs) resist aggregation in high salt conditions, protein solutions, and undiluted human blood serum.

Additionally, the EK-GNP platform can include specific function by extending the peptide sequence, without the need for chemical conjugation. To demonstrate this versatility, a specific cell targeting sequence (cyclic RGD) was added to the low fouling EK peptide. A short linker (SGG) was included between the targeting moiety and the remainder of the peptide to improve receptor-ligand interactions. Particles containing specific targeting moieties (cRGD-EK-GNPs) are uptaken by cells possessing the appropriate receptor. Conversely, particles lacking the specific targeting moiety (EK-GNPs) or particles containing a scrambled sequence (cRDG-EK-GNPs) are not uptaken by cells and maintain stealth properties. The peptide sequence c[RGDfE(SGG-KEKEKE-PPPPC-Am)] used in this work is illustrated in Figure 3-1b. This multifunctional peptide contains biomolecular recognition, ultra-low fouling, and surface anchoring properties in one sequence. Moreover, this system is easily constructed in one step by mixing gold nanoparticles and self-assembling peptides.

3.2 Experimental Methods

3.2.1 Materials

N-Fluorenylmethoxycarbonyl (Fmoc)-protected amino acids with the amine and side chain protected (Fmoc-Arg(Pbf)-OH, Fmoc-Asp(OtBu)-OH, Fmoc-Cys(Trt)-OH , Fmoc-Glu(OAll)-OH, Fmoc-Glu(OtBu)-OH, Fmoc-Gly-OH, Fmoc-Lys(Boc)-OH, Fmoc-D-Phe-OH, Fmoc-Pro-OH, Fmoc-Ser(tBu)-OH), Rink amide AM resin, O-Benzotriazole-N,N,N',N'-tetramethyl-uronium-

hexafluoro-phosphate (HBTU), N-hydroxybenzotriazole (HOBt), and N,N-dimethylformamide (DMF) were bought from AAPPTec (Louisville, KY). N,N-diisopropylethylamine (DIPEA) and N-methylmorpholine (NMM) was bought from TCI America (Portland, OR). Citric acid trisodium salt dehydrate was bought from Fisher Scientific (Waltham, MA). Sodium chloride was purchased from Avantor (Center Valley, PA). Trifluoroacetic acid (TFA), sodium hydroxide (NaOH), and Omni Trace nitric acid (HNO_3) was bought from EMD (Darrnstadt, Germany). Piperidine, dichloromethane (DCM), triisopropylsilane (TIS), 1,2-ethanedithiol (EDT), gold (III) chloride trihydrate ($HAuCl_4$), tetrakis(triphenyl-phosphine) palladium (0) ($Pd(PPh_3)_4$), sodium diethyldithiocarbamate trihydrate (NaDEDTC), acetonitrile (AcOH), chloroform (CH_3Cl_3), phosphate buffered saline (PBS), fibrinogen from bovine plasma, and lysozyme from chicken egg white were purchased from Sigma Aldrich (St. Louis, MO). Pooled human blood serum was purchased from BioChemed Services (Winchester, VA). Bovine aortic endothelial cells (BAEC) and mouse macrophage RAW 264.7 cells were purchased from ATCC (Manassas, VA). Dulbecco's Modified Eagle Medium (DMEM), fetal bovine serum (FBS), and penicillin-streptomycin (PS) were purchased from Invitrogen (Carlsbad, CA). Water used in experiments was purified using a Millipore water purification system (Darmstadt, Germany) with a minimum resistivity of 18.0 MΩ•cm.

3.2.2 Peptide Synthesis

All peptides were synthesized by solid-phase techniques using the AAPPTec Titan 357 automated synthesizer (Louisville, KY). Polystyrene Rink amide AM resin with a 0.58 mmol/g loading capacity was used. Coupling was performed using amino acid monomer, HBTU, HOBt, and DIPEA prepared in DMF in a molar ratio of 1.1:1:1:2 in four times excess of the loading capacity of the resin. Deprotection of Fmoc groups was achieved using 20% piperidine in DMF. Cyclization of

peptides containing the RGD moiety was achieved by selective deprotection of the allyl group[105]. Briefly, removal of the allyl group was performed using 3 equivalents of $Pd(PPh_3)_4$ in a mixture solvent of CH_3Cl_3/AcOH/NMM (37:2:1) under nitrogen for two hours. Following deprotection, the resin was rinsed three times with 0.5% DIPEA in DMF (v/v), 0.5% NaDEDTC in DMF (w/w), and 0.5% HoBt in DMF (w/w), successively. Next the Fmoc group was removed with 20% piperidine. Finally, the resulting linear peptide was cyclized using HBTU, HOBt, and DIPEA in a DMF solution using 1.5, 2, and 4 equivalents of the loading capacity of the resin, respectively. The final cleavage of peptides from the resin was performed by a TFA (77.5%), DCM (15%), water (2.5%), TIS (2.5%), and EDT (2.5%) (v/v/v/v/v) cleavage cocktail. Peptide purity was evaluated by preparative reverse phase high performance liquid chromatography (RP-HPLC) and purified as needed. The purity of all peptide sequences is higher than 95%. Peptides were analyzed by matrix-assisted laser desorption/ionization time-of-flight mass spectrometry (MALDI-TOF-MS) to confirm accurate molecular weights of products.

3.2.3 Citrate-Capped Gold Nanoparticle Synthesis

Gold nanoparticles (13 nm) were prepared by reduction of $HAuCl_4$ with citric acid. A vigorously stirred aqueous solution of $HAuCl_4$ (250 mL, 1 mM) was refluxed at which point a solution of sodium citrate was quickly added (25 mL, 38.8 mM). Reflux was continued for 20 minutes. The solution was then removed from heat and stirred for another 20 min. The solution was filtered through a 0.2 μm filter to remove any precipitates.

3.2.4 EK-Capped Gold Nanoparticle Assembly

Citrate-capped gold nanoparticles were adjusted to a pH of 7 using a 0.1 M NaOH solution. EK-capped gold nanoparticles were prepared by mixing citrate-capped gold nanoparticles (pH 7)

with a 0.69 mM peptide solution in PBS in a volume ratio of 10 to 1. In the case of cRGD-EK-GNPs or cRDG-EK-GNPs peptide solutions were composed of 5% (mol) c[RGDfE(SGG-KEKEKE-PPPPC-Am)] or c[RDGfE(SGG-KEKEKE-PPPPC-Am)] and 95% (mol) EKEKEKE-PPPPC-Am peptide. Self-assembly was performed for 24 hours. An Econo-Pac 10DG desalting column from Bio-Rad Laboratories (Hercules, CA) was used to remove free peptide from solution and to perform a buffer exchange into PBS.

3.2.5 Characterization of Gold Nanoparticles

UV-vis absorption spectra were recorded at room temperature with a Smart Spec 3000 spectrophotometer (Bio-Rad Laboratories, Hercules, CA) or a Cytation 3 multi-mode plate reader (BioTek, Winooski, VT) from 300 to 800 nm. The core gold size and morphology of particles was determined by transmission electron microscopy (TEM) using a Tecnai G2 F20 (FEI, Hillsboro, OR). Samples were prepared by evaporating 5 μL of GNP solution onto carbon-supported copper grids. For the determination of particle size, over 200 particles were counted from multiple pictures from different areas of the TEM grid using ImageJ software. The hydrodynamic size and zeta potential of the particles was analyzed by dynamic light scattering (DLS) using the Zetasizer Nano-ZS (Malvern, Worcestershire, United Kingdom). Measurements were carried out at 25 ˚C in aqueous media. The zeta potential was calculated from the electrophoretic mobility based on the Smoluchowski theory. For zeta potential measurements, Cit-GNPs were analyzed in QW and EK-GNPs were analyzed in a 10% (vol) PBS.

3.2.6 Stability Experiments

To evaluate the stability of peptide-capped gold nanoparticles, samples were centrifuged to remove dispersion solution and resuspended in either Millipore water (QW), PBS, 1 mg/mL

fibrinogen, 1 mg/mL lysozyme, 20% (wt) NaCl, or undiluted human serum. Stability tests in salt and single protein solutions were conducted for 1 hour. UV-vis measurements were performed using the corresponding testing solution as a blank. Samples were then centrifuged at 12k rpm and rinsed with PBS twice before being measured by DLS. For serum stability tests particles were centrifuged at 12k for EK-GNPs and 8k for citrate-capped GNPs and then resuspended in undiluted human serum and placed in an incubator at 37°C. Samples were removed at various time points over a period of 24 hours. Each aliquot was centrifuged (EK-GNPs at 12k and Cit-GNPs at 8k) and redispersed in PBS (EK-GNPs) or QW (Cit-GNPs) twice. Aliquots were measured by DLS. Control samples in PBS (EK-GNPs) and QW (Cit-GNPs) were evaluated concurrently with all samples during stability experiments.

3.2.7 Cytotoxicity Assay

Cell viability of BAEC and RAW 264.7 cells was tested by an Alamar Blue cytotoxicity assay (Invitrogen, Carlsbad, CA). Cells were seeded in a 96-well culture plate in 100 µL of DMEM supplemented with 10% (v/v) FBS and 1% (v/v) PS. Cells were incubated at 37°C in 5% CO_2 and 100% relative humidity, until they reached 80-90% confluence. On the day of the test, cells were incubated with 100 µL of fresh medium containing various concentrations of peptide-capped GNPs. After 24 hours, cells were rinsed with PBS three times and incubated with 100 µL of phenol free DMEM supplemented with 10% FBS and 1% PS and 10 µL of Alamar Blue for another four hours. Fluorescence measurements were performed on a Victor^3 V plate reader (PerkinElmer, Waltham, MA) at an excitation wavelength of 544 nm, and the emission spectra was collected at 595 nm. Percent viability was calculated by dividing the fluorescence emission of cells exposed to GNPs by the fluorescence emission of cells in media. Three independent measurements were performed for each sample.

3.2.8 Cell Uptake Experiments

BAEC and RAW 264.7 cells were seeded in 6 well plates in 2 mL of DMEM supplemented with 10% FBS (v/v) and 1% PS (v/v) and incubated at 37°C in 5% CO_2 and 100% relative humidity until they reached 80-90% confluence. On the day of the test, cells were washed with fresh medium and then incubated with 2 mL of nanoparticle solutions at various concentrations. Cells were incubated for four hours and then rinsed with PBS three times. Cells were lysed with 200 μL of 50 mM NaOH. The lysed cell solution was digested in 50% HNO_3 for 24 hours. Samples were then diluted to 2% HNO_3 and analyzed for gold concentration by ICP-MS using the ELAN-DRCe (PerkinElmer, Waltham, MA).

3.3 Results and Discussion

3.3.1 Peptide Synthesis Characterization

All synthesized peptides were characterized by reverse phase high performance liquid chromatography (RP-HPLC) for known sequences and purified as needed (Figure 3-2). The purity of all synthesized sequences was greater than 95%. Peptides were also analyzed by matrix-assisted laser desorption/ionization time-of-flight mass spectrometry (MALDI-TOF-MS) to confirm accurate molecular weight values.

a) EKEKEKE-PPPPC-Am

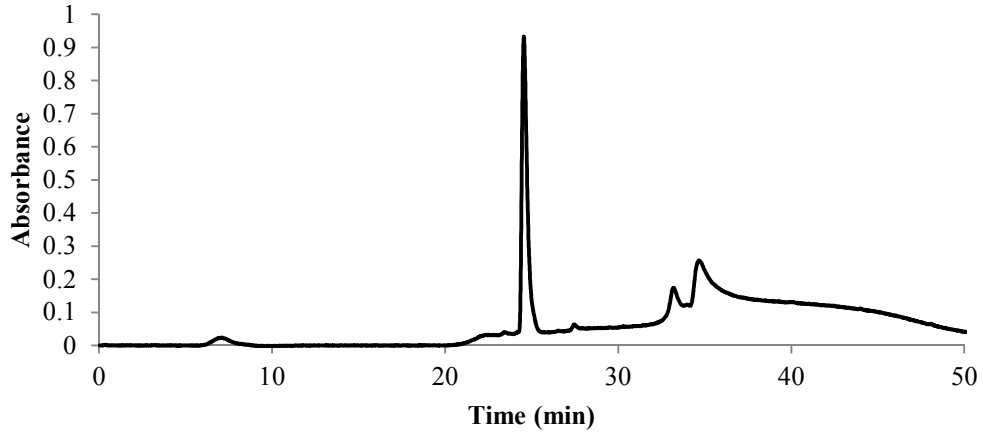

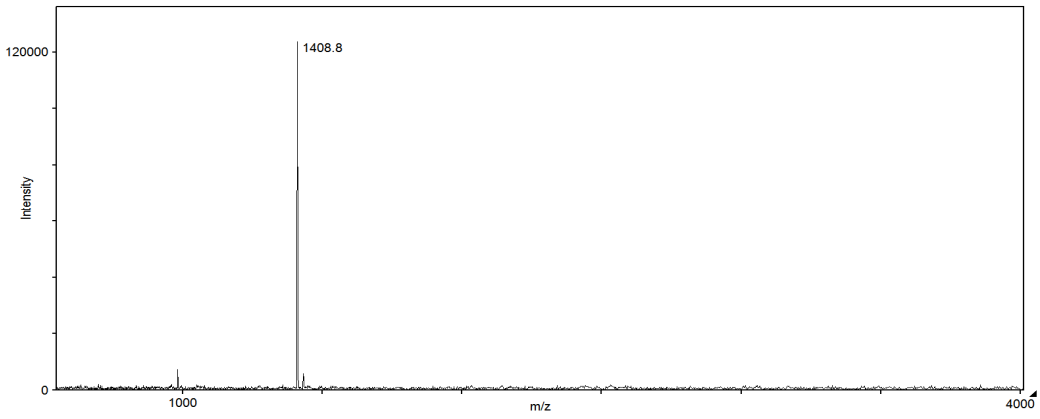

b) c[RGDfE(SGG-KEKEKE-PPPPC-Am)]

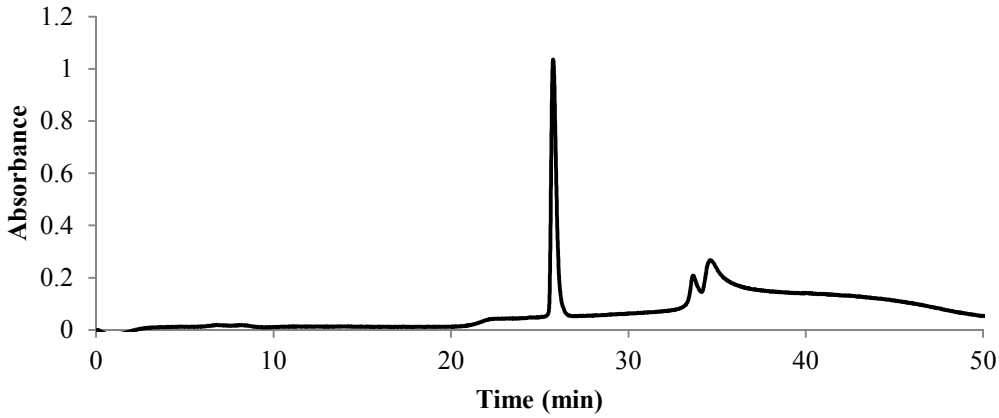

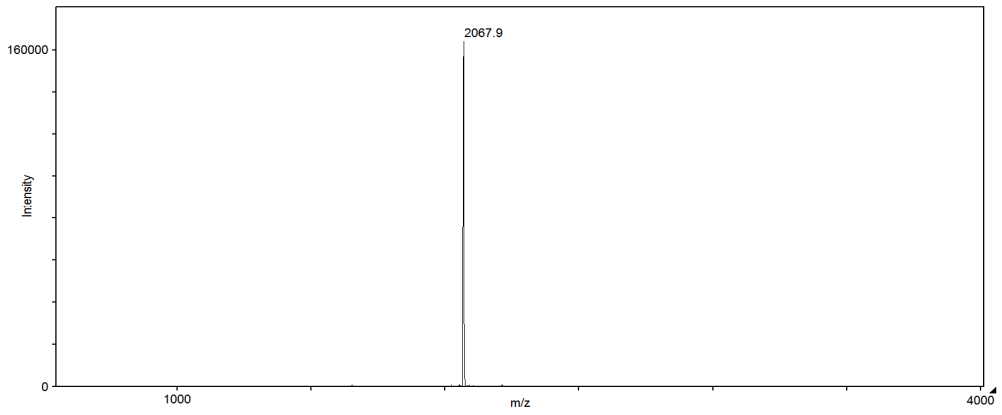

c) c[RDGfE(SGG-KEKEKE-PPPPC-Am)]

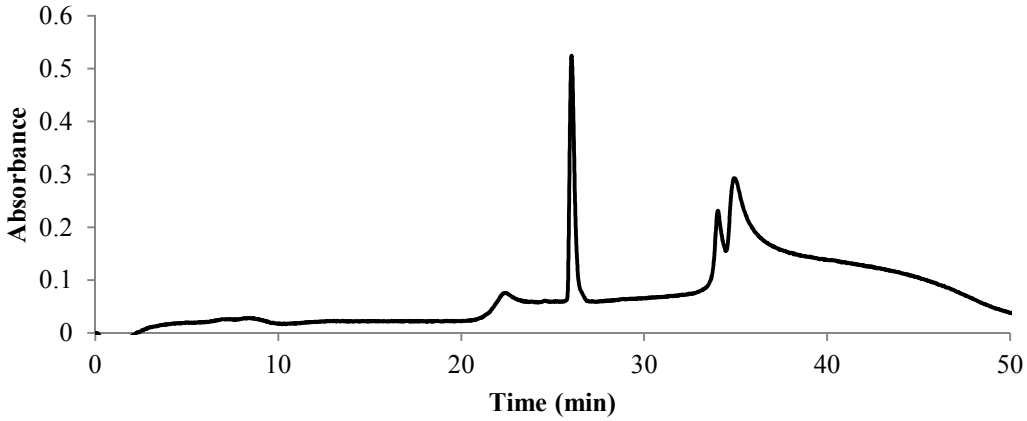

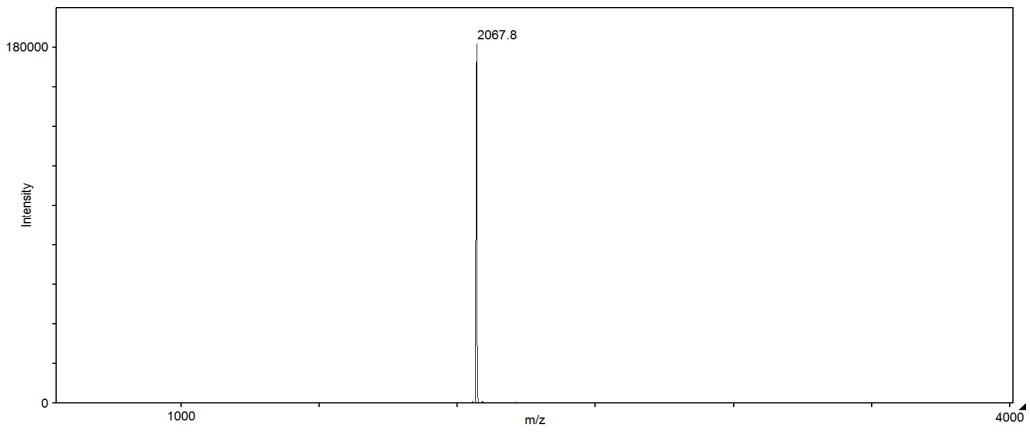

Figure 3-2. RP-HPLC and MALDI peptide synthesis characterization.
RP-HPLC (top) and MALDI (bottom) data for synthesized peptide sequences. (a) EKEKEKE-PPPPC-Am (b) c[RGDfE(SGG-KEKEKE-PPPPC-Am)] (c) c[RDGfE(SGG-KEKEKE-PPPPC-Am)].

3.3.2 EK-GNP Synthesis and Characterization

Citrate-capped gold nanoparticles (Cit-GNPs) were synthesized following the Turkevich method[106,107] by adding sodium citrate to a refluxed solution of chloroauric acid ($HAuCl_4$). Peptide-capped GNPs were formed by self-assembling peptides on the surface of gold nanoparticles over 24 hours. Capped EK-GNPs were purified from free peptide and transferred to phosphate buffered saline (PBS) by passing through a desalting column. Cit-GNPs were left in water since adding PBS will immediately cause particle aggregation due to screening of the electrostatic repulsion between particles by salt[108].

The Cit-GNPs and EK-GNPs were characterized by transmission electron microscopy (TEM), optical spectroscopy (UV-vis), and dynamic light scattering (DLS) as seen in Figure 3-3. TEM image analysis indicates that the core gold nanoparticle diameter of the Cit-GNPs and the EK-GNPs is 12.9 ± 1.0 nm. Peptide capping does not affect the gold core size if particles do not aggregate during assembly. On the basis of the TEM images and the constant gold core diameter, it is evident that EK-GNPs remain monodisperse after capping. From UV-vis, Cit-GNPs show a plasmon band at 519 nm. The particle diameter can be calculated from the concentration of gold nanoparticles and the absorbance at the surface plasmon resonance and is in agreement with a diameter of 13 nm[109]. For EK-GNPs, the plasmon band absorbance shifts to 527 nm. The hydrodynamic diameter (volume percentage) of Cit-GNPs and EK-GNPs was measured by DLS to be 13.9 ± 0.1 nm and 16.0 ± 0.2 nm, respectively. Zeta potential measurements indicate that the charge of the Cit-GNPs is -45.2 ± 1.8 mV in water and the charge of EK-GNPs is -16.4 ± 0.3 mV in 10% (vol) PBS. The differences observed between Cit-GNPs and EK-GNPs in UV-vis, DLS, and zeta potential measurements show evidence that the EK peptide is effectively capping the GNPs. The shift to a higher plasmon band and the hydrodynamic diameter size increase by 2 nm after

addition of peptide is consistent with the formation of a peptide layer on the surface[95]. In addition, the reduction of charge from -45.2 mV to -16.4 mV indicates displacement of negatively charged citric acid by the EK peptide. The slightly negative charge remaining on the EK-GNPs is most likely due to a small amount of residual citrate molecules remaining on the surface after ligand exchange.

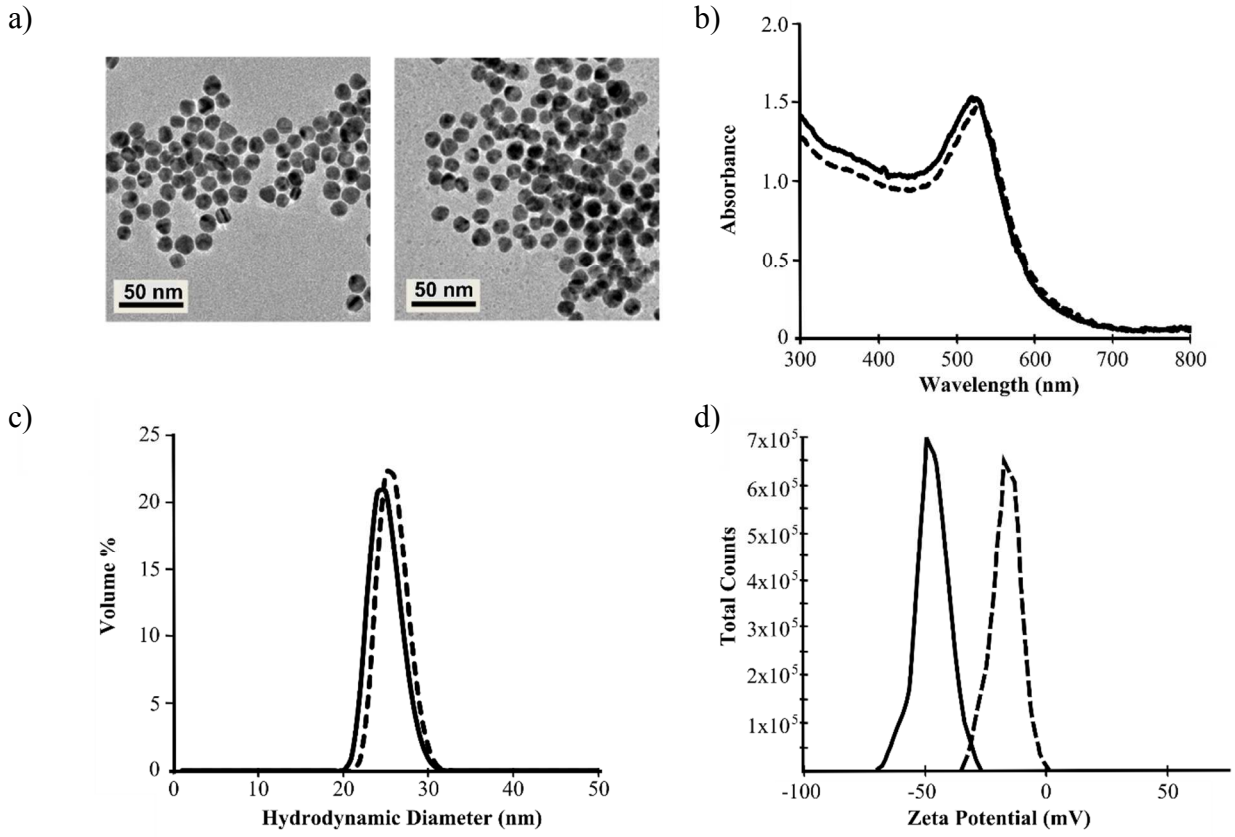

Figure 3-3. Characterization of EK-GNPs and Cit-GNPs.
(a) TEM images of Cit-GNPs in QW (left) and EK-GNPs in PBS (right). (b) UV-vis spectra of Cit-GNPs in QW (solid line) and EK-GNPs in PBS (dashed line). (c) Hydrodynamic diameter (volume %) (nm) measured by DLS of Cit-GNPs in QW (solid line) and EK-GNPs in PBS (dashed line). (d) Zeta potential distribution (mV) of Cit-GNPs in QW (solid line) and EK-GNPs in 10% (vol) PBS (dashed line).

3.3.3 Stability of EK-GNPs in Protein, High Salt, and Undiluted Human Serum

Stability in PBS is the first criteria for developing a robust, biocompatible system. However, if particles are to be utilized in more complex environments, such as *in vivo*, then harsher conditions need to be evaluated. Particle stability was assessed by monitoring the hydrodynamic diameter of

particles using UV-vis and DLS. First, particles were evaluated in 1 mg/mL fibrinogen and lysozyme protein solutions. Fibrinogen is a negatively charged protein and lysozyme is a positively charged protein. It is important to test proteins of both charges to ensure that the EK-GNPs are not stable due to electrostatic repulsion from similarly charged proteins. Fibrinogen surface adsorption is challenging to resist since it is rather sticky. Resisting fibrinogen adsorption is relevant because it plays a key role in platelet adhesion and clotting in the body[1]. As seen in Figure 3-4a, EK-GNPs maintain the same hydrodynamic diameter after exposure to 1 mg/mL fibrinogen and lysozyme solutions.

Next, we examined EK-GNP stability under high salt conditions. Most particles aggregate as salt is added due to the screening of any electrostatic repulsion; however, zwitterionic and mixed charge materials can resist aggregation due to the presence of a strongly bound surface hydration layer[93,94,110]. In addition to examining particle stability in PBS solutions, the stability of EK-GNPs was also measured in higher salt concentrations. EK-GNPs maintain stability in concentrations of even 20% (wt) salt. This result verifies the formation of a peptide coated layer on the surface. UV-vis spectra for single protein solution and high salt stability tests support DLS data with no shift observed in the plasmon band for all samples (Figure 3-4b).

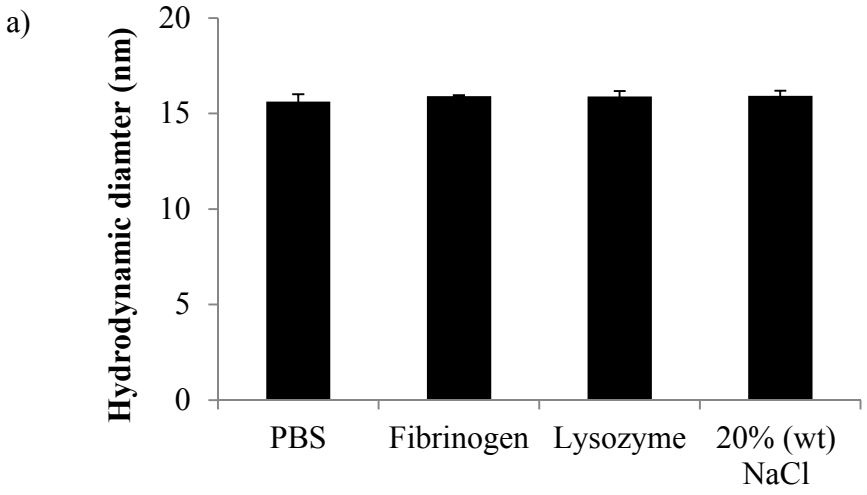

b)

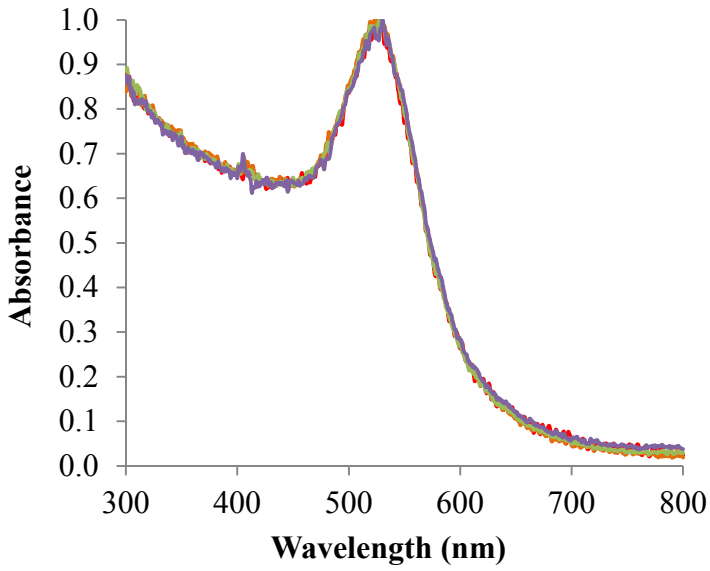

Figure 3-4. Stability in single protein solutions and high salt concentration.
(a) DLS measurements of the hydrodynamic diameter (volume percentage) (nm) of EK-GNPs after exposure to PBS, 1 mg/mL fibrinogen in PBS, 1 mg/mL lysozyme in PBS, and 20% (wt) NaCl solution for one hour. Each data point represents an average value ± standard deviation from at least three independent measurements. (b) UV-vis spectra for stability tests performed in PBS (red line), 1 mg/mL fibrinogen (orange line), 1 mg/mL lysozyme (green line), and 20% (wt) NaCl (purple line). Spectra were all normalized to have a maximum absorbance at 1 for comparison. Blanks for each sample were composed of the stability solution being evaluated, i.e. PBS, 1 mg/mL fibrinogen, etc.

EK-GNPs were also exposed to undiluted human serum at 37°C for 24 hours to determine stability under physiologically relevant conditions. Human serum contains thousands of proteins and is an extremely challenging environment for particles to retain stability[89]. Most particle stability tests are performed in aqueous buffers which are not representative of the *in vivo* environment. Even studies that examine stability in culture medium often do not contain more than 10% serum in solutions. In this stability test, samples were removed at several time points and measured by DLS to determine their hydrodynamic size. Since undiluted serum contains many proteins that interfere with the signal of the gold nanoparticles during DLS analysis, the samples were centrifuged to separate EK-GNPs from serum proteins. Final measurements were conducted in PBS after a series of two rinses. In addition to collecting DLS data, UV-vis spectra were collected for samples while still in

undiluted human serum to ensure that particles were not aggregating during centrifugation (Figure 3-5).

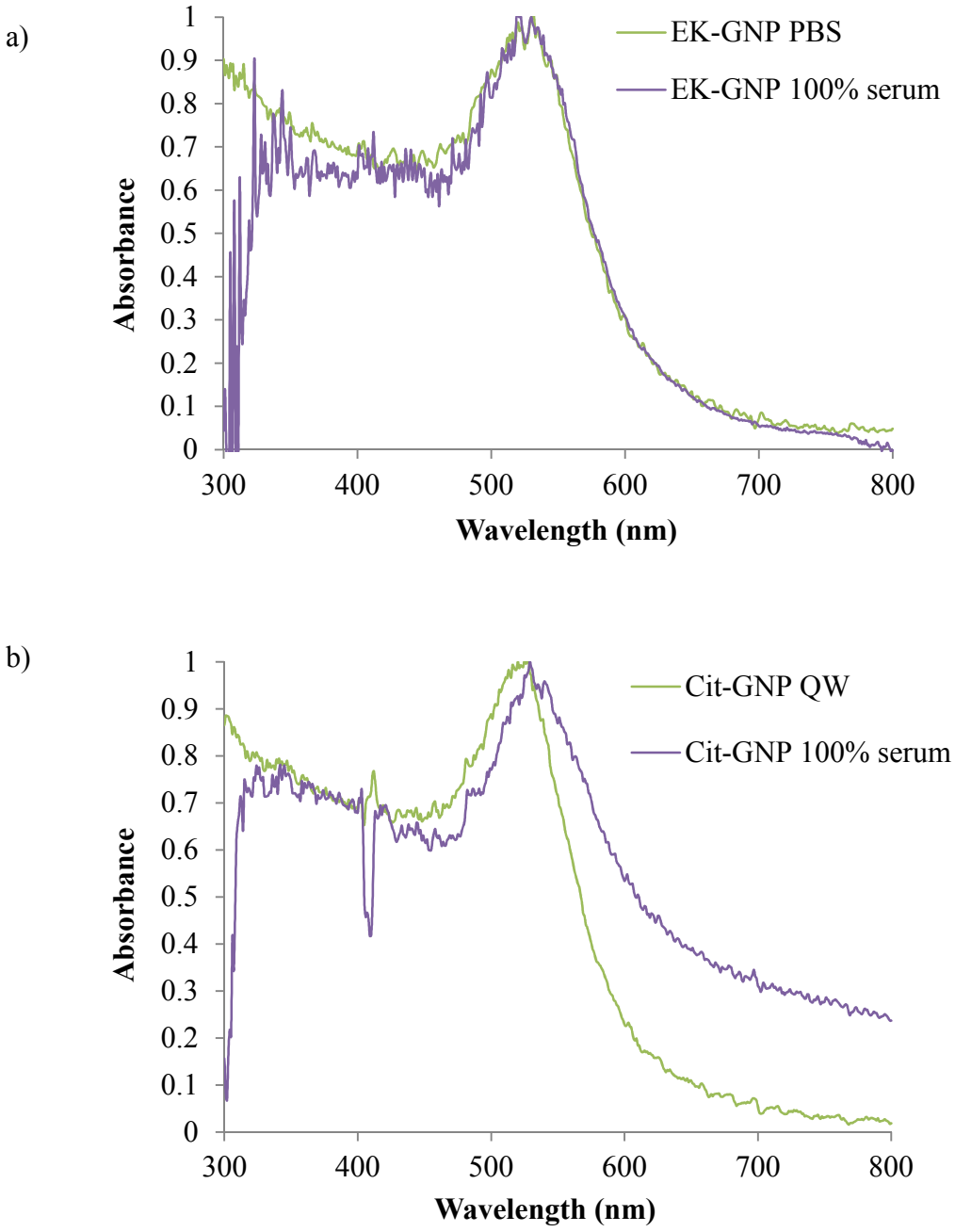

Figure 3-5. UV-vis spectra for particles in undiluted human serum.
(a) UV-vis spectra for EK-GNPs in PBS (green line) and undiluted human serum (purple line) after 24 hours. (b) UV-vis spectra for Cit-GNPs in QW (green line) and undiluted human serum (purple line) after 24 hours. Serum samples were run with a serum blank. Samples with serum contain some noise due to interference from proteins in the serum solution.

EK-GNPs exposed to undiluted human serum maintained a constant size of 18.8 ± 0.3 nm throughout 24 hours (Figure 3-6a). However, Cit-GNPs aggregated almost immediately to a constant size of 98.2 ± 4.3 nm. The Cit-GNPs did not precipitate out of solution and retained a constant size most likely due to the adsorption of serum proteins. The size increase of Cit-GNPs was evident from the immediate color change to dark purple upon addition of undiluted human serum indicating an increase in the surface plasmon band. EK-GNPs in undiluted human serum maintained a deep red color similar to their color in PBS (Figure 3-6b). As a control, EK-GNPs in PBS at 37 °C were tested and maintained a diameter size of 18.6 ± 0.8 nm, the same size as EK-GNPs exposed to undiluted human serum. The Z-average value was used to track the hydrodynamic diameter for serum stability tests due to the larger polydispersity of Cit-GNPs once exposed to serum.

a)

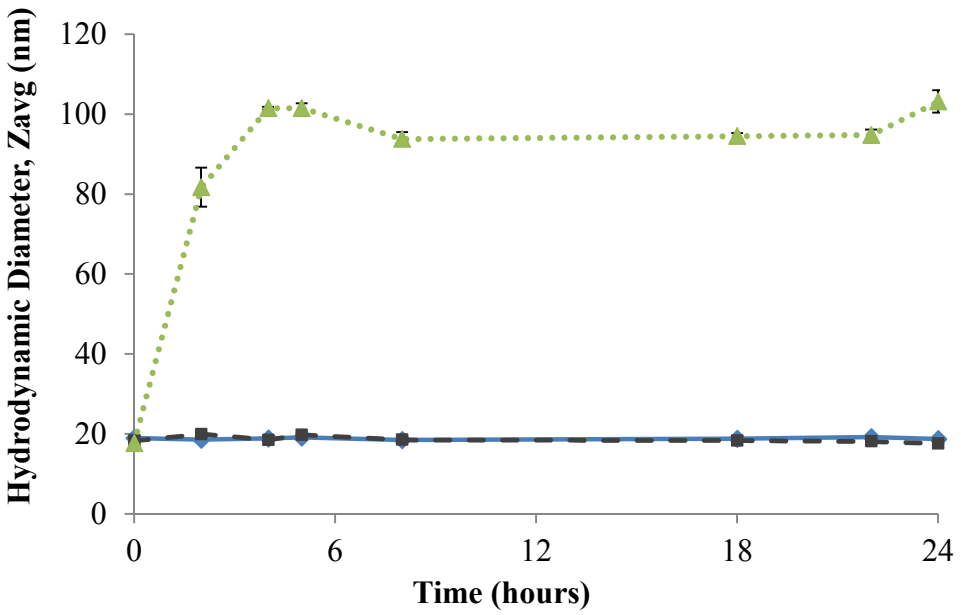

b)

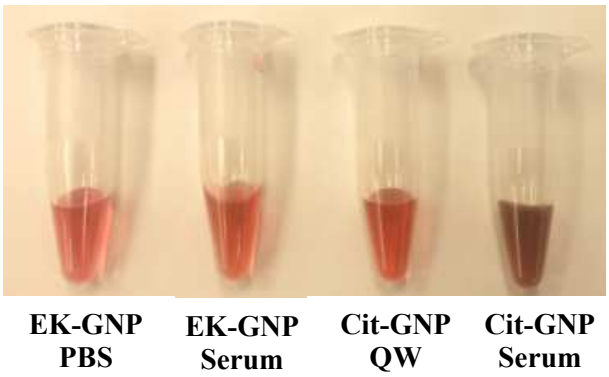

Figure 3-6. Stability of EK-GNPs and Cit-GNPs in undiluted human serum.
(a) DLS measurement of the Z_{avg} hydrodynamic diameter (intensity percentage) (nm) of EK-GNPs in human serum (blue solid line, diamonds), EK-GNPs in PBS (gray dashed line, squares), and Cit-GNPs in human serum (green dotted line, triangles) over 24 hours. All samples were kept at 37° C. Each data point represents an average value ± standard deviation from at least three independent measurements. (b) Picture showing the difference in color between EK-GNPs in PBS, EK-GNPs in undiluted human serum, Cit-GNPs in QW, and Cit-GNPs in undiluted human serum (left to right).

3.3.4 Stability in Culture Medium and Cytotoxicity of EK-GNPs

Ensuring stability in cell culture medium is an important factor when performing *in vitro* experiments. The stability of EK-GNPs in 10% fetal bovine serum (FBS) supplemented cell culture medium (DMEM) was monitored by UV-vis spectroscopy (Figure 3-7). UV-vis is sensitive to aggregation as shown by spectrum shape and plasmon peak shifts[108]. The plasmon peak and spectrum shape did not change for EK-GNPs in cell culture medium over a period of 48 hours, compared to EK-GNPs in PBS. Cit-GNPs aggregated almost immediately in cell culture medium as evidenced by a shift to a higher plasmon peak and broadening of the spectrum shape. Cit-GNPs most likely aggregate due to the coating by proteins found in FBS and the higher salt content of cell culture medium.

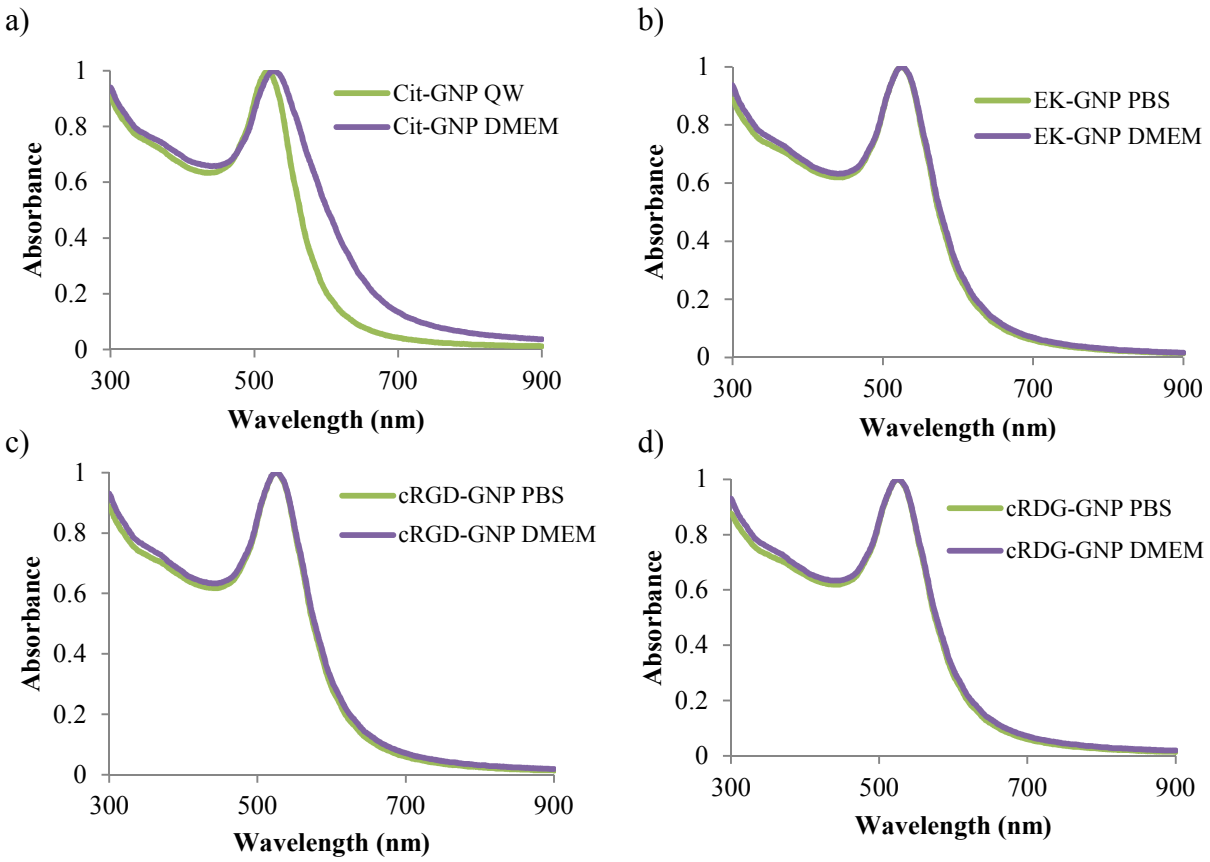

Figure 3-7. UV-vis spectra for GNPs in cell culture medium.
UV-vis spectra for (a) Cit-GNPs, (b) EK-GNPs, (c) cRGD-EK-GNPs, and (d) cRDG-EK-GNPs in QW/PBS (green line) and cell culture medium DMEM supplemented with 10% FBS and 1% PS (purple line) after 48 hours.

The cytotoxicity of EK-GNPs to bovine aortic endothelial cells (BAEC) and mouse macrophage (RAW 264.7) cells was evaluated by an Alamar Blue assay after 24 hour incubation in various EK-GNP concentrations (Figure 3-8a). Alamar Blue incorporates an oxidation-reduction indicator that both fluoresces and changes color in response to chemical reduction of growth medium resulting from cell growth. Percent viability was calculated by dividing the fluorescence signal from cells exposed to GNPs by the fluorescence signal from control cells exposed only to growth medium. There was no obvious cytotoxicity in all test concentrations for the EK-GNPs. Since EK-GNPs possess stealth properties and do not aggregate in cell culture medium it is likely that they do not

interact with the cells and thus do not affect cell viability. Particles containing cyclic RGD (Figure 3-8b) and cyclic RDG (Figure 3-8c) targeting moieties were also not cytotoxic to cells.

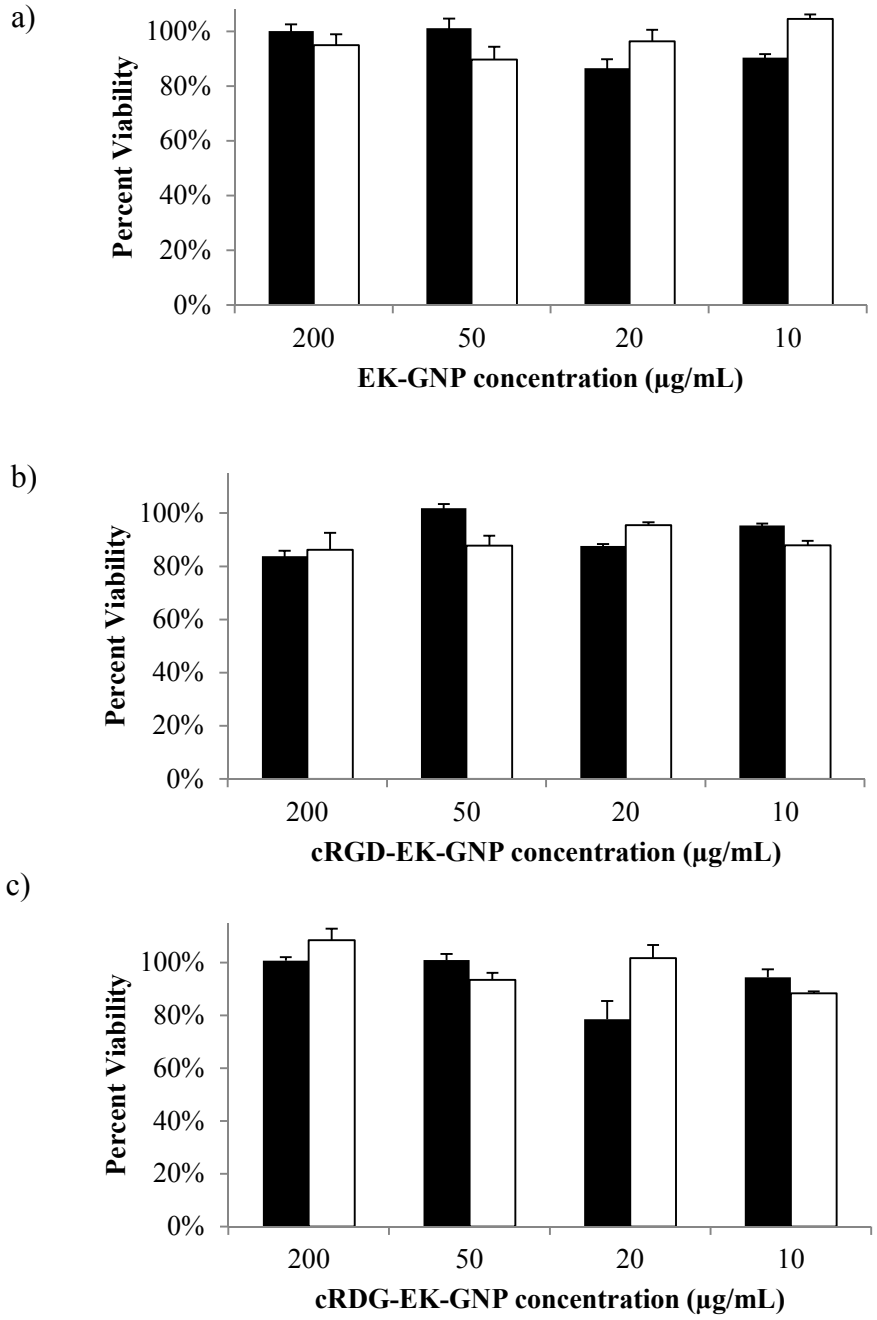

Figure 3-8. *In vitro* cytotoxicity assay.
Alamar Blue cytotoxicity assay of BAEC (black) and RAW 264.7 (white) cells exposed to varying concentrations of (a) EK-GNPs (b) cRGD-EK-GNPs and (c) cRDG-EK-GNPs for 24 hours. Each data point represents an average value ± standard deviation from three measurements.

3.3.5 Resistance to Cell-Uptake

In order for particles to have long circulation times in the body, they need to resist cellular uptake. Of particular importance is resisting uptake by macrophage cells, which are abundant in the liver and spleen and are well-known for removing particles from blood circulation, as most particles end up in these locations[88,111]. For uptake experiments, phagocytic RAW 264.7 and nonphagocytic BAEC cells were seeded in 6 well plates and allowed to grow to 90% confluence. EK-GNPs and Cit-GNPs were added to wells in concentrations of 10 μg/mL and 20 μg/mL. After four hours of incubation, the wells were rinsed three times with PBS and cells were lysed with 50 mM sodium hydroxide. Samples were analyzed for gold content after concentrated acid digestion via inductively coupled plasma mass spectrometry (ICP-MS). Cells that were not exposed to gold nanoparticles were analyzed as a negative blank control. EK-GNPs were not selectively uptaken by either RAW 264.7 or BAEC cells (Figure 3-9). However, the Cit-GNPs were uptaken by both cell types. The phagocytic macrophage cells had slightly higher uptake numbers for EK-GNPs at 20 μg/mL most likely due to their high rate of environment sampling compared to other cell lines[111]. As expected, the cells exposed to a higher concentration of Cit-GNPs had double the amount of gold uptaken. Higher uptake of Cit-GNPs is most likely due to coating by serum proteins and an increase in size[89]. The amount of citrate capped nanoparticles ingested by RAW 264.7 and BAEC cells are similar to other values reported in the literature[88,112].

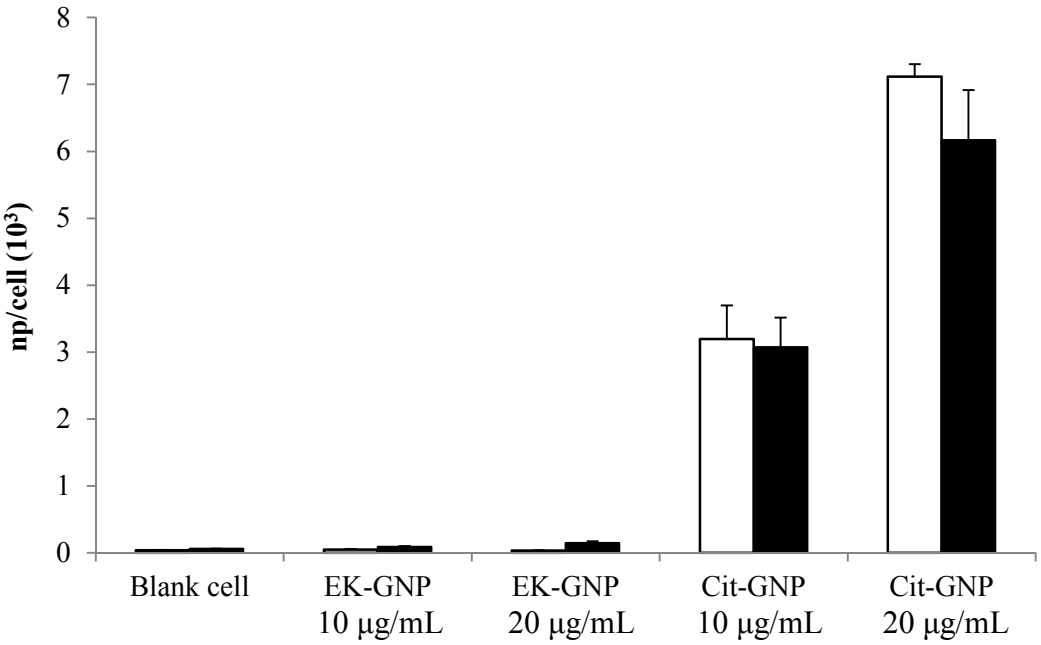

Figure 3-9. Cell uptake of GNPs in BAEC and RAW 264.7.
Cell uptake of EK-GNPs and Cit-GNPs (number of gold nanoparticles per cell 10^3) in BAEC (white) and RAW 264.7 (black) cells measured by ICP-MS. Each data point represents an average value ± standard deviation from at least three independent measurements.

3.3.6 Specific Cell-Uptake by Functionalized cRGD-EK-GNPs

In addition to being able to resist nonspecific uptake by cells, it is desirable to target specific cells for uptake. Several cell types contain integrins on their cell surface which can specifically recognize the RGD sequence, including BAEC[113]. To demonstrate specific cell uptake, we extended the peptide sequence EKEKEKE-PPPPC-Am with the cell-binding sequence cyclic RGD. To incorporate the cell-binding sequence onto gold nanoparticles the assembly peptide solution was composed of 5% (mol) c[RGDfE(SGG-KEKEKE-PPPPC-Am)] and 95% (mol) EKEKEKE-PPPPC-Am. A peptide containing a scrambled sequence with cyclic RDG was used as a control sequence. Cells were seeded and allowed to grow to 90% confluence and then were incubated with varying concentrations of cRGD-EK-GNPs and the scrambled cRDG-EK-GNPs. Particles containing cyclic RGD were uptaken by cells in a concentration dependent manner, whereas particles containing the

scrambled sequence cyclic RDG were uptaken similarly to the blank and EK-GNPs (Figure 3-10). These results demonstrate that the interactions of cRGD-EK-GNPs with cells are sequence specific and that the EK portion of the peptide sequence maintains a low fouling background.

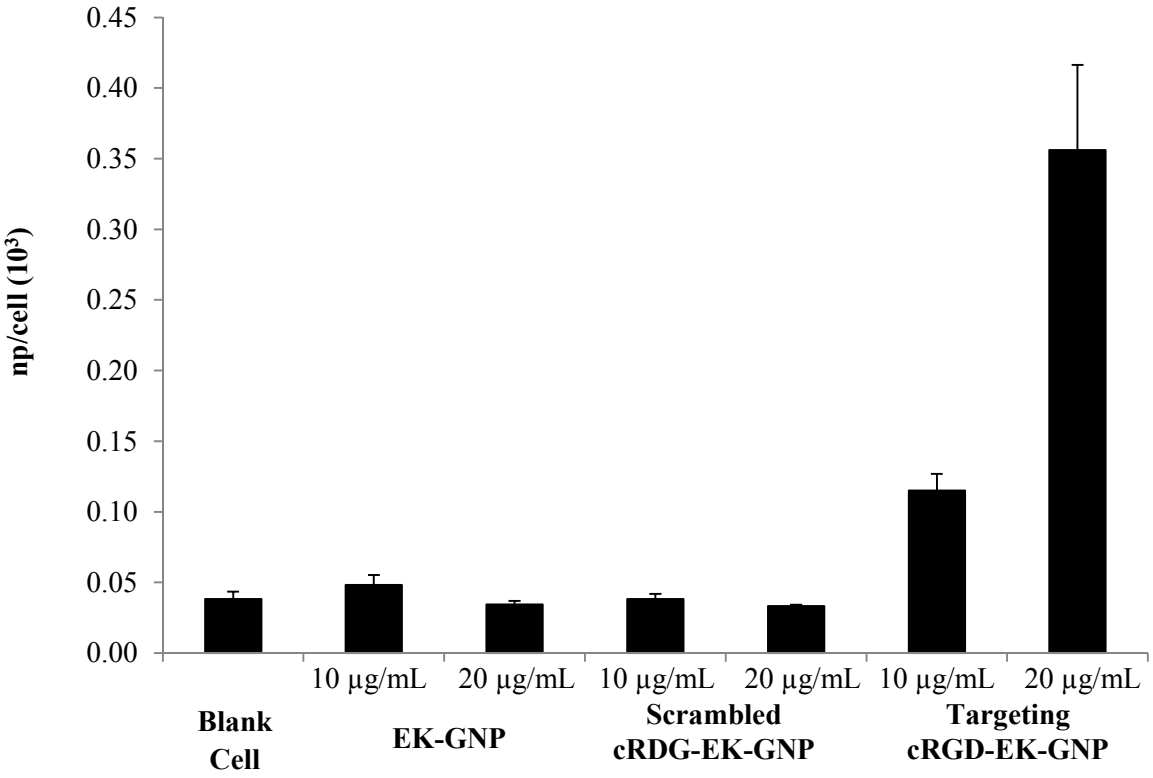

Figure 3-10. Specific cell uptake with cyclic RGD.
Cell uptake of EK-GNPs, scrambled cRDG-EK-GNPs, and targeting cRGD-EK-GNPs (number of gold nanoparticles per cell 10^3) in BAEC cells measured by ICP-MS. Exposure concentration was 10 µg/mL and 20 µg/mL for each peptide-GNP tested. Each data point represents an average value ± standard deviation from at least three independent measurements.

3.4 Conclusions

We have developed a stealth peptide coating inspired by the surfaces of proteins in the human body. This low fouling peptide coating is composed of alternating negatively charged glutamic acid (E) and positively charged lysine (K) residues, which create a strong hydration layer near the surface. Gold nanoparticles are capped by self-assembly and a rigid, hydrophobic linker (-PPPPC) is included in the peptide sequence to facilitate surface anchoring. EK-GNPs display

stability in high salt and protein solutions without aggregating. Furthermore, EK-GNPs are stable in undiluted human serum at 37°C for 24 hours and show low macrophage cell uptake suggesting that EK-GNPs could achieve long blood circulation half-life *in vivo*. Importantly, the particles can be functionalized without the need for chemical conjugation simply by extending the peptide sequence with a specific targeting moiety. In this work, the cell recognition sequence cyclic RGD was added as an example of specific cell targeting while maintaining a low fouling background. This system provides an all-natural coating that can be easily adapted for stealth applications in many particle based platforms.

Chapter 4: EK-PLGA for Drug Delivery Applications

Biodegradable polymers play an important role in a wide range of applications including drug delivery, gene transfer, tissue engineering, and regenerative medicine. Polylactic-*co*-glycolic acid (PLGA) is one of the most commonly used polymers to form drug delivery nanocarriers due to its complete biodegradability and ability to form micelles. However, PLGA suffers from drawbacks of rapid clearance from the body upon intravenous injection and lack of targeting capabilities. Stealth materials such as poly(ethylene glycol) (PEG) and zwitterionic polymers have been conjugated to PLGA in order to alleviate stability issues *in vivo*. However, these synthetic polymers are not fully biodegradable and may induce an immune system response. In this work, we conjugate the stealth peptide sequence glutamic acid/lysine (EK) to PLGA to form an EK-PLGA polymer conjugate. The use of a fully biocompatible and biodegradable stealth poly(amino acid) coating has advantages including low toxicity, easily metabolized degradation products, and potentially lower immunogenicity than non-biodegradable polymer systems. EK-PLGA diblock copolymers having hydrophilic EK segments of various lengths were synthesized. An EK-PLGA diblock copolymer containing eight EK repeats ($[EK]_8$-PLGA) was assembled into micelles utilizing nanoprecipitation techniques. Formed $[EK]_8$-PLGA micelles were characterized using dynamic light scattering (DLS), zeta potential, and scanning electron microscopy (SEM). Future work for this project will include optimization of EK-PLGA micelle formation containing various hydrophilic EK segment lengths. In addition, more extensive stability testing in protein solutions and undiluted human serum, as well as drug loading release studies should be performed.

4.1 Introduction

Nanoparticle systems are commonly used to deliver small molecule drugs, vaccines, and biological macromolecules[114–116]. One of the most successfully used biodegradable polymers is poly(lactic-*co*-glycolic acid) (PLGA). Utilizing PLGA in drug delivery formulations allows for controlled release in a time dependent manner which can improve therapeutic efficacy, reduce the required dosage of drug needed, and minimize unwanted side effects[117]. Degradation rates can be controlled by varying the molecular weight and copolymer ratio[118]. PLGA is convenient because degradation products are endogenous and easily metabolized to carbon dioxide and water or excreted in the kidneys[119].

One of the limitations of *in vivo* applications of PLGA particles is recognition and rapid clearance by the reticuloendothelial system (RES) due to the hydrophobic nature of the surface. As soon as particles enter the blood stream the binding of opsonin proteins from blood serum occurs leading to macrophage attachment and subsequent internalization by phagocytosis[117]. In order to prevent rapid clearance of PLGA nanoparticles, these particles are often synthesized with an additional stealth coating to prevent recognition by the RES. The most common surface modification utilized to create stealth coatings is poly(ethylene glycol) (PEG)[120–122]. While PEG has been successfully utilized as a stealth surface coating it has several disadvantages[16]: (1) potentially interferes with nanoparticle cell interactions; (2) elicits an antibody immune response; (3) degrades under oxidative conditions. Alternative polymers utilized as stealth coatings include polyoxazolines[123], n-(2-hydroxypropyl)methacrylamide (HPMA)[124], polyglycerols[125], and zwitterionic polybetaines[126].

One potential disadvantage common to synthetic polymer systems is the lack of biodegradability which can affect clearance of the polymer from the body and cause potential

cytotoxic effects from accumulation in organs such as the liver[16]. Two biodegradable alternatives are the use of polysaccharides[127] or poly(amino acids)[34,128]. These materials are biocompatible and readily degradable in the body reducing the risk of accumulation and related toxicity. Several poly(amino acid) polymers have been synthesized for drug delivery applications including polymers derived from phenylalanine[129], arginine[130], aspartic acid[131], tyrosine[132], glutamic acid[133], proline[134], lysine[135], and cysteine[136].

It has been recently shown that polypeptides based on alternating glutamic acid and lysine residues possess stealth properties[13,104]. These mixed charge peptides are based on zwitterionic materials which possess better resistance to nonspecific protein adsorption than PEG, but have the advantage of being completely biodegradable. In this work, we propose the development of an EK-PLGA diblock copolymer which can be self-assembled into a polymer micelle for controlled drug delivery applications. A synthesis method was developed to form EK-PLGA by performing a coupling reaction between an amine terminated side-chain protected EK peptide of varying lengths and a carboxylic acid terminated PLGA polymer (Figure 4-1). Following deprotection of amino acid side chains, the EK-PLGA diblock copolymers can form micelles with a PLGA core and an EK shell. EK-PLGA micelles were characterized for size, charge, and morphology via dynamic light scattering (DLS), zeta potential, and scanning electron microscopy (SEM), respectively. Future work will involve testing for stability in complex media, cytotoxicity to cells, and drug release kinetics.

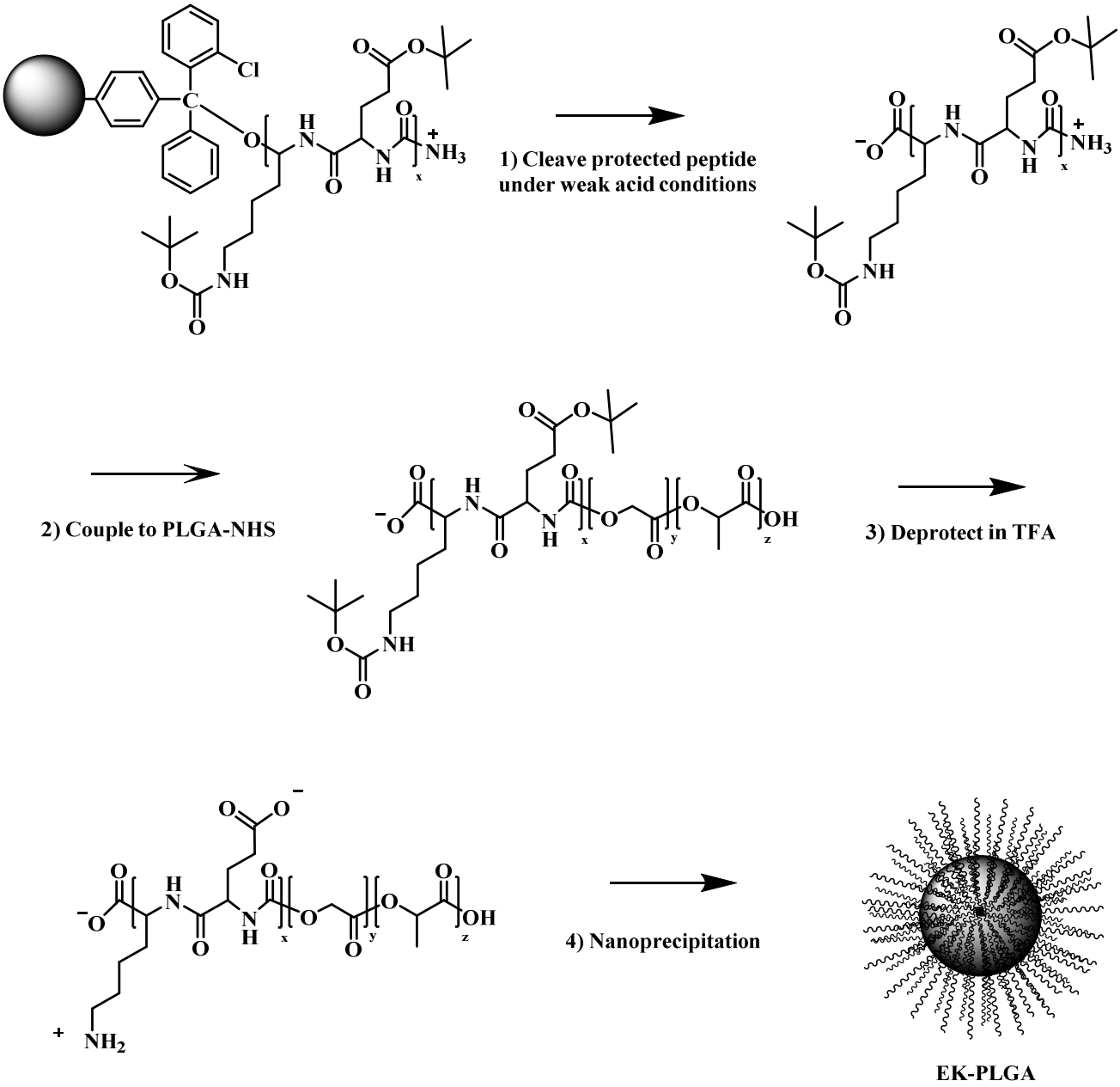

Figure 4-1. Synthesis of EK-PLGA copolymers and formation of EK-PLGA nanoparticles.

4.2 Experimental Methods

4.2.1 Materials

Poly(D,L-lactide-*co*-glycolide) (PLGA) with a 50:50 monomer ratio was purchased from Durect Corporation (Pelham, Al). 2-Chlorotrityl chloride (CTC) resin (1.54 mmol Cl^-/g resin) was purchased from Thermo Fisher AnaSpec (Waltham, MA). N-Fluorenylmethoxycarbonyl (Fmoc)-protected amino acids with the amine and side chain protected (Fmoc–Glu(OtBu)–OH, Fmoc–Lys(Boc)–OH), piperidine, and N,N-dimethylformamide (DMF) were purchased from AAPPTec (Louisville, KY). N,N-Diisopropylethylamine (DIPEA), thionyl chloride, and triethylamine (TEA) were purchased from TCI America (Portland, OR). Trifluoroacetic acid (TFA) and acetic acid were purchased from EMD (Darmstadt, Germany). Anhydrous dichloromethane (DCM), dichloromethane (DCM), methanol (MeOH), diethyl ether, hexane, triisopropylsilane (TIS), thioanisole, 1,8-Diazabicyclo[5.4.0]undec-7-ene (DBU), 2,2,2-trifluoroethanol (TFE), N-hydroxy-succinimide (NHS), and phosphate buffered saline (PBS) were purchased from Sigma Aldrich (St. Louis, MO). N-methylpyrrolidone (NMP) and acetonitrile (AcOH) were purchased from Fisher Scientific (Waltham, MA). N-(3-Dimethylaminopropyl)-N'-ethylcarbodiimide hydrochloride (EDC) was purchased from Oakwood Products Inc. (West Columbia, SC). O-(1*H*-6-Chlorobenzotriazol-1-yl)-*N*,*N*,*N*',*N*'-tetramethyluronium hexafluorophosphate (HCTU) was purchased from Chem-Impex International Inc. (Wood Dale, IL).

4.2.2 Loading of First Amino Acid onto CTC resin

The first amino acid was manually loaded onto 2-chlorotrityl chloride (CTC) resin. If needed the resin was first regenerated using methods described in the literature[137]. Briefly, CTC resin was rinsed with DMF and three times with anhydrous DCM. The resin was then treated with a 1.7%

thionyl chloride solution in DCM (v/v) for one hour at room temperature. Finally, the resin was rinsed with DMF and DCM. The activated resin was used directly. 1 g of CTC resin was placed in a round bottom flask and was deoxygenated by five repetitions of a strong vacuum followed by nitrogen backfill. 10 mL of anhydrous DCM was added to allow swelling of the resin. After 10 min of swelling, 0.75 equivalents of Fmoc–Lys(Boc)–OH and 3.75 equivalents of DIPEA were added in 10 mL of anhydrous DCM. The resin was allowed to react for 30 minutes and then drained. To endcap any remaining reactive 2-chlorotrityl groups 20 mL of a DCM (85%), MeOH (10%), and DIPEA (5%) (v/v/v) solution was added for 20 minutes. The resin was then washed (10 mL/g resin) three times with DCM, two times with DMF, two times with DCM, three times with MeOH, and dried under reduced pressure overnight.

Estimation of loading of the CTC resin was determined using an Fmoc sensitive assay[138]. Approximately, 10 mg of dry, Fmoc-amino acid loaded resin was weighed into a 20 mL scintillation vial and 2 mL of a 2% DBU in NMP solution (v/v) was added in order to cleave the Fmoc groups. The solution was swirled for 15 min and then diluted to 10 mL with AcOH. Next, 2 mL of this solution was taken and diluted to 25 mL. A reference solution was prepared in the same manner, but without the addition of resin. Cuvettes were loaded with 1 mL of solution and the absorbance was measured at 304 nm via a Cytation 3 multi-mode plate reader (BioTek, Winooski, VT). Fmoc loading of the resin can be estimated using the following equation:

$$\text{Fmoc loading } \left(\frac{\text{mmol}}{\text{g resin}}\right) = \frac{\left(\text{Absorbance}_{\text{sample}} - \text{Absorbance}_{\text{reference}}\right) \times 16.4}{\text{mg of dry resin}}$$

The Fmoc loading of the resin was determined to be 0.48 mmol/g.

4.2.3 Peptide Synthesis

All peptides were synthesized by solid-phase techniques using the AAPPTec Titan 357 automated synthesizer (Louisville, KY). Lysine-loaded CTC resin with a 0.48 mmol/g loading capacity was used. Coupling was performed using amino acid monomer, HCTU, and DIPEA prepared in DMF in a molar ratio of 1.1:1:2 in six times excess of the loading capacity of the resin. All amino acid additions underwent double coupling. Deprotection of Fmoc groups was achieved using 20% piperidine in DMF.

In order to verify that expected molecular weights were achieved and to assess purity, peptides were cleaved from the resin and deprotected for analysis. The cleavage and side-chain deprotection of the peptide product was performed using a TFA (85%), DCM (10%), TIS (2%), thioanisole (2%), and water (1%) (v/v/v/v/v) cleavage cocktail. Peptides were precipitated into diethyl ether, dried, and the peptide purity was evaluated by reverse phase high performance liquid chromatography (RP-HPLC) to determine purity. The purity of the peptide sequences was 100% for NH_2-$[EK]_8$-COOH, 78% for NH_2-$[EK]_{16}$-COOH, and 72% for NH_2-$[EK]_{24}$-COOH. Peptides were also analyzed by matrix-assisted laser desorption/ionization time-of-flight mass spectrometry (MALDI-TOF-MS) to confirm molecular weight values.

4.2.4 Cleavage of Protected EK Peptide from CTC Resin

In order to obtain side-chain protected peptides, low acid cleavage can be performed on CTC resin[139,140]. Peptide-loaded CTC resin was suspended in a 1:1:8 by volume mixture of acetic acid/TFE/DCM (10 mL per gram of resin) for 1 hour. The resin was then filtered and washed with additional cleavage solution. The filtrates were combined and 15 times the volume of hexane was added. The solvent was removed under reduced pressure. The acetic acid is removed as an azeotrope

with hexane. The peptide was then dissolved in cold methanol and precipitated with water. The precipitated peptide was rinsed twice with water and then dried under reduced pressure.

4.2.5 EK-PLGA Conjugation

In order to conjugate side-chain protected EK peptide segments to PLGA, EDC/NHS chemistry was utilized. First, PLGA was modified in order to form PLGA-NHS. Briefly, 2 g of COOH terminated PLGA (0.20 dl/g), 54 mg of NHS, and 92 mg of EDC were reacted in 6 mL of anhydrous DCM for 4.5 hours at room temperature. The reaction was precipitated into 45 ml of cold diethyl ether. The resulting PLGA-NHS was washed with a cold 2:1 by volume mixture of diethyl ether and methanol five times to remove any residual EDC and NHS. The final product was then dried under high vacuum.

To form an $[EK]_8$-PLGA conjugate, 30 mg of an amine-terminated $[EK]_8$ protected peptide and 265 mg of PLGA-NHS were placed in a round bottom flask and were deoxygenated by five repetitions of a strong vacuum followed by nitrogen backfill. The conjugation reaction proceeded in 6 mL of anhydrous DCM and 50 µL of TEA for 40 hours at room temperature under nitrogen. The resulting $[EK]_8$-PLGA diblock copolymer was precipitated into cold methanol. Any unreacted $[EK]_8$ protected peptide was removed by repeated washing in methanol. The polymer was then dried under high vacuum. Conjugation was verified by analyzing conjugation reaction samples and control reaction samples on a size exclusion column (SEC). Gel permeation chromatography (GPC) samples were run on an Agilent 1200 Infinity Series (Agilent Technologies, Santa Clara, CA) connected to a Viscotek I-Series Mixed Bed Low MW and Mixed Bed Mid MW columns (Malvern, Worcestershire, United Kingdom) at 1 mL/min in DMF with 0.05 M LiBr. Samples were monitored

with a Mini Dawn Treos light scattering detector and an Optilab T-rex refractive index detector (Wyatt Technology, Santa Barbara, CA).

4.2.6 Deprotection of Peptide Side Chains on EK-PLGA

To remove side-chain protecting groups from the protected EK peptide, the $[EK]_8$-PLGA polymer was deprotected using a TFA (94%), TIS (3%), and thioanisole (3%) (v/v/v) solution for 1 hour. From previous work it has been shown that PLGA treated with TFA for up to 6 hours did not show significant molecular weight changes[126]. The resulting deprotected $[EK]_8$-PLGA polymer was precipitated into diethyl ether, and re-dissolved in a small amount of TFE and precipitated in diethyl ether repeatedly. The polymer was then dried under high vacuum.

4.2.7 Formation of EK-PLGA Micelles via Nanoprecipitation

Polymer micelles were formed via nanoprecipitation methods. $[EK]_8$-PLGA copolymer was dissolved in a 2.25:1 by volume mixture of TFE and MeOH at a concentration of 0.6 mg/mL. The copolymer solution was then added dropwise to water stirring at 1,000 rpm. A four time excess of water by volume was used relative to the amount of copolymer solution. In addition to adding copolymer solution to water, a second method was explored where water was added to the copolymer solution instead. In both cases, the solution was left stirring for 2 hours in order to allow evaporation of organic solvents to occur. The particles were then concentrated and exchanged to PBS using an Amicon Ultracel Centrifugal Filter Unit with a nominal molecular weight limit (NMWL) of 30 kDa (Millipore, Billerica, MA). If necessary, particles were filtered through a Millex-GV 0.22 μm polyvinylidene fluoride (PVDF) syringe filter (Millipore, Billerica, MA).

Control PLGA nanoparticles can be synthesized utilizing single emulsion solvent evaporation techniques[141]. Briefly, polymer is dissolved in an organic phase such as dichloromethane and the resulting solution is dropped at a constant speed into water. The formed oil-in-water emulsion is gently stirred at room temperature to evaporate the organic solvents. Particles can then be washed and lyophilized until use.

4.2.8 Characterization of EK-PLGA Micelles

The hydrodynamic size and zeta potential of $[EK]_8$-PLGA micelles was analyzed by dynamic light scattering (DLS) using the Zetasizer Nano-ZS (Malvern, Worcestershire, United Kingdom). Measurements were carried out at 25 ˚C in aqueous media. The zeta potential was calculated from the electrophoretic mobility based on the Smoluchowski theory. For zeta potential measurements, $[EK]_8$-PLGA micelles were analyzed in water or a 10% (vol) PBS solution. The morphology of particles was determined by scanning electron microscopy (SEM) using a Dual Beam FIB (FEI, Hillsboro, OR). SEM samples were prepared by evaporating 5 μL of micelle solution onto a silica wafer.

4.3 Results and Discussion

4.3.1 Comparison of Synthesis Routes for EK-PLGA

Two methods were considered for synthesis of EK-PLGA, each with its advantages and disadvantages. The first method consists of coupling a carboxylic acid terminated PLGA polymer to an amine terminated EK peptide. This method is advantageous because the EK peptide sequence can be precisely controlled. The disadvantage is that solid-phase peptide synthesis is limited to peptide sequences composed of up to 50 amino acids in length (~6500 Da). Coupling reactions between amine groups and carboxylic acids can be achieved via many different reactions[142]. One possibility

is the use of peptide coupling chemistry to add a carboxylic acid-terminated PLGA polymer to the end of a peptide containing a free amine group on a polymer resin. The standard peptide coupling reaction can be monitored using a ninhydrin test to ensure coupling has gone to completion[143]. However, when this approach was tried yield coupling on resin was very low. Another possibility is to synthesize EK peptides on a polymer resin that allows for cleavage of fully protected peptide sequences. The coupling of EK peptide and PLGA polymer can then be achieved in solution and much higher coupling yields can be obtained. Following conjugation of the EK peptide and PLGA polymer, a trifluoroacetic acid cleavage cocktail can be used to remove the side chain protecting groups on the peptide. PLGA polymers are stable in trifluoracetic acid solutions[126,131]. The product can then be precipitated into diethyl ether and dried under vacuum.

The second method consists of performing a random ring opening polymerization of glutamic acid and lysine off of a polylactic acid (PLA) macroinitiator. This method allows access to longer length EK polymer chains. The disadvantage of this method is that there is no control over the sequence, resulting in a random EK sequence. However, as long as a 50:50 monomer ratio of glutamic acid to lysine is used then the overall fouling properties will remain low[13,40]. Polymerization of glutamic acid/lysine polymers using ring opening polymerization has been previously reported[13]. The synthesis of n-carboxy anhydrides (NCAs) of γ-benzyl-$_L$-glutamate and N_ε-benzyloxycarbonyl-$_L$-lysine are also reported in the literature[13,144]. This procedure can be modified to polymerize off of a PLA macroinitiator containing an amine group[135,145]. Following polymerization, a deprotection step needs to be performed in order to remove protecting groups off of NCA monomer side chains. Finally, the product can be precipitated into diethyl ether for purification and dried under vacuum.

Here, we decided to pursue synthesis of EK-PLGA through conjugation of amine terminated side-chain protected EK peptide and PLGA-NHS (Figure 4-1). With this synthesis method complete control over the resulting EK peptide sequence was achieved. This ensures that equal amounts of glutamic acid and lysine residues will be present in the polymer in a strictly alternating order.

4.3.2 Synthesis of Amine Terminated Side-Chain Protected EK Peptide

Direct conjugation of EK peptide to PLGA is difficult because of their dramatic difference in polarity. Mixed charge EK is only soluble in water or methanol, whereas PLGA is not soluble in either solvent. In addition, PLGA can become hydrolyzed in the presence of water[118]. In order to overcome these difficulties, CTC resin was used to synthesize EK peptide which allows for cleavage of fully protected peptide sequences in weak acidic conditions. Side chains of glutamic acid are protected with *tert*-butyl ester groups (OtBu) and side chains of lysine are protected with *tert*-butyloxycarbonyl groups (Boc). Protected peptides consisting of three varying EK lengths were synthesized utilizing CTC resin: NH_2-$[EK]_8$-COOH, NH_2-$[EK]_{16}$-COOH, and NH_2-$[EK]_{24}$-COOH. In order to determine peptide purity, a small sample of each peptide was fully deprotected and cleaved from the resin utilizing a TFA cleavage cocktail. Analysis by RP-HPLC shows that peptide purity was 100% for NH_2-$[EK]_8$-COOH, 78% for NH_2-$[EK]_{16}$-COOH, and 72% for NH_2-$[EK]_{24}$-COOH (Figure 4-2). In addition to analyzing peptide sequences by RP-HPLC for purity, peptides were also analyzed by MALDI-TOF to confirm accurate molecular weights. Since these peptides are larger in size they were analyzed in linear mode by MALDI-TOF (Figure 4-3). Although the purity for NH_2-$[EK]_{16}$-COOH and NH_2-$[EK]_{24}$-COOH peptide sequences is slightly lower, most impurities are simply sequences missing a glutamic acid or lysine residue as indicated by MALDI-TOF. The NH_2-$[EK]_{16}$-COOH and NH_2-$[EK]_{24}$-COOH peptide sequences are 32 and 48 residues long,

respectively. These longer peptide sequencess are approaching the maximum lenght for solid phase peptide synthesis on resin, which is typically limited to 50 residues[146]. In order to achieve higher molecular weight EK peptide segments synthesis strategies such as recombinant DNA technology, native chemical ligation, or convergent synthesis could be considered[147].

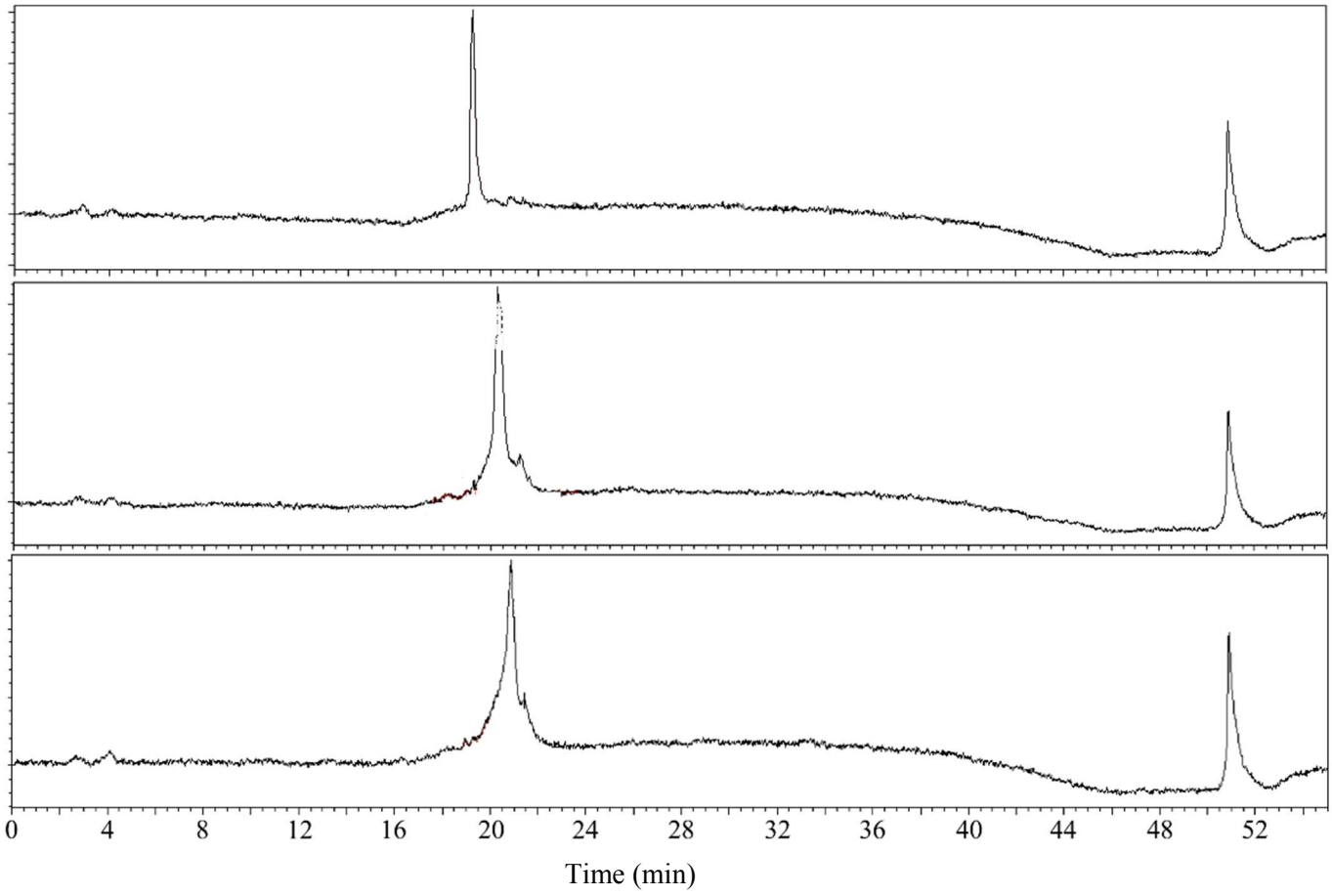

Figure 4-2. Synthesis of EK peptide of varying lengths.
RP-HPLC chromatograms of fully deprotected EK peptides. Top panel is NH_2-$[EK]_8$-COOH (100 % purity), the middle panel is NH_2-$[EK]_{16}$-COOH (78% purity), and the bottom panel is NH_2-$[EK]_8$-COOH (72% purity).

a) NH_2-$[EK]_8$-COOH

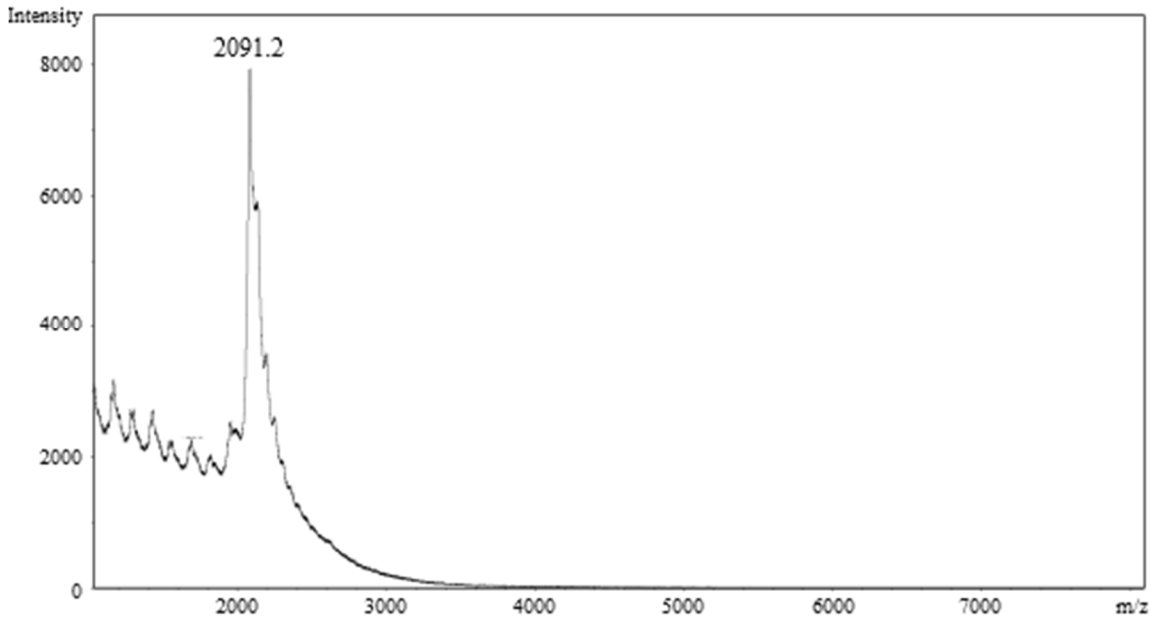

b) NH_2-$[EK]_{16}$-COOH

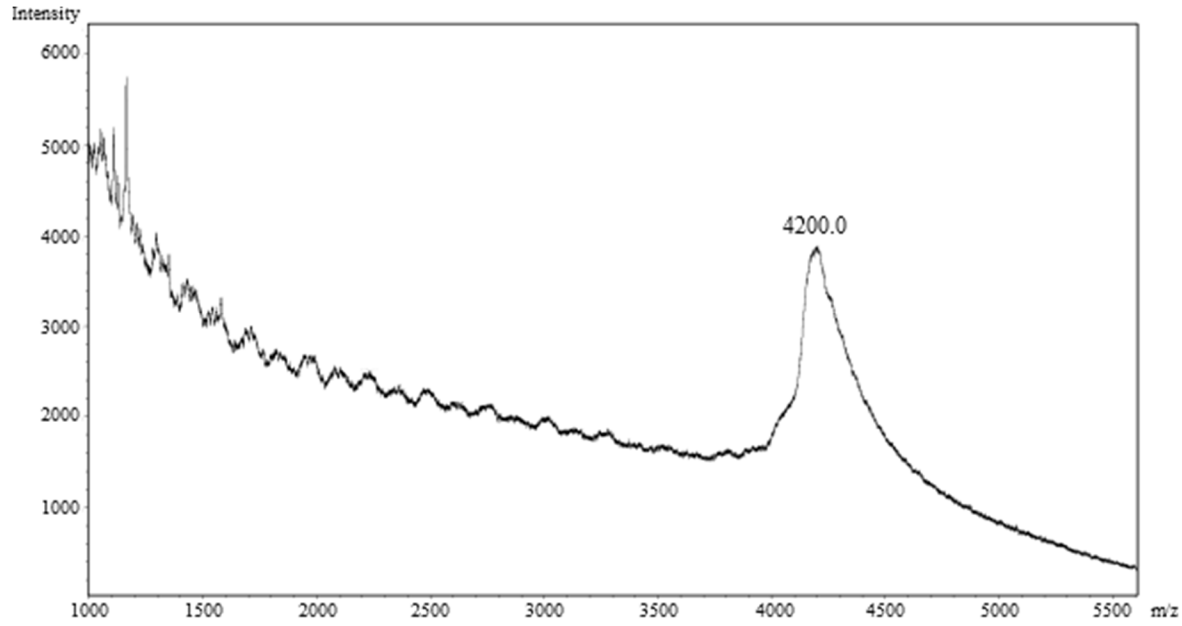

c) NH_2-$[EK]_{24}$-COOH

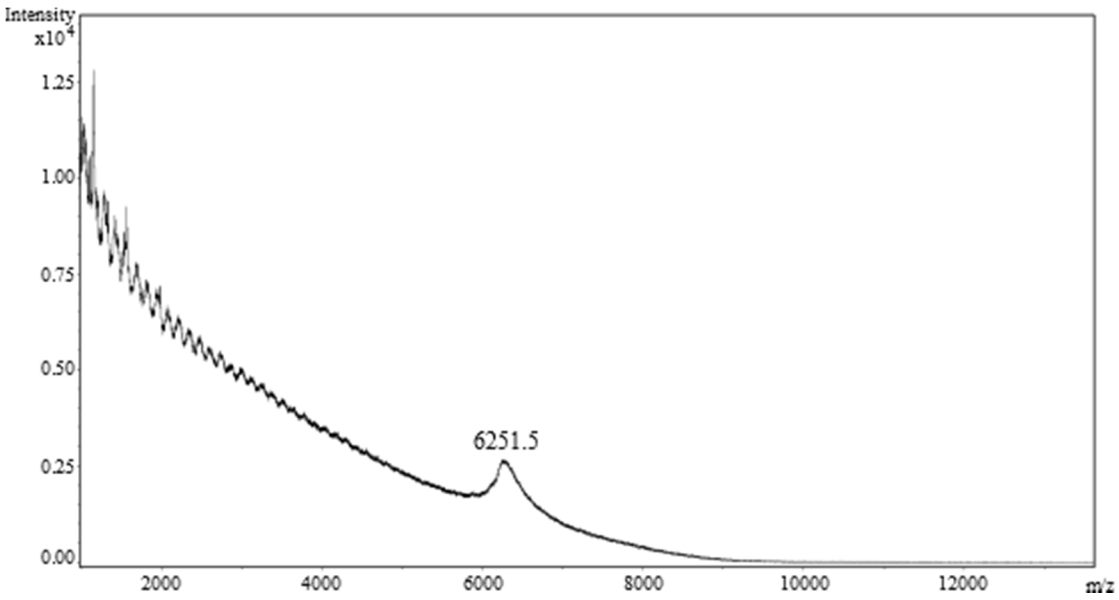

Figure 4-3. MALDI peptide synthesis characterization.
Linear mode MALDI spectra for synthesized peptide sequences. (a) NH_2-$[EK]_8$-COOH (b) NH_2-$[EK]_{16}$-COOH (c) NH_2-$[EK]_{24}$-COOH.

4.3.3 Conjugation of $[EK]_8$ Peptide to PLGA

Following synthesis of EK peptide, cleavage of fully side-chain protected peptide sequences was achieved through weak acid cleavage in a 1:1:8 by volume mixture of acetic acid/TFE/DCM. The cleaved EK peptide sequences display good solubility in organic solvents, thus allowing conjugation to PLGA-NHS in anhydrous DCM to form protected EK-PLGA diblock copolymers. To verify successful conjugation, GPC was used to monitor molecular weight changes of PLGA-NHS before and after conjugation. Two reactions were set up with one containing $[EK]_8$ peptide and PLGA-NHS and the other containing $[EK]_8$ peptide and PLGA. Three control vials containing PLGA-NHS, PLGA, and $[EK]_8$ peptide alone were also prepared. All samples were analyzed by GPC on a SEC Viscotek I-series column at 1mL/min in 0.05 M LiBr DMF (Figure 4-4).

a)

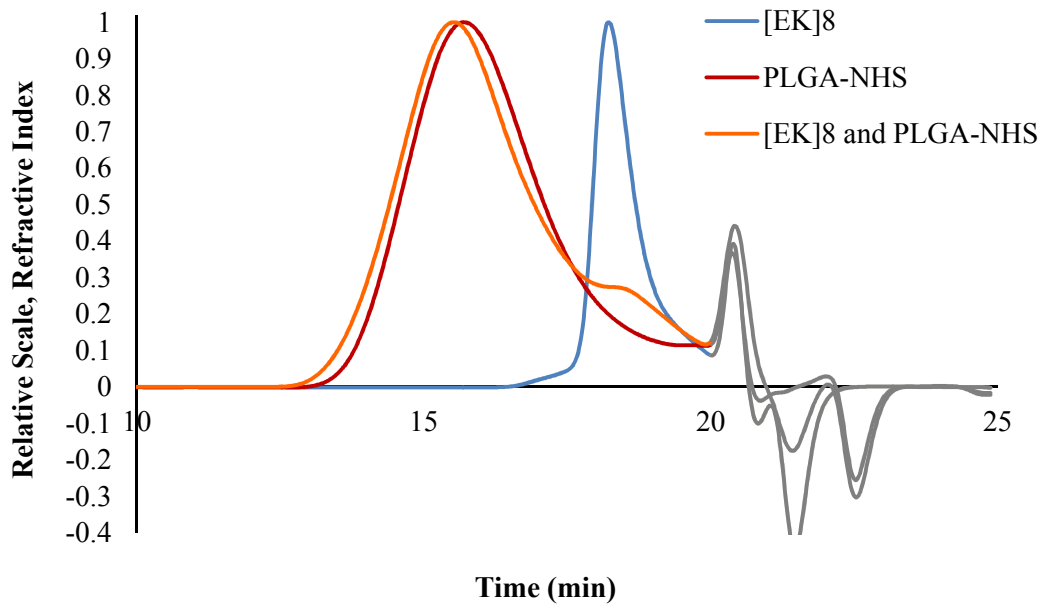

b)

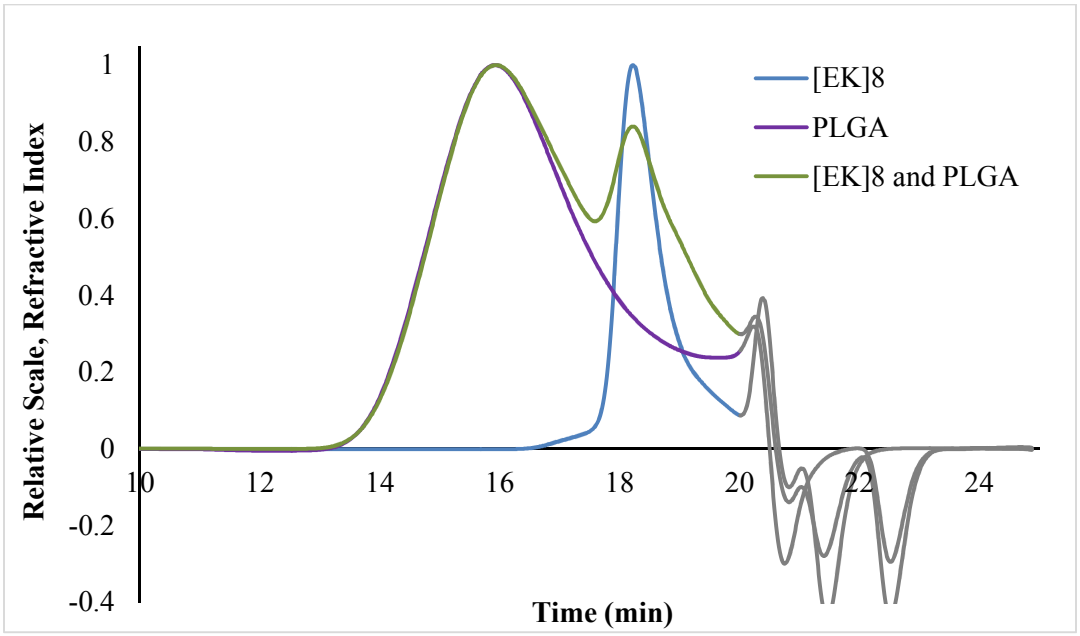

Figure 4-4. GPC analysis of EK-PLGA conjugation reaction.
(a) GPC chromatograms of conjugation reaction showing $[EK]_8$ peptide (blue line), PLGA-NHS (red line), and $[EK]_8$ and PLGA-NHS (orange line). (b) GPC chromatograms of negative control conjugation reaction showing $[EK]_8$ peptide (blue line), PLGA (purple line), and $[EK]_8$ and PLGA (green line). Solvent peaks are colored in grey for all spectra.

From the GPC chromatogram, the reaction containing $[EK]_8$ peptide and PLGA-NHS shows a shift to a larger polymer size in reference to simply PLGA-NHS alone. In addition, the $[EK]_8$ peptide peak has decreased significantly indicating its consumption in the conjugation reaction. In contrast, the control reaction containing $[EK]_8$ peptide and PLGA shows no difference in reference to PLGA alone. In addition, the $[EK]_8$ peptide peak has high signal indicating it has not reacted. This is as expected, since there should be no conjugation reaction occurring in the presence of unmodified PLGA. Conjugation should only take place in the presence of the NHS group.

Following conjugation of EK peptide to PLGA-NHS, the diblock copolymer needs to be deprotected in order to remove OtBu and Boc protecting groups present on glutamic acid residues and lysine residues, respectively. This was accomplished through deprotection in a TFA cleavage solution for 1 hour. From previous work, it has been shown that PLGA can withstand TFA treatment for up to 6 hours without destroying the ester backbone[126]. The resistance of PLGA[148] and polylactic acid (PLA)[131,149,150] to acid degradation has also been reported in the literature. This synthesis strategy can also be applied to generate any amphiphilic block copolymer containing a hydrophilic EK peptide block and a hydrophobic polymer block.

4.3.4 Micelle Formation of $[EK]_8$-PLGA via Nanoprecipitation

To formulate EK-PLGA micelles a nanoprecipitation method was used in which the block copolymer is dissolved in an organic solvent that is water-miscible[126]. Upon introduction of water, in which the EK block is soluble but the PLGA block is not, PLGA core/EK shell structured nanoparticles (NPs) are formed. With time, the organic solvent evaporates while stirring, and leaves an aqueous solution in which the NPs harden. Hydrophobic drugs can be encapsulated in the hydrophobic core of the NP by mixing the drug with the copolymer solution during formation.

The diblock copolymer $[EK]_8$-PLGA was dissolved in a solution of 2.25:1 by volume mixture of TFE and MeOH at a concentration of 0.6 mg/mL. The inclusion of methanol helps to improve the solubility of the EK block in TFE. The $[EK]_8$-PLGA polymer solution was then mixed with a volume of water four times in excess of the copolymer solution. Two approaches were used to mix the copolymer solution and water. In the first approach, the polymer solution was added dropwise to the water. In the second approach, water was added dropwise to the polymer solution. In both cases, the solution was stirred for 2 hours to allow evaporation of the organic solvents. Particles were then concentrated using a 30 kDa molecular weight cut-off Amicon filter, and then exchanged into PBS using the same method.

4.3.5 Characterization of $[EK]_8$-PLGA Micelles

Dynamic light scattering (DLS) was used to characterize the hydrodynamic size and zeta potential of particles formed during nanoprecipitation from both methods (Table 4-1). Particles formed by adding polymer solution to water had a hydrodynamic size of 134.4 ± 2.6 nm with a polydispersity (PDI) of 0.24 ± 0.01 and a zeta potential of -12.5 ± 0.9 mV. After exchange into PBS, the nanoparticles partially aggregated, but aggregates were able to be removed with a filter. The resulting hydrodynamic size in PBS was 174.0 ± 4.0 nm with a polydispersity (PDI) of 0.09 ± 0.07 and a zeta potential of -16.2 ± 2.2 mV. These results suggest that not enough EK is present on the surface of particles in order to stabilize them after transfer into PBS solution. The high PDI in water indicates that particles are not uniformly formed and is most likely contributing to the instability upon transfer to PBS. However, once particles have been filtered the PDI indicates that there is a monodisperse population of particles.

Table 4-1. Hydrodynamic size and zeta potential of $[EK]_8$-PLGA nanoparticles.
DLS data of $[EK]_8$-PLGA nanoparticles prepared via two different nanoprecipitation methods: 1) polymer solution added to water 2) water added to polymer solution. The hydrodynamic diameter (nm), PDI, and zeta potential (mV) are shown for each nanoparticle in both water and PBS.

	Polymer Solution Added to Water			**Water Added to Polymer Solution**		
	Size (nm)	PDI	Zeta (mV)	Size (nm)	PDI	Zeta (mV)
Water	134.4 ± 2.6	0.24 ± 0.01	-12.5 ± 0.9	690.9 ± 16.3	0.14 ± 0.02	-27.2 ± 0.6
PBS	174.0 ± 4.0	0.09 ± 0.07	-16.2 ± 2.2	619.4 ± 23.5	0.15 ± 0.04	n/a

Particles formed by adding water to the polymer solution resulted in much larger sizes than particles formed by adding polymer solution to water. The hydrodynamic size was nearly five times larger at 690.9 ± 16.3 nm with a PDI of 0.14 ± 0.02, and a zeta potential of -27.2 ± 0.6 mV. Upon addition of 50% PBS to the particle solution, the hydrodynamic size decreased slightly to 619.4 ± 23.5 nm and the PDI remained similar at 0.15 ± 0.04. The larger size of these particles and the more negative zeta potential indicate less incorporation of the EK block into the shell of the particle. The addition of water into the organic polymer solution may not have allowed for the EK block to become solubilized as quickly and there may have been some reverse micelles forming with EK in the core and PLGA in the shell.

In addition to using DLS to characterize particles, scanning electron microscopy (SEM) was used to probe particle morphology. A sample of $[EK]_8$-PLGA micelles in water formed by adding polymer solution to water were deposited on a silica wafer and examined by SEM (Figure 4-5). Particles of around 150 nm in size can be seen, corresponding with DLS data. A few of the particles appear to be clustered in groups upon drying, but the majority maintain a rounded morphology.

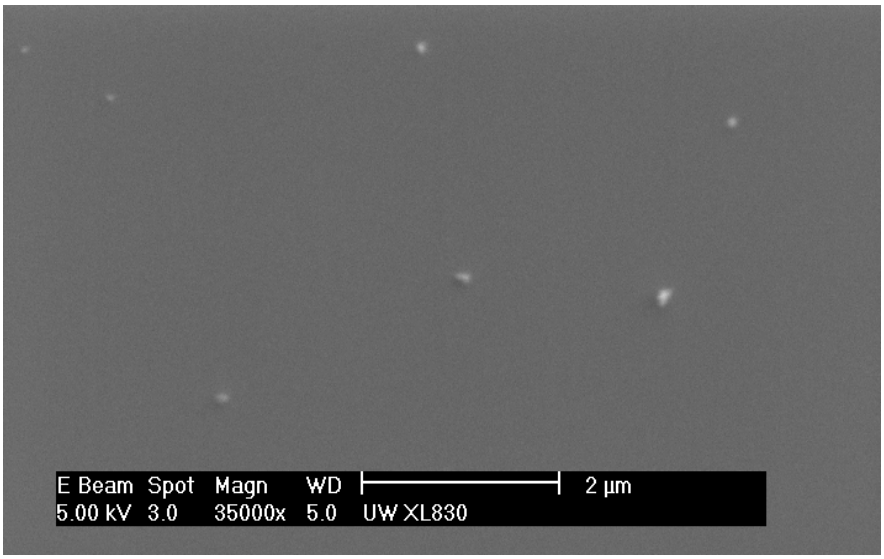

Figure 4-5. SEM image of $[EK]_8$-PLGA nanoparticles in water.
SEM image of $[EK]_8$-PLGA nanoparticles prepared by adding copolymer solution into water. The sample was prepared by depositing 5 µL of solution onto a silica wafer.

Initial nanoprecipitation results show promise for forming stable $[EK]_8$-PLGA micelles, however, the process needs to be optimized. There are several parameters that can be adjusted in order to fine tune the nanoprecipitation process including: adjusting the concentration of polymer, changing the organic solvent used, adjusting the amount of water added, and changing the order of addition. It is also possible that a chain length consisting of only eight EK repeats may be too short in order to stabilize the EK-PLGA particles. It will be beneficial to compare micelle formation of particles made with $[EK]_{16}$ and $[EK]_{24}$.

4.4 Conclusions

In this work, we propose a synthesis route to develop the diblock copolymer EK-PLGA which can be used to form stealth nanoparticle drug delivery carriers. Stealth properties are achieved from the superhydrophilic EK peptide block composed of alternating negatively charged glutamic acid (E) and positively charged lysine (K) residues. Drug loading capabilities are introduced by the inclusion of a hydrophobic PLGA block. This system is unique compared to PEG-PLGA and other

synthetic polymer systems because it is completely biodegradable and can be metabolized by the body to nontoxic degradation products. In addition, EK-PLGA particles may display nonimmunogenic properties *in vivo*. Nanoprecipitation methods were used to form $[EK]_8$-PLGA nanoparticles that were stable upon transfer to PBS after filtering. Future work for this project will involve optimizing the nanoprecipitation method and forming micelles with varying EK block lengths. In addition, stability testing in single protein solutions and undiluted human serum, as well as, cytotoxicity tests will be performed. Finally, drug release kinetics will be studied.

4.5 Future Work

4.5.1 Optimization of EK-PLGA Micelle Formation

The formation of EK-PLGA needs to be optimized. This will involve changing the nanoprecipitation parameters including adjusting the concentration of polymer, changing the organic solvent used, adjusting the amount of water added, and changing the order of addition. In addition, several EK-PLGA polymers will be analyzed containing varying lengths of the EK peptide block. It may also be beneficial to alter the conjugation reaction between EK and PLGA in order to have the EK peptide in excess. Currently, PLGA is in excess and it may still be present in the reaction following conjugation. It will be much easier to remove unreacted EK peptide than to separate EK-PLGA from unreacted PLGA. The drawback to having excess EK peptide is that it is much more challenging to make and the peptide synthesis would need to be scaled up significantly.

4.5.2 Stability Testing of EK-PLGA in Single Protein Solutions and Undiluted Human Serum

To evaluate the stability of EK-PLGA micelles and PLGA micelles, concentrated samples will be incubated in water, PBS, 1 mg/mL fibrinogen, 1 mg/mL lysozyme, or undiluted human

serum. Stability tests will be conducted for at least 1 hour. After the allotted exposure time, samples will be analyzed via dynamic light scattering to evaluate the hydrodynamic radius and via zeta potential to evaluate surface charge.

4.5.3 *In vitro* Cytotoxicity Study

The EK-PLGA and control PLGA particles will be assessed for cytotoxicity by performing a cell viability assay. Particles are expected to be nontoxic based on the biocompatibility of PLGA polymer[151] and the biocompatibility of EK peptides (Figure 3-8). HepG2 cells will be exposed to varying concentrations of EK-PLGA particles up to 10 mg/mL for 24 hours. Cells will then be analyzed for viability using an Alamar Blue cytotoxicity assay.

4.5.4 Drug Release Profile

Finally, the drug release profile will be examined for EK-PLGA particles and control PLGA particles. Micelles will be loaded with docetaxel as a model drug. The drug loading for polymer micelles can be determined by centrifuging solutions containing drug-loaded nanoparticles and solutions containing free drugs. Both samples are then analyzed for drug content using reverse-phase high performance liquid chromatography (RP-HPLC). Release kinetics can be determined by placing drug loaded particles in mini dialysis microtubes. At varied time points, three microtubes can be removed and drug content inside the nanoparticles can be determined by RP-HPLC. Samples need to be mixed with an equal volume of acetonitrile overnight in order to ensure complete drug release before running RP-HPLC. We expect the drug release kinetics to be similar between EK-PLGA and control PLGA polymers. The kinetics can be tuned by changing the length of the PLGA blocks and the copolymer composition[152].

Chapter 5: Discovering Low Fouling Peptides via Combinatorial Chemistry

Rational design of low fouling peptides via known zwitterionic principles and biomimetics can successfully lead to the discovery of novel sequences possessing stealth properties. However, rational design is limited to the analysis of tens of sequences at a time. Applying combinatorial screening methods on one-compound-one-bead libraries can increase the number of peptide sequences tested to thousands of compounds. Traditional screening techniques such as phage display and resin display seek to identify specific binding targets and cannot be used for the identification of low fouling sequences due to the interference of background binding. Here, we explore a new screening platform that allows for facile formation of a combinatorial library via amine modification of controlled pore glass substrates. A combinatorial library was created using a mix and split technique to include cationic, anionic, hydrophobic, aromatic, and hydrophilic residues. This library was screened with fluorescently labeled fibrinogen and evaluated via confocal microscopy to identify substrates containing low fouling peptide sequences. Peptide sequences can be recovered using partial Edman degradation in combination with matrix-assisted laser desorption/ionization time-of-flight mass spectrometry. However, the current controlled pore glass substrate does not possess enough peptide mass per substrate to successfully recover sequences. Other substrate options were explored and recommendations are made for improvement to the combinatorial library screening method. Fundamental understanding and mechanistic insights into why surfaces are nonfouling at the molecular level can be gained through the identification of nonfouling sequences.

5.1 Introduction

Nonfouling properties are relevant to many biomedical applications including drug delivery, surface coatings, and biosensing[15]. Natural materials such as peptides can offer several advantages as

biomaterials: they are biocompatible, well-defined, nonimmunogenic, biodegradable, multifunctional, and offer nearly infinite sequence combinations to explore[33]. Recently, we have identified several low fouling peptide sequences including glutamic acid/lysine (EK) and asparagine (N) through rational and biomimetic design[40,104]. However, rational and biomimetic design only allow access to a limited number of sequences for testing. Combinatorial screening methods can increase the number of compounds from tens of sequences to thousands of sequences. Combinatorial screening methods are traditionally utilized to identify sequences possessing specific binding properties. Screening a larger pool of compounds allows for the discovery of sequences containing new specific functions and has been used to identify mineral binding peptides[153], antimicrobial peptides[154], cancer-targeting peptides[155], enzyme binding motifs[156], and protease cleavage sites[157].

Commonly used display platforms for the screening of peptides include phage[43], yeast[44], bacterial[45], ribosome[131] or polymer resin display[158,159]. Phage display is the most frequently used for identification of specific binding peptides due to several advantages: (1) synthesis and sequencing is performed using established DNA technologies, since the peptide sequence is encoded in the phage DNA; (2) multiple rounds of scanning can be performed to enhance resolution; (3) biological amplification is straightforward[160]. In this work, we want to identify low binding sequences and therefore traditional platforms cannot be used due to background interference. For example, in phage display the envelope proteins would cause nonspecific binding preventing the identification of low fouling peptide sequences. Similarly, when traditional polymer resins such as TentaGel are used for peptide synthesis they are susceptible to swelling and protein entrapment[47]. To overcome these limitations we developed a novel protein adsorption screening technique utilizing a controlled pore glass (CPG) substrate coated with peptides.

The newly developed CPG substrate can be used to synthesize a combinatorial library utilizing mix and split techniques. The created one-bead-one-compound (OBOC) library can then be subjected to screening using fluorescently labeled fibrinogen. Confocal microscopy can be utilized to identify low fouling substrates (CPG substrates with low fluorescence). Finally, sequence identification can be achieved using partial Edman degradation (PED) in combination with matrix-assisted laser desorption/ionization time-of-flight mass spectrometry (MALDI-TOF-MS). A diagram of the entire screening procedure is shown in Figure 5-1.

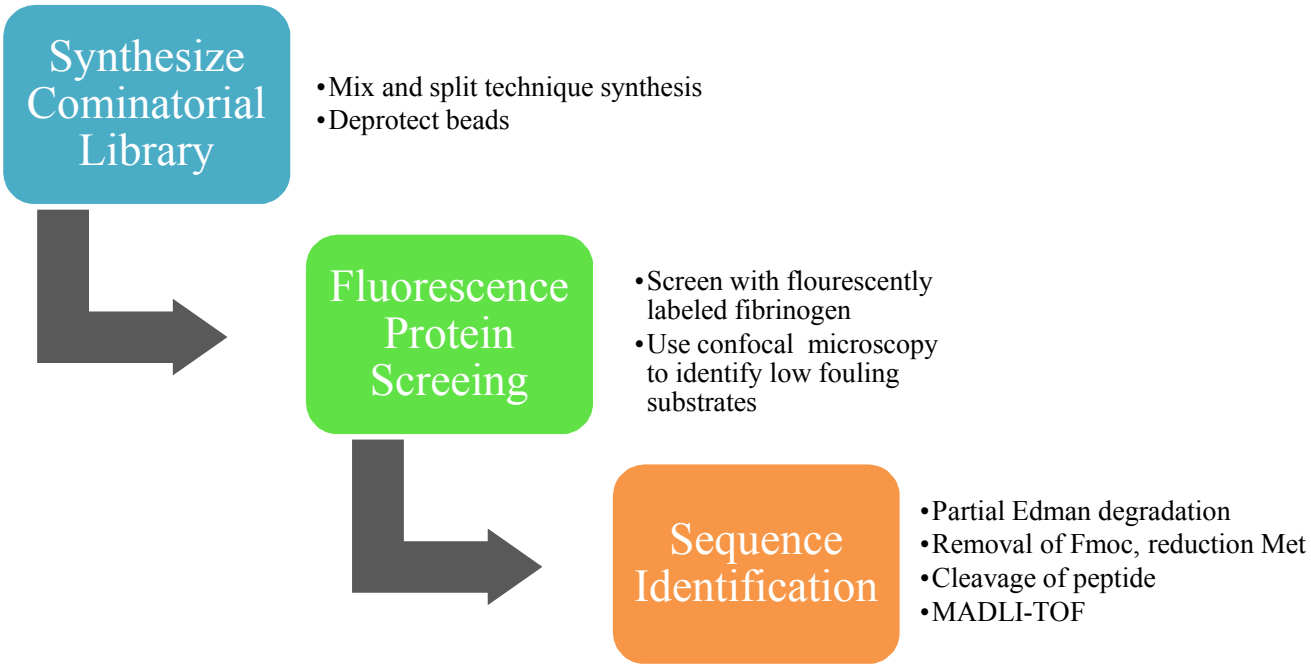

Figure 5-1. Schematic of combinatorial peptide screening for nonfouling sequences.

Here, we create an eight-residue peptide combinatorial library containing cationic, anionic, hydrophobic, aromatic, and hydrophilic groups on an amine modified CPG substrate. This one-bead-one-compound (OBOC) library was screened for protein adsorption using fluorescently tagged fibrinogen. Low fouling sequences were identified using confocal microscopy, a technique previously utilized for OBOC libraries[161]. Several known control sequences were synthesized and

evaluated along with the library in order to serve as benchmarks for low and high fouling values. After screening 100 randomly selected CPG substrates, in addition to three known fouling peptide controls (leucine, glycine, glutamic acid/lysine), 37% of the library was found to have lower fouling than previously identified ultra-low fouling glutamic acid/lysine. Successful recovery of peptide sequences via partial Edman degradation (PED) and matrix-assisted laser desorption/ionization time-of-flight mass spectrometry (MALDI-TOF) was hindered due to mass limitations. A second CPG substrate containing smaller pore sizes was then evaluated as a replacement substrate. While the mass signal was improved for the system, sequence recovery on individual substrates was still hindered. In the future, a more appropriate CPG substrate needs to be identified to facilitate successful peptide sequence recovery.

5.2 Experimental Methods

5.2.1 Materials

Triisopropylsilane (TIS), 9-Fluorenylmethyl *N*-succinimidyl carbonate (Fmoc-OSU), protein sequencing grade phenyl isothiocyanate (PITC), trifluoroacetic acid (TFA), γ-glycidoxypropyltrimethoxysilane (GPTMS), N,N-diisopropylethylamine (DIPEA), bromotrimethylsilane, thioanisole, phenol, methanol (MeOH), anhydrous pyridine, anhydrous dichloromethane (DCM), anhydrous trifluoroaetic acid (TFA), dimethyl sulfide, sodium bicarbonate ($NaHCO_3$), alpha-cyano-4-hydroxycinnamic acid matrix, and fibrinogen from bovine plasma were purchased from Sigma-Aldrich (St. Louis, MO). Controlled pore glass substrates with 1000 Å (CPG1000A) and 3000 Å (CPG3000A) pores and amino-PEGA resin were purchased from EMD Millipore (Billerica, MA). Tetraethyleneglycol diamine (PEO_4-Bis Amine) was purchased from Molecular Biosciences (Boulder, CO). Alexa Fluor® 488 Carboxylic Acid, 2,3,5,6-Tetrafluorophenyl Ester, 5-iosmer (Alexa Fluor® 488 5-TFP), acetonitrile (AcOH), dichloromethane

(DCM), N,N-dimethylformamide (DMF), and pyridine were purchased from Fisher Scientific (Waltham, MA). N-Fluorenylmethoxycarbonyl (Fmoc)-protected amino acids with the amine and side chain protected (Fmoc–Ala–OH, Fmoc–Arg(Pbf)–OH, Fmoc–Asn(Trt)–OH, Fmoc–Asp(OtBu)–OH, Fmoc–Glu(OtBu)–OH, Fmoc–Gly–OH, Fmoc–His(Trt)–OH, Fmoc–Leu–OH, Fmoc–Lys(Boc)–OH, Fmoc–Met–OH, Fmoc–Phe–OH, Fmoc–Ser(OtBu)–OH, Fmoc–Thr(OtBu)–OH, Fmoc–Val–OH) piperidine, N-hydroxybenzotriazole (HOBt), and O-benzotriazole-N,N,N',N'-tetramethyl-uronium-hexafluoro-phosphate (HBTU) were purchased from AAPPTec (Louisville, KY). Sulfuric acid and toluene were purchased from Macron Fine Chemicals (Center Valley, PA). Hydrogen peroxide was purchased from JT Baker (Austin, TX). Ammonium hydroxide and acetic anhydride were purchased from EMD (Darrnstadt, Germany). Triethylamine (TEA) was purchased from TCI America (Portland, OR). Ammonium iodide and cyanogen bromide were purchased from Acros Organics (Geel, Belgium). Water used in experiments was purified using a Millipore water purification system (Darmstadt, Germany) with a minimum resistivity of 18.0 MΩ•cm.

5.2.2 Modification of Controlled Pore Glass Substrates

Controlled pore glass substrates were treated with a piranha solution composed of H_2SO_4 (80%) and H_2O_2 (20%) (v/v) for 15 minutes. The substrates were rinsed several times with water and NH_4OH was added until the pH became basic. The CPG substrates were then treated with a Millipore water (QW) (70%), NH_4OH (15%), and H_2O_2 (15%) (v/v/v) solution for 10 minutes. The CPG substrates were washed several times with QW to remove any residual salts and then several times with methanol to remove residual QW. The CPG substrates were dried under reduced pressure and then placed in an oven at 150°C overnight to remove any trace water. After cooling to room temperature the CPG substrates were added to a solution of anhydrous toluene (90%) and GPTMS

(10%) (v/v) under nitrogen. Silination was performed at 80°C for 18 hours. The CPG substrates were then rinsed several times with anhydrous toluene, followed by DCM, and then dried under reduced pressure. The silanized CPG substrates were next added to a solution of tetraethyleneglycol diamine (2%) in anhydrous toluene (98%) (v/v) at 80°C for 18 hours. The CPG substrates were then rinsed several times with anhydrous toluene, followed by acetonitrile, and then dried under reduced pressure. Unreacted surface epoxide groups were deactivated by incubating in a solution of H_2SO_4 (0.1%) in QW (99.9%) (v/v) overnight. Finally, the CPG substrates were rinsed with water, methanol, and then dried under reduced pressure.

5.2.3 Synthesis of Combinatorial Peptide Library

Standard Fmoc-solid phase peptide synthesis was used to form an eight amino acid length library on a Titan 357 peptide synthesizer (AAPPTec, Louisville, KY). Amino acids possessing cationic, anionic, hydrophilic, hydrophobic, and aromatic properties were used to create the library including: arginine (R), histidine (H), lysine (K), aspartic acid (D), glutamic acid (E), serine (S), threonine, (T), asparagine (N), glycine (G), alanine (A), valine (V), leucine (L), and phenylalanine (F). One-bead-one-compound (OBOC) peptide libraries were constructed using a mix and split synthesis technique. CPG3000A substrates were evenly distributed into 13 reaction vessels (one per amino acid in the library) where the addition of one amino acid residue took place. The CPG substrates were then removed from all vessels, recombined, mixed, and evenly redistributed. This process was repeated eight times to create an 8-length amino acid library. Each CPG substrate contains one unique peptide sequence which can be screened for fouling properties. A common peptide linker (surface-MTRTET) was included at the base of each CPG substrate in order to facilitate peptide cleavage from the substrate and molecular weight identification by MALDI-TOF.

Coupling was performed in solutions containing 80 mM amino acid, 80 mM HBTU, 80 mM HOBt, and 160 mM DIPEA in DMF for two, consecutive 60 minute cycles. Following coupling, any unreacted amine groups were acetylated using acetic anhydride (5%), pyridine (5%), and DMF (90%) (v/v/v). Deprotection was performed using a 20% piperidine solution in DMF. All washing steps between deprotection and coupling were performed using DMF. Following peptide synthesis, the CPG substrates were rinsed with DCM and methanol, then dried under reduced pressure. Acid cleavable protecting groups for side chains were deprotected after synthesis using a solution of TFA (79%), bromotrimethylsilane (10%), thioanisole (10%), and phenol (1%) (v/v/v/v) for two hours. Finally, CPG substrates were rinsed with TFA, DCM, methanol, and then dried under reduced pressure.

5.2.4 Synthesis of Control Peptide Sequences

Several known control peptide sequences were synthesized on CPG3000A and CPG1000A beads. Coupling was performed using amino acid monomer, HBTU, HOBt, and DIPEA prepared in DMF in a molar ratio of 1.1:1:1:2 in six times excess of the loading capacity of the resin. All amino acid additions underwent double coupling. Following coupling, any unreacted amine groups were acetylated using acetic anhydride (5%), pyridine (5%), and DMF (90%) (v/v/v). Deprotection of Fmoc groups was achieved using 20% piperidine in DMF. All washing steps between deprotection and coupling were performed using DMF. Following peptide synthesis, the CPG substrates were rinsed with DCM and methanol, then dried under reduced pressure. Acid cleavable protecting groups for side chains were deprotected after synthesis using a solution of TFA (79%), bromotrimethylsilane (10%), thioanisole (10%), and phenol (1%) (v/v/v/v) for two hours. Finally, CPG substrates were rinsed with TFA, DCM, methanol, and then dried under reduced pressure.

5.2.5 Fmoc Loading Assay

Estimation of loading of the CPG substrate was determined using an Fmoc sensitive assay[138]. Approximately, 100-200 mg of dry, Fmoc–Met–OH loaded resin was weighed into a 20 mL scintillation vial and 2 mL of a 2% DBU in NMP solution (v/v) was added in order to cleave the Fmoc groups. The solution was swirled for 15 min and then diluted to 10 mL with AcOH. Next, 2 mL of this solution was taken and diluted to 25 mL. A reference solution was prepared in the same manner, but without the addition of resin. Cuvettes were loaded with 1 mL of solution and the absorbance was measured at 304 nm via a Cytation 3 multi-mode plate reader (BioTek, Winooski, VT). Fmoc loading of the resin can be estimated using the following equation:

$$\text{Fmoc loading } \left(\frac{\text{mmol}}{\text{g resin}}\right) = \frac{\left(\text{Absorbance}_{\text{sample}} - \text{Absorbance}_{\text{reference}}\right) \times 16.4}{\text{mg of dry resin}}$$

5.2.6 Screening of Combinatorial Library Utilizing Fluorescently Tagged Fibrinogen

Fluorescently labeled fibrinogen was prepared by conjugation with Alexa Fluor® 488 5-TFP. Briefly, 30 mg of fibrinogen was dissolved in 3 mL of 100 mM $NaHCO_3$, pH 9. This solution was added to a vial containing ~1 mg Alexa Fluor® 488 5-TFP. After 2 hours, the labeled conjugates were twice purified using 10 mL Bio-Gel P-6DG disposable size exclusion columns (Bio-Rad Laboratories, Hercules, CA).

Prior to fluorescent protein screening CPG substrates were rinsed several times with phosphate buffered saline (PBS). Next, CPG substrates were incubated in a 0.5 mg/mL solution of Alexa Fluor 488 labeled fibrinogen for two hours. After adsorption, CPG substrates were rinsed five times with PBS to remove unbound protein and quickly analyzed using a Zeiss LSM 510 (Jena, Germany) confocal microscope. Cross-sectional fluorescent images of the CPG substrates were

taken (X-Z plane) using a 488 nm argon laser for excitation and detecting an emission signal between 500-550 nm. In addition to combinatorial CPG substrate analysis, several controls of known low and high fouling sequences were evaluated in parallel.

5.2.7 Evaluation of Peptide Sequences via PED and MALDI-TOF

Peptide sequence determination was performed using partial Edman degradation (PED) and matrix-assisted laser desorption/ionization time-of-flight mass spectrometry (MALDI-TOF). CPG substrates were subjected to partial Edman degradation to form segmented versions of the peptide sequence on the same CPG substrate. PED degradation can be performed without cleaving the peptide sequences from the CPG substrate allowing the reaction to be performed on groups of CPG substrates. The PED degradation takes place in small reaction vessels fitted with a porous glass frit to facilitate solvent removal between steps.

For each cycle of partial Edman degradation CPG substrates were first rinsed with pyridine followed by a 2:1 (v/v) pyridine/water solution containing 0.1% triethylamine. Then the CPG substrates were suspended in a 160 µL aliquot of 2:1 (v/v) pyridine/water solution containing 0.1% triethylamine. A degradation reagent mixture containing 583 mM PITC and 9-16 mM Fmoc-OSU was prepared in pyridine (ratio of PITC/Fmoc-OSU ~65-36:1). A 172 µL aliquot of this mixture was added to the pyridine/water solution containing 0.1% triethylamine and the reaction was allowed to proceed for 6 minutes at room temperature with intermittent stirring. The solution was then drained and the CPG substrates were washed with anhydrous pyridine, anhydrous dichloromethane, and anhydrous TFA. Next, the CPG substrates were treated twice with anhydrous TFA at room temperature for 6 min each to cleave the PITC bound amino acids. Chains that were bound with an Fmoc group remain protected from degradation for the entirety of the procedure. CPG substrates

were then washed extensively with dichloromethane and then pyridine. This PED procedure was repeated for $n - 1$ times, where n is the number of residues to be sequenced.

After PED degradation, Fmoc groups added to the amine terminus of peptide chains and Fmoc groups added to the side chains during the protocol were removed by 20% piperidine in DMF (v/v). CPG substrates were rinsed with DCM and methanol and the solvent was evaporated under reduced pressure. Next, CPG substrates were suspended in 1 mL of TFA containing 20 μL dimethyl sulfide, and 50 mg ammonium iodide for 20 minutes to reduce any oxidized methionine. CPG substrates were then washed with copious amounts of water and methanol to remove any remaining ammonium iodide. Finally, individual CPG substrates were manually transferred into vials for cleavage such that each vial contains one CPG substrate. Cleavage from the CPG substrate was achieved using 10 μL of a 40 mg/mL cyanogen bromide in 70% TFA/30% H_2O (v/v) solution in the dark. After overnight cleavage, the cleavage solution was removed under reduced pressure. The remaining peptide residue was dissolved in 2 μL of MALDI matrix solution (60 mg/mL alpha-cyano-4-hydroxycinnamic acid matrix dissolved in 1:1 acetonitrile to water with 0.1% TFA), mounted on a stainless steel MALDI plate, and analyzed via MALDI-TOF.

5.3 Results and Discussion

5.3.1 Traditional Polymer Resins Result in Salting Out Effect

From previous work it was determined that traditional peptide resins were unsuitable for low fouling peptide screening. When charged peptide sequences were synthesized on traditional resins, such as TentaGel, salting out of the fluorescent screening proteins occurred within the polymer scaffold in the presence of highly charged peptide sequences[47] (Figure 5-2a). TentaGel resin is composed of a polystyrene matrix containing a PEG spacer from which peptide sequences are

synthesized. The swelling ratio of TentaGel in DMF is 5 mL/g and the swelling ratio of TentaGel in water is 3.6 mL/g[162]. If highly charged peptides are synthesized on the resin then fluorescently labeled proteins will salt out into the resin and become trapped during screening. This salting-out effect is due to the attraction of water molecules to charged species (in this case EK peptide), which decreases the number of water molecules available to interact with other species (in this case fibrinogen). As a result of the increased demand for solvent molecules, the protein-protein interactions exceed the solvent-solute interactions and the protein molecules precipitate out[163]. In fact, high concentrations of amino acids have been reported to salt-out proteins such as egg albumin[164], carboxyhemoglobin[164], fibrinogen[165,166], and antihemophilic factor[167]. In addition, the presence of hydrophobic polystyrene in the resin most likely contributes to the precipitation of protein into the resin.

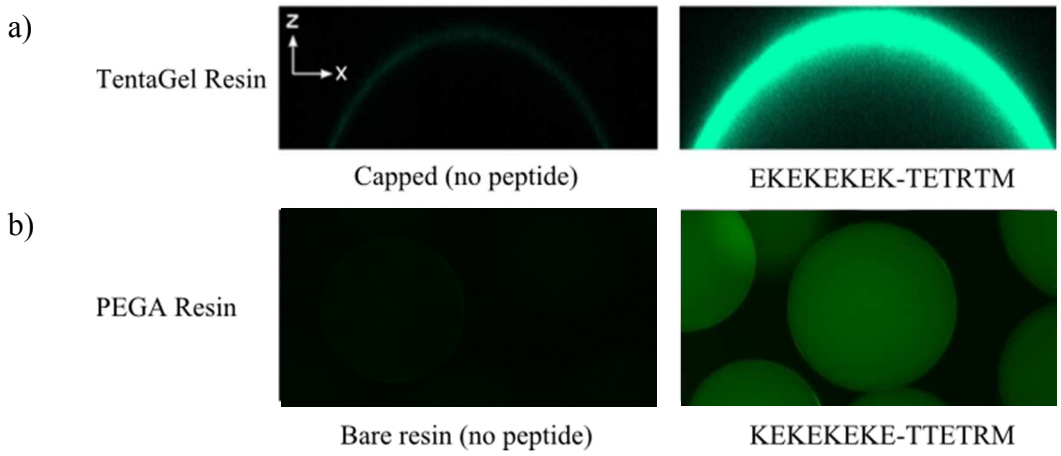

Figure 5-2. Salting out effect of fluorescently labeled fibrinogen in traditional polymer resins.
(a) Confocal image of TentaGel Resin containing a capping agent with no peptide (left) and EKEKEKEK-TETRTM-TentaGel (right) after screening with fluorescently labeled fibrinogen. (b) Fluorescence microscope image of PEGA resin containing no peptide (left) and KEKEKEKE-TTETRM-PEGA (right) after screening with fluorescently labeled fibrinogen.

In order to prevent the salting out effect of TentaGel Resin, a PEGA resin was also tested. PEGA resins consist of dimethyl acrylamide and mono-2-acrylamidoprop-1-yl[2-aminoprop-1-yl]

poly(ethylene glycol) cross-linked with bis 2-acrylamidoprop-1-yl poly(ethylene glycol)[168]. These resins swell much more extensively than TentaGel with a swelling ratio of 11 mL/g in DMF and a swelling ratio of 16 mL/g in water[162]. In addition, they lack the hydrophobic polystyrene present in TentaGel. They are permeable to macromolecules up to 35 kDa and are commonly used for on-resin enzyme assays. To determine if PEGA resin would show improvement over TentaGel, bare resin containing no peptide and resin containing KEKEKEKE-TTETRM-PEGA were exposed to 0.5 mg/mL of fluorescently labeled fibrinogen. After extensive rinsing in PBS, samples were evaluated under a fluorescent microscope. While, the salting-out effect was reduced compared to TentaGel resin, there was still indication of the salting-out of fibrinogen occurring (Figure 5-2b). This confirms that traditional polymer resins are an unsuitable substrate for screening low fouling peptides.

5.3.2 Development of CPG Substrate for Nonspecific Screening

To prevent the interference of complex adsorption events a rigid surface scaffold was selected to remove background effects. To allow for sequence recovery after screening a balance was needed between a rigid scaffold and a high surface area. Controlled pore glass (CPG) substrates containing a diameter of ~150 μm and pores of 300 nm (±10%) (CPG-3000A) and substrates containing a diameter of ~150 μm and pores of 100 nm (±10%) (CPG-1000A) were selected. The selection was based on the criteria that the substrates should have sufficient surface area to synthesize adequate amounts of peptide for sequence recovery and possess pores large enough to prevent protein entrapment during screening. In theory, this platform should provide enough peptide per individual CPG substrate to be within the detection range of the MALDI-TOF instrument.

The CPG substrates were modified with amines in order to allow for standard Fmoc-solid phase peptide synthesis (Figure 5-3). This was accomplished by modification with an epoxy silane, followed by a tetraethylene glycol diamine linker. A four spacer ethylene glycol linker was used as an alternative to shorter diamines in order to improve amino acid coupling[169]. Peptides were then synthesized from the amine groups utilizing standard solid phase peptide synthesis.

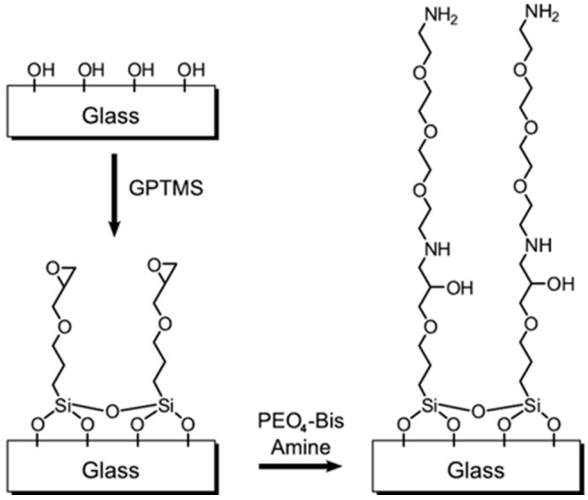

Figure 5-3. Surface modification of glass substrate for peptide synthesis.
After cleaning, controlled pore glass substrates were modified with GPTMS to introduce a monolayer of epoxide groups to the surface. Next, the epoxide surface was exposed to PEO_4-Bis Amine to attach reactive amine groups needed for peptide synthesis. Finally, peptides were grown using standard Fmoc solid phase peptide synthesis.

To verify that the salting-out effect was not occurring on the CPG substrate, a control low fouling EK peptide sequence was synthesized on both CPG1000A and CPG3000A substrates and compared to a hydrophobic fouling control. On both CPG3000A (Figure 5-4a) and CPG1000A (Figure 5-4b) substrates there was no evidence of a salting-out effect occurring. As expected, substrates containing high fouling surfaces displayed high fluorescence and substrates containing EK peptide displayed low fluorescence.

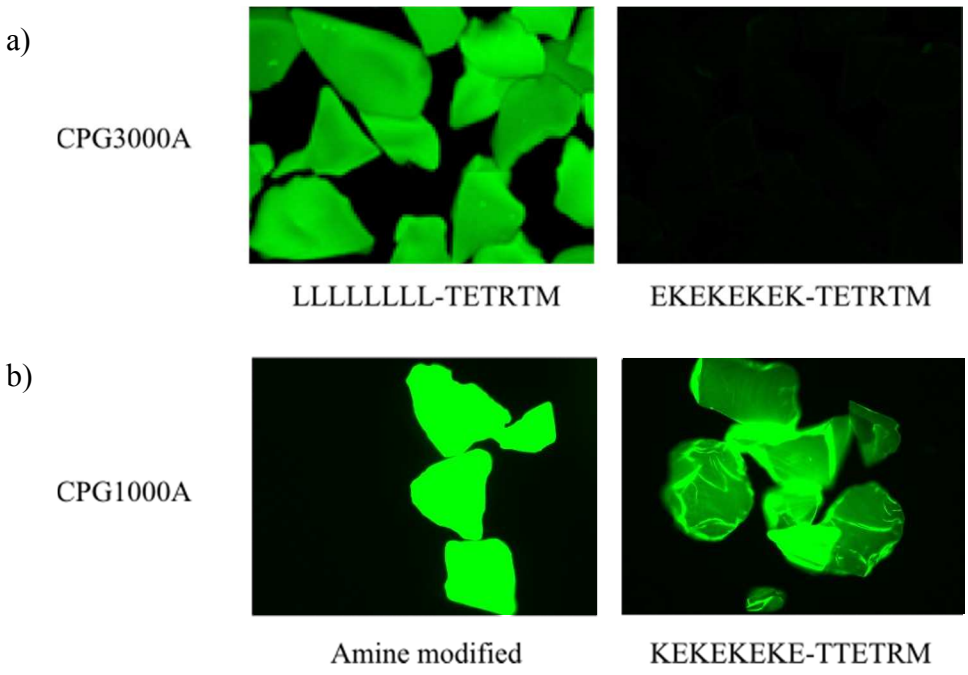

Figure 5-4. Protein screening of CPG substrates.
(a) Fluorescence microscope image of CPG3000A containing a high fouling LLLLLLLL-TETRTM-CPG3000A sequence (left) and a low fouling EKEKEKEK-TETRTM-CPG3000A peptide (right) after screening with fluorescently labeled fibrinogen. (b) Fluorescence microscope image of CPG1000A containing a high fouling amine modified CPG1000A substrate (left) and a low fouling KEKEKEKE-TTETRM-CPG1000A peptide (right) after screening with fluorescently labeled fibrinogen.

5.3.3 Evaluation of Fibrinogen Fouling on Control Sequences via Confocal Microscopy

Control peptide sequences possessing known low fouling and high fouling properties were synthesized and screened as controls to validate the proposed screening method (Figure 5-5a). The sequence KEKEKEKE-TETRTM-CPG3000A was used as a low fouling control and the sequence FFFFFFFF-TETRTM-CPG3000A was used as a high fouling control. The peptide sequence TETRTM is included as a linker. CPG substrates were exposed to 0.5 mg/mL fluorescently labeled fibrinogen for two hours and then rinsed extensively with PBS. Evaluation of fouling was conducted using confocal microscopy. By integrating the fluorescence signal across the surface of the CPG substrate a numerical value can be assigned to each sequence. The fluorescence intensity of the low fouling glutamic acid/lysine (EK) surface was 2,279 and the fluorescence intensity of the high

fouling phenylalanine (F) surface was 80,890 (Figure 5-5b). The inclusion of known sequences in addition to sequences from the library is important since absolute measurements of fouling cannot be obtained. Only values relative to known low fouling sequences that have simultaneously gone through the screening can be identified.

a)

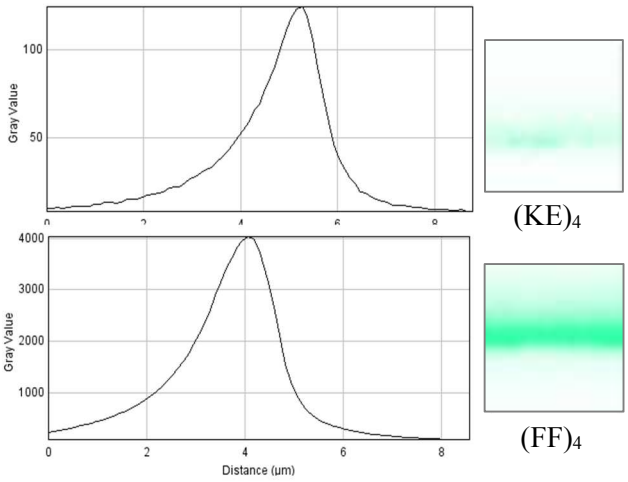

b)

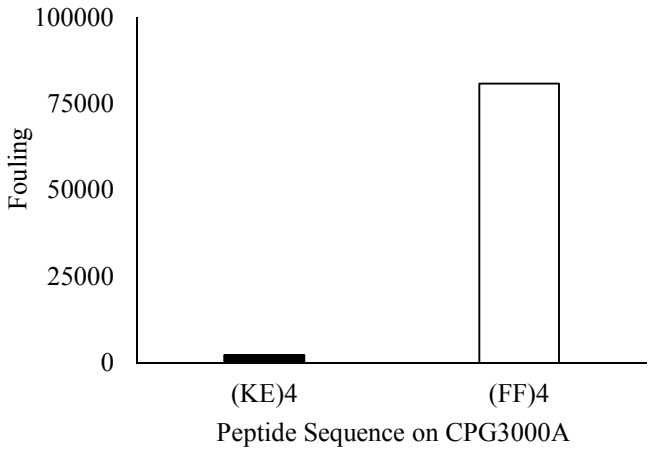

Figure 5-5. Protein screening of known low and high fouling peptide sequence controls.
Confocal microscopy analysis of fluorescence screening to known sequences KEKEKEKE-TETRTM-CPG3000A (low fouling) and FFFFFFFF-TETRTM-CPG3000A (high fouling). Intensity of fluorescence is analyzed via integration of the signal through the CPG substrate.

5.3.4 Design of Combinatorial Peptide Library

After development of a suitable substrate platform for screening, a combinatorial peptide library was developed. A selection of 13 amino acids containing cationic, anionic, hydrophilic, hydrophobic, and aromatic residues was used to synthesize the combinatorial library including: arginine (R), histidine (H), lysine (K), aspartic acid (D), glutamic acid (E), serine (S), threonine, (T), asparagine (N), glycine (G), alanine (A), valine (V), leucine (L), and phenylalanine (F) (Figure 5-6). Several amino acids needed to be excluded due to limitations of the PED/MALDI-TOF technique. Proline (P) was avoided due to its incompatibility with partial Edman degradation. Cysteine (C) was not used due to its ability to form disulfide bonds. MALDI-TOF cannot discriminate between amino acids of the same molecular weight. There are two instances where this occurs: glutamine (Q) and lysine (K) both have a molecular weight of 146 g/mol and leucine (L) and isoleucine (I) both have a molecular weight of 131 g/mol. Since glutamine (Q) is chemically similar to asparagine (N), it was excluded. Similarly, isoleucine (I) was also excluded. Tryptophan (W) and tyrosine (Y) were excluded due to difficulty in synthesis and their possession of reactive protecting groups that can cause undesired side reactions. Finally, methionine (M) was left out because the thioester side group interferes with the final peptide cleavage.

For all sequences synthesized a known peptide linker was first added to all CPG substrates. The linker consisted of *surface*-methionine-threonine-arginine-threonine-glutamic acid-threonine-NH_2 (surface-MTRTET-NH_2). The inclusion of a linker serves two purposes: 1) provides additional molecular weight to the peptide required for detection by MALDI-TOF and 2) the methionine at the peptide base is used to cleave the peptide from the CPG substrate upon exposure to cyanogen bromide[170]. In the future, modification of the linker to avoid having a threonine (T) residue directly following the methionine (M) would prove beneficial to improve cleavage of peptide from the resin.

Cyanogen bromide induced bond cleavage at a methionine residue has an efficiency of greater than 90%, except in situations where a serine (S) or threonine (T) residue follows methionine (M) in the amino acid sequence[171].

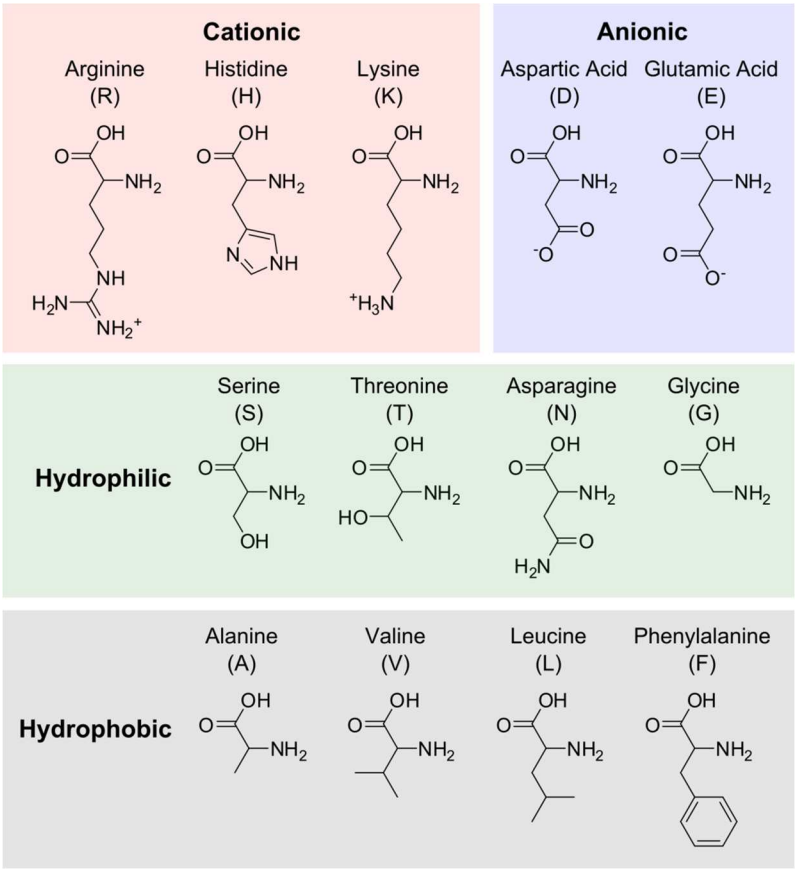

Figure 5-6. Natural amino acids used to create combinatorial library.
Cationic, anionic, hydrophilic, hydrophobic, and aromatic amino acid residues were used to create an 8 length amino acid combinatorial peptide library on the CPG3000A substrate.

To verify successful synthesis of the peptide library, eight CPG3000A substrates were randomly selected for cleavage from the resin and analyzed by MALDI-TOF (Figure 5-7). Expected molecular weights of cleaved peptides in the library range from 1144.4 (GGGGGGGG-TETRTM) to 1937.5 (RRRRRRRR-TETRTM). Out of eight selected beads for cleavage, six showed a single peptide peak indicating successful synthesis of the library (Figure 5-7a-f). Two beads had no signal in the expected peptide library range (Figure 5-7g-h).

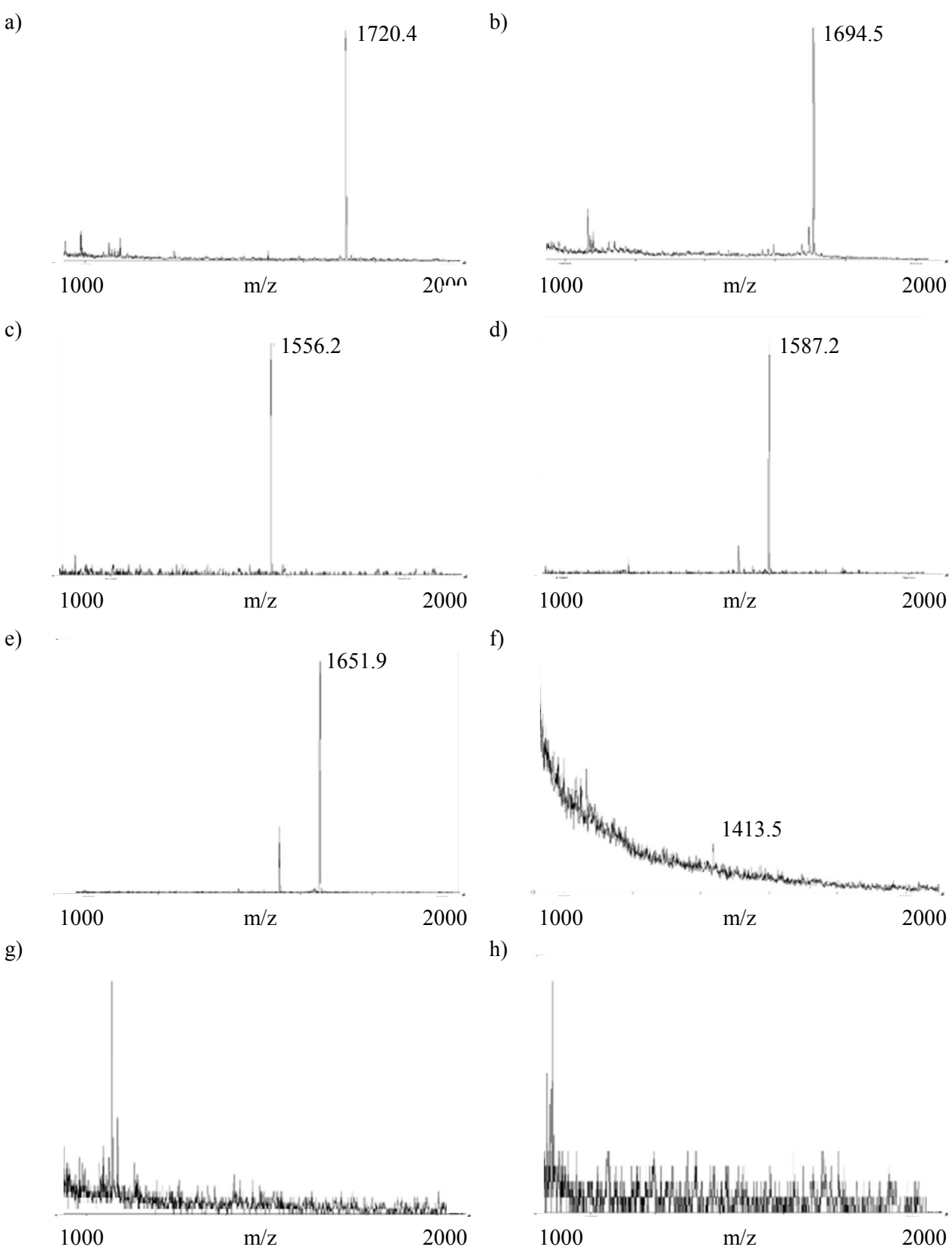

Figure 5-7. MALDI evaluation of single CPG3000A substrates from combinatorial library.
(a)-(h) Cleavage of peptide from single CPG3000A substrates selected randomly from the library.

5.3.5 Combinatorial Peptide Library Screening with Fluorescently Labeled Fibrinogen

Using a mix and split technique in combination with Fmoc solid phase peptide synthesis, a diverse library of CPG substrates was created with varying degrees of fouling (Figure 5-8a). Several sequences with lower fouling than the EK sequence were identified through confocal microscopy. After screening 100 randomly selected CPG substrates, in addition to three known fouling peptide controls (leucine, glycine, glutamic acid/lysine), 37% of the library was found to have lower fouling than ultra-low fouling glutamic acid/lysine (Figure 5-8b).

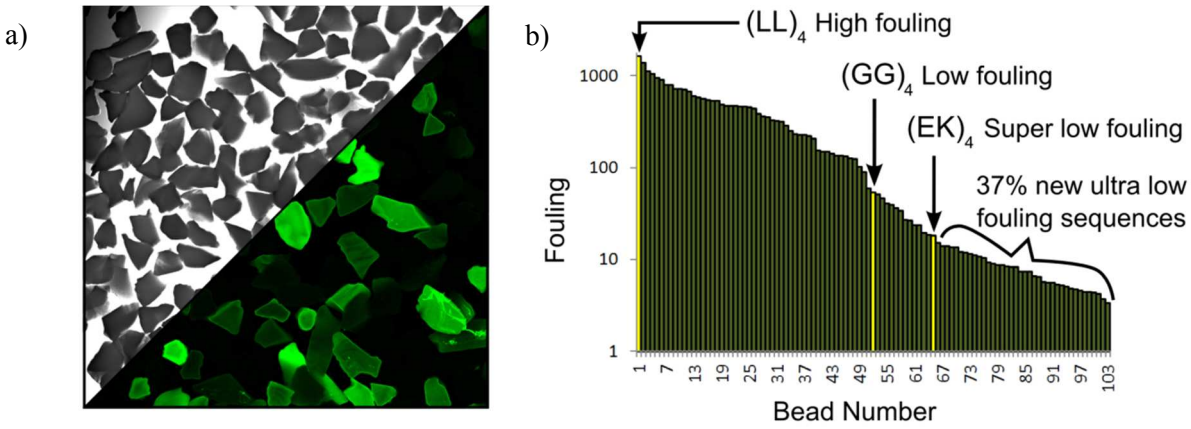

Figure 5-8. Fluorescent protein screening of combinatorial peptide library.
(a) Bright field image of glass substrate used for combinatorial synthesis (top). Fluorescence screening of combinatorial peptide library to Alexa Fluor 488 labeled fibrinogen (bottom). (b) Through integration of fluorescent signal across the CPG substrate, numerical values can be assigned to each sequence. This is fouling data for 100 randomly selected CPG substrates and three known control sequences (LLLLLLLL-TETRTM-CPG3000A, GGGGGGGG-TETRTM-CPG3000A, and EKEKEKEK-CPG3000A). 37% of the library is found to have lower levels compared to EKEKEKEK-CPG3000A.

In the future, the screening method can potentially be improved by adding a fluorescently labeled positively charged protein to the procedure. Currently, only a negatively charged protein is used for screening which may bias the screening to select for negatively charged peptides. To implement the use of different charged proteins for screening, most likely two separate screening steps would need to be performed to prevent precipitation of proteins out of solution.

5.3.6 Peptide Sequence Recovery via PED and MALDI-TOF

Following protein adsorption screening of the library and selection of low fouling CPG substrates via confocal microscopy, the peptide sequences must be recovered. Partial Edman degradation (PED) can be used to break down the peptide into shorter chains[172]. Following cleavage of segmented peptides from a single CPG substrate, MALDI-TOF can be used to identify a molecular weight for each degradation product from PED. The differences between peaks found in the MALDI-TOF spectra correspond to the amino acid sequence[173].

PED was performed on random CPG3000A substrates selected from the eight-residue peptide combinatorial library. Ten substrates were pulled out after 2, 4, 6, and 8 cycles of PED were performed. These CPG substrates were then cleaved to recover peptide and evaluated with MADLI-TOF. After 2 cycles of PED all ten substrates showed identifiable peptide peaks corresponding to the first amino acid residue of the sequence. However, after 4 cycles of PED only one substrate out of ten displayed a clearly identifiable peptide sequence (Figure 5-9). No identifiable peptide sequences were recovered after 6 and 8 cycles of PED. Even after optimizing the PED procedure the signal was not able to be improved indicating that there is not enough mass present on one individual substrate to reliably recover the peptide sequence.

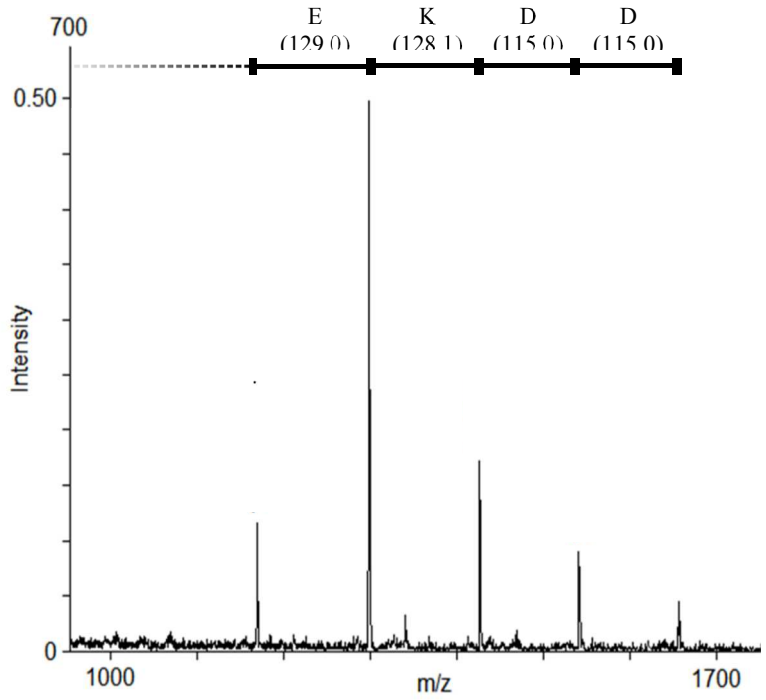

Figure 5-9. MALDI-TOF of randomly selected CPG3000A substrate from library after 4 cycles of PED.

To improve the peptide sequence recovery procedure a new substrate needed to be selected that met the following conditions: 1) enough mass on one substrate to obtain sufficient signal for MALDI-TOF, 2) rigid substrate to prevent salting-out of the screening protein, and 3) large enough pore sizes to prevent entrapment of screening protein. A CPG substrate containing smaller pore sizes (1000 Å) was tested in order to increase the surface area available for peptide synthesis, but to maintain a rigid substrate. Control peptide sequences containing varying hydrophobic properties were synthesized to evaluate the CPG1000A substrate. The following sequences were synthesized: NEKSGRDH-TTETRM-CPG1000A (Control A), DAKTGRLG-TTETRM-CPG1000A (Control B), and NAVSGTLG-TTETRM-CPG1000A (Control C). In addition to changing the substrate, the linker was also modified in order to avoid a threonine (T) directly following the methionine (M) residue, which can significantly impede cleavage of the peptide sequence[171].

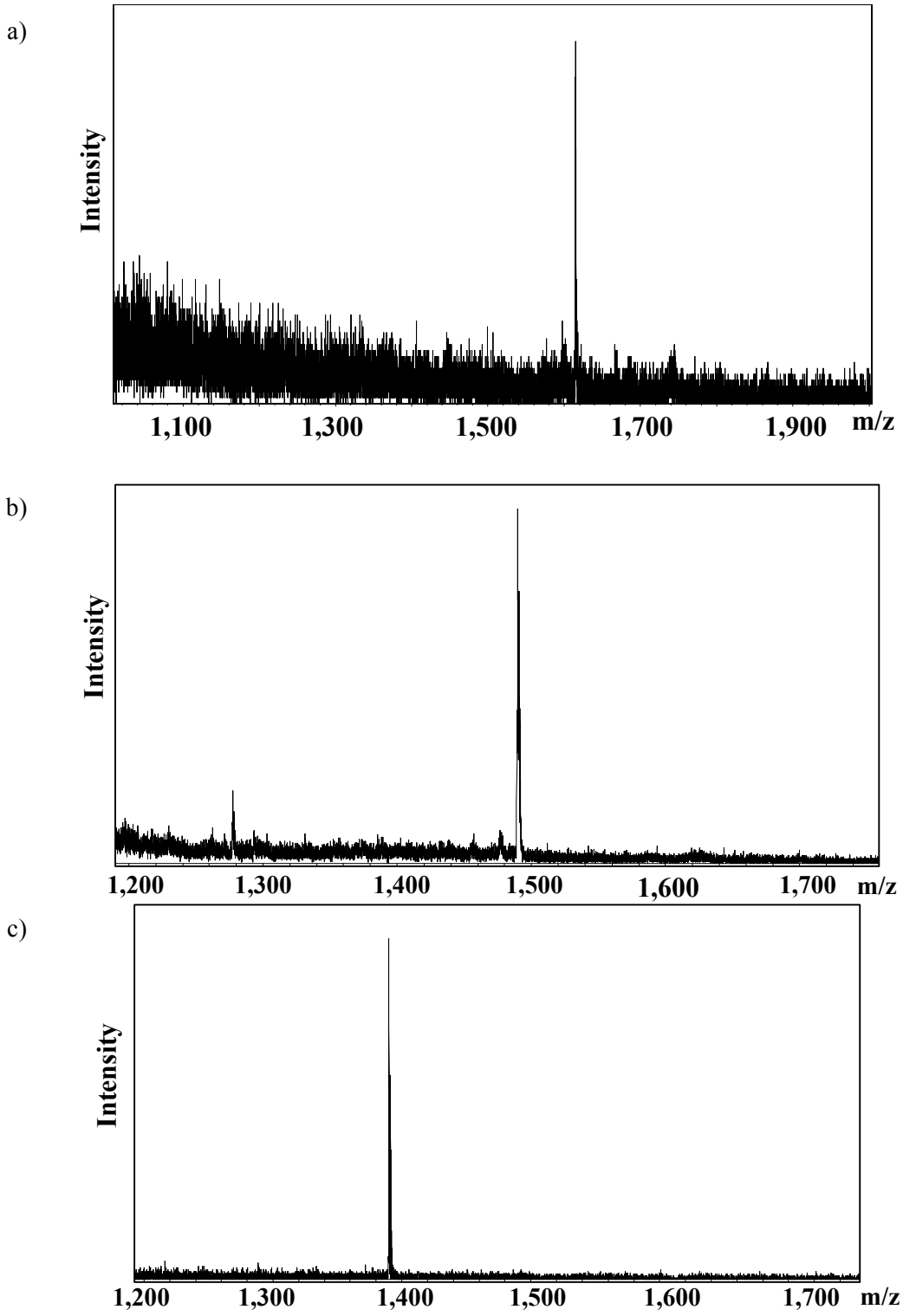

Figure 5-10. MADLI-TOF spectra of single substrate cleavage of control peptide sequences. MALDI-TOF of control peptide sequences cleaved from a single CPG1000A substrate. (a) Control A, NEKSGRDH-TTETRM-CPG1000A (MW: 1611.9) (b) Control B, DAKTGRLG-TTETRM-CPG1000A (MW: 1486.9) (c) Control C, NAVSGTLG-TTETRM-CPG1000A (MW: 1387.8).

Control peptide sequences were successfully synthesized and high signal is achieved when peptide is cleaved from a single CPG1000A substrate (Figure 5-10).

Following verification of correct sequences for control peptide sequences, 3 cycles of PED was performed to determine if there is sufficient mass for peptide sequence recovery. Groups of 50, 10, 5, and 1 CPG1000A substrates were cleaved and analyzed by MALDI-TOF. Good signal was obtained for groups of down to 5 beads, however, single CPG1000A substrates did not possess enough signal to be observed by MALDI-TOF. Representative MALDI-TOF spectra are shown for groups of 5 beads for all three control sequences after 1, 2, and 3 cycles of PED (Figure 5-11). While the signal has improved compared to the CPG3000A substrates and the overall quality of the MALDI-TOF spectra after PED have improved, there is still not enough mass present on one CPG1000A substrate for robust recovery of the peptide sequence.

In the future, a platform that can have more mass per individual substrate is needed. Once a suitable platform is identified a new library can be generated and screened. In addition to finding a new platform, there are several parameters that can affect the quality of the partial Edman degradation procedure and optimization should be performed for the platform selected. The most important parameter affecting the results of the degradation is the ratio of Fmoc-OSU to PITC[173,174]. This ratio determines which chains will be capped and which chains will be degraded on a single CPG substrate. Chains that are capped with an Fmoc-OSU group will be shielded from degradation. If the ratio of Fmoc-OSU is too high then there will not be enough uncapped chains remaining to degrade the peptide completely to the linker. Conversely, if the ratio of PITC is too high then all the chains will be degraded too quickly. The PED procedure needs to be consistent and work every single time for a variety of peptide sequences to have successful recovery of peptide sequences.

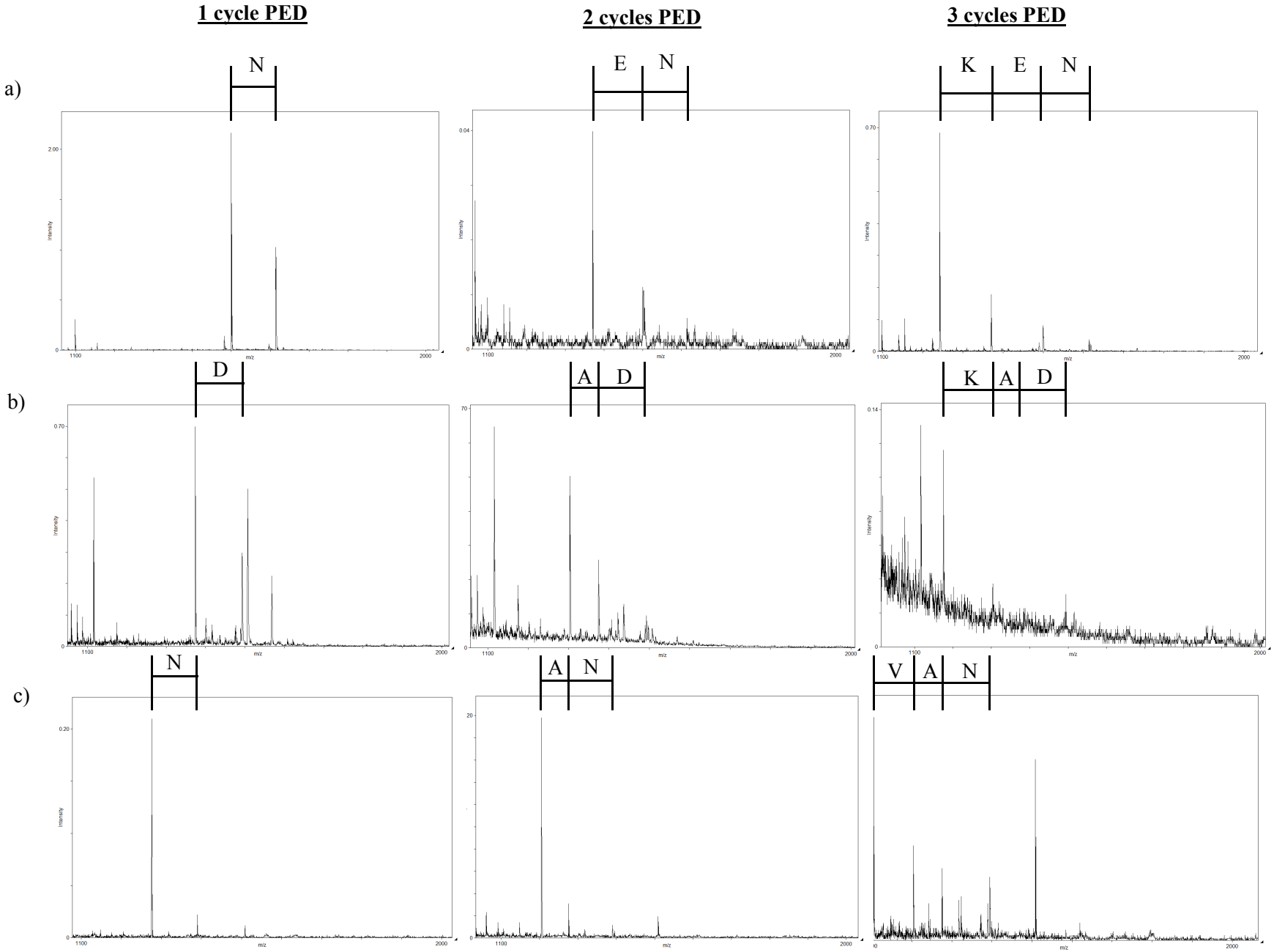

Figure 5-11. MADLI-TOF of control peptide sequences from groups of 5 CPG1000A substrates after 1, 2, and 3 cycles of PED.
(a) Control A, NEKSGRDH-TTETRM-CPG1000A (b) Control B, DAKTGRLG-TTETRM-CPG1000A (c) Control C, NAVSGTLG-TTETRM-CPG1000A.

In addition to performing PED successfully, the MALDI spotting method needs to be optimized in order to maximize the signal. Since we are analyzing peptide from a single CPG substrate, the signal is much closer to the detection limit of the instrument and is more difficult to analyze compared to signal from traditional peptide resins which contain much higher concentrations of peptide. Parameters influencing MALDI signal include the matrix solution composition, the rate of matrix crystal growth, matrix additives, and contamination products[175–177].

5.3.7 Fmoc Loading Assay to Evaluate Future CPG Substrates

An Fmoc loading assay was performed on CPG1000A and CPG3000A substrates to quantitatively measure how much peptide is loaded on the substrate. CPG1000A substrates were determined to have a loading of 0.0074 mmol per gram of substrate, which translates to an average of 580 fmol of peptide per substrate after 8 PED cycles. Conversely, CPG3000A substrates were determined to have a loading of 0.026 mmol per gram of substrate, corresponding to an average of 6,516 fmol peptide per substrate after 8 PED cycles. These loading values were compared to the loading of TentaGel resin which is 10,926 fmol peptide per each resin bead (Figure 5-12). The CPG3000A substrate was found to have 5 ± 2% of the loading capacity of TentaGel, whereas the CPG1000A substrate was found to have 60 ± 2% of the loading capacity of TentaGel.

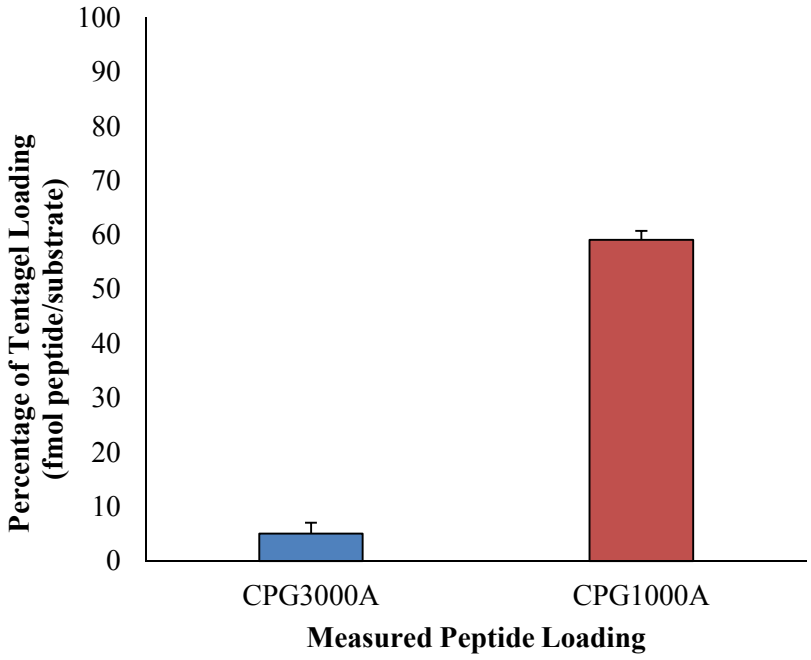

Figure 5-12. Measured peptide loading on CPG3000A and CPG1000A substrates.
Measured peptide loading of CPG3000A (blue) and CPG1000A (red) substrates normalized to the peptide loading of TentaGel resin.

While the loading of peptide on the CPG1000A substrate seems reasonable, we were unable to successfully perform PED. The actual number of peptides recovered per substrate may be lower due to incomplete cleavage of methionine from the residue, losses of peptide due to volume transfers and test tube surfaces, and overestimation of the substrate volume of one CPG unit. In the future, a platform with more peptide mass per substrate unit is needed. The Fmoc loading assay and control peptide sequences described here can be a robust first step in identifying a suitable platform.

5.4 Conclusions

A new combinatorial screening method utilizing controlled pore glass substrates was explored to screen for low binding peptide sequences. Known control peptide sequences were synthesized and evaluated to validate the new screening platform. Following platform validation, a combinatorial

library was created and screened for nonfouling activity. Several nonfouling sequences containing lower binding levels than previously known low fouling sequences were discovered. PED and MALDI-TOF techniques were developed to recover low fouling peptide sequences from the screening. It was determined that mass limitations prevented successful recovery through PED on a single substrate. Alternative platforms were evaluated for library screening including PEGA resin and CPG substrates with varying pore sizes. Future criteria for a successful substrate platform were identified: 1) a rigid substrate 2) sufficient mass per substrate for MALDI-TOF 3) large enough pore sizes to prevent protein entrapment. Identification of a suitable platform would allow recovery of low fouling peptide sequences leading to the examination of properties that characterize low fouling peptides. If sufficient low fouling sequences are identified then structure-property quantity relationships can be established. Mechanistic insight and a deeper fundamental understanding of low fouling mechanisms can be gained from this work. The identification of new low fouling sequences can provide novel insights into the fundamental understanding of molecular-level nonfouling mechanisms and the development of new nonfouling materials.

Chapter 6: Zwitterionic Mucus-Penetrating Particles

Mucosal barriers pose a challenge for drug delivery due to the sticky, hydrophobic nature of mucus and its rapid turnover rate in the body. A particle that could efficiently penetrate the mucosal barrier and provide uniform and longer delivery would greatly improve therapeutic approaches for a number of diseases. Zwitterionic and mixed charged materials have already been shown to have excellent low fouling properties when applied to the surfaces of nanoparticles. In this work, we explore the use of poly(carboxybetaine acrylamide) and poly(sulfobetaine methacrylate) zwitterionic polymers to coat dye-loaded polystyrene particles. Both graft-to and graft-from polymer synthesis is explored for forming zwitterionic coated particles. The stability of particles is evaluated via dynamic light scattering and zeta potential measurements in phosphate buffered saline and single protein solutions. Particle tracking experiments are performed in synthetic mucus to evaluate the effectiveness of the zwitterionic polymer coating on the mucus penetration capabilities of the particles. Particles coated with poly(sulfobetaine methacrylate) display mucus-penetrating properties.

6.1 Introduction

The development of systems that can penetrate mucosal barriers in the human body, such as those of the lung airways, gastrointestinal tract, female reproductive tract, nose, and eye, can have many relevant biomedical applications such as drug delivery[49], gene therapy[50], and vaccination[51]. A method that could provide more uniform and longer lasting delivery to mucosal surfaces can greatly improve therapeutic approaches for a number of diseases including sexually transmitted infections, cystic fibrosis, chronic rhinosinusitis, inflammatory bowel disease, and glaucoma[48]. However, penetration of mucosal barriers is difficult due to the efficient trapping and removal of foreign

particles and hydrophobic molecules by the human body[178,179]. Mucus is a sticky, viscoelastic layer that is composed of cross-linked and entangled mucin fibers coated with a diverse array of proteoglycans[180]. Mucus forms adhesive interactions with introduced particulates via hydrophobic, electrostatic, and hydrogen bonding interactions[48]. In addition to the challenging chemical environment of mucus, the mucosal layer in the body is continuously secreted, then shed and discarded or digested and recycled. The mucosal turnover rate varies from several minutes to hours depending on the location in the body providing another obstacle to efficient delivery[48].

Two strategies to overcome the mucosal barrier include mucoadhesion and mucopenetration. Mucoadhesive systems focus on enhancing the association of particles to the mucus layer in order to slow particle transit time to the time scale of mucus renewal, thereby enhancing drug absorption[181]. Common biomaterials used to make mucoadhesive particles include chitosan[182], poly(ethylene glycol)[183], derivatives of poly(acrylic acid)[184], poly(methacrylates)[185], and poly(sebacic acid)[186]. These particles achieve mucoadhesion via electrostatic interaction, hydrogen bonding, polymer entanglement, hydrophobic interactions, or a combination of these mechanisms. Although mucoadhesion can increase the bioavailability of drugs delivered there are several important fundamental limitations. Since mucoadhesive systems are bound to the mucus layer the transit time of these systems is determined by the physiological turnover time of the mucus layer[48]. In addition, mucoadhesive systems are incapable of penetrating across the mucus layer and are unsuitable for applications requiring intracellular delivery to the underlying epithelial cells.

To overcome the limitations of mucoadhesive systems, there has been an interest in developing mucus-penetrating particles (MPP) that can avoid adherence to mucus and diffuse through the low viscosity pores without steric obstruction. Norris et al. observed the transport of surface-modified carboxyl, sulfate, and amidine nanoparticles. Despite the slow transport of all

particles, the most hydrophilic surface (amidine) was found to have the fastest transport[187]. Sakuma et al. studied nanoparticles containing surface poly(*N*-isopropylacrylamide), poly(*N*-vinylacetamide), poly(vinylamine), and poly(methacrylic acid) chains and observed increased mucoadhesion for all nanoparticles except poly(*N*-vinylacetamide)[188]. The most successful MPP particles developed up to date are particles containing a high density of low molecular weight poly(ethylene glycol) (PEG)[49,189]. In addition, mixed charge peptide materials[190] and mixed charge polymers[191] have also been shown to possess mucus-penetrating properties.

An alternative approach to using PEG for mucus-penetrating particles would be to use zwitterionic materials. Polymers containing zwitterionic moieties such as carboxybetaine and sulfobetaine have already been shown to resist interactions in complex environments such as whole blood, tissue, and marine environments[15]. Carboxybetaine polymers possess increased resistance to protein adsorption when compared with traditionally used PEG and can be functionalized easily through the use of the carboxylic acid side chain. Previously, poly(carboxybetaine acrylamide) (polyCBAA) was shown to be an ultra-stable and functionalizable coating for gold nanoparticles in undiluted blood serum[93]. Nature has already employed the concept of zwitterionic materials to cross the mucus layer. Many viruses that are known to penetrate the mucosal barrier including poliovirus, Norwalk virus, and human papilloma virus (HPV), are densely coated with both positively and negatively charged groups on the surface, while maintaining a net neutral charge[192].

In this work, we explore the use of a zwitterionic coated particle for mucus penetration. Fluorescently labeled carboxylate-modified polystyrene particles are coated with zwitterionic polymers utilizing either a graft-to or graft-from approach. Coated particles are characterized by dynamic light scattering (DLS) and zeta potential (ZP). In addition, stability of particles in PBS and single protein solutions of fibrinogen and lysozyme was tested. A synthetic mucus formulation was

used to perform particle tracking experiments and to assess mucus penetration properties. Poly(sulfobetaine methacrylate) (SBMA) coated particles are shown to have mucus-penetrating properties.

6.2 Experimental Methods

6.2.1 Materials

2% (w/v) FluoSpheres® carboxylate-modified microspheres, 0.1 μm, yellow-green fluorescent (505/515) were purchased from Invitrogen (Carlsbad, CA). Copper (I) bromide (99.999%), copper (II) bromide (>99.0%), 2-bromoisobutyryl bromide, t-Boc-aminoethyl alcohol, 2,2'-bipyridine (Bpy), Tween20 detergent, bovine plasma fibrinogen, chicken lysozyme egg white, dried porcine gastric mucin type III, imidurea, methylparaben, propylparaben, sodium borate, sodium bicarbonate ($NaHCO_3$), magnesium sulfate, diethyl ether, tetrahydrofuran (THF), methanol (MeOH), [2-(methacryloyloxy)ethyl]-dimethyl-(3-sulfopropyl)-ammonium hydroxide (SBMA monomer) and phosphate buffered saline (PBS, 0.01 M phosphate, 0.138 sodium chloride, 0.0027 M potassium chloride, pH 7.4) were purchased from Sigma Aldrich (St. Louis, MO). N-(3-Dimethylaminopropyl)-N'-ethylcarbodiimide hydrochloride (EDC), sulfo-N-hydroxysuccinimide (sulfo-NHS), and 2-(N-morpholino)ethanesulfonic acid (MES) were purchased from Acros Organics (Geel, Belgium). Sodium hydroxide (NaOH) and trifluoracetic acid (TFA) were purchased from EMD (Darmstadt, Germany). SupercolU guar gum was kindly donated by Hercules (Wilmington, DE). Triethylamine (TEA) was purchased from TCI America (Portland, OR). Dichloromethane (DCM) was purchased from Fisher Scientific (Waltham, MA). Methoxyl PEG Amine (5kDa) was purchased from NanoCS (New York, NY). (3-Acryloylamino-propyl)-(2-carboxy-ethyl)-dimethyl-ammonium (CBAA monomer) was synthesized as previously reported[93]. Water used in experiments

was purified using a Millipore water purification system (Billerica, MA) with a minimum resistivity of 18.0 MΩ•cm.

6.2.2 Synthesis of Amine-Terminated ATRP Initiator

An ATRP initiator with an NH_2 functional group was synthesized via a modified method based on established procedures previously reported[126]. Briefly, 3.57 g of 2-bromoisobutyryl bromide was added to a solution of 2.5 g t-Boc-aminoethyl alcohol and 1.73 g triethylamine in 8 ml methylene chloride in an ice bath. After 4 hours, the salts were filtered off and the filtrate was extracted with saturated sodium bicarbonate solution. The DCM phase was dried over magnesium sulfate and evaporated. The resulting t-Boc-aminoethyl 2-bromoisobutyrate was treated with 15 ml trifluoroacetic acid (TFA) for 2 hours and crystallized upon addition of diethyl ether (yield 95%).

6.2.3 Polymer Synthesis of CBAA and SBMA

An amine terminated CBAA polymer was synthesized via atom transfer radical polymerization (ATRP). Copper (I) bromide (11.8 mg), copper (II) bromide (3.7 mg), and Bpy (30.9 mg) were weighed into a vial and deoxygenated by five repetitions of a strong vacuum followed by nitrogen backfill. In a separate vial, CBAA monomer (2 g) and amine-terminated ATRP initiator (26.7 mg) was weighed and also deoxygenated. 7 mL of MeOH (bubbled with nitrogen) was added to the monomer solution and 3 mL of MeOH (bubbled with nitrogen) was added to the initiator solution. Solutions were stirred for 15 minutes under nitrogen and then combined. The ATRP reaction was run overnight under nitrogen. Next, the polymer was precipitated into THF then centrifuged and dried. Dialysis was performed using Slide-A-lyzer® dialysis cassette with a 3,500 molecular weight cutoff (MWCO) (Thermo Scientific, Waltham, MA) in water in order to remove

unreacted monomer, copper (I) bromide, copper (II) bromide, and Bpy ligand. Polymers were then lyophilized and analyzed by gel permeation chromatography (GPC) to determine the molecular weight.

Amine-terminated poly(sulfobetaine methacrylate) polymers (SBMA) were synthesized in a very similar manner. Copper (I) bromide (11.8 mg), copper (II) bromide (3.7 mg), and Bpy (30.9 mg) were weighed into a vial and deoxygenated by five repetitions of a strong vacuum followed by nitrogen backfill. In a separate vial, SBMA monomer (565 mg) and amine-terminated ATRP initiator (26.7 mg) was weighed and also deoxygenated. 7 mL of MeOH (bubbled with nitrogen) was added to the monomer solution and 3 mL of MeOH (bubbled with nitrogen) was added to the initiator solution. Solutions were stirred for 15 minutes under nitrogen and then combined. The ATRP reaction was run overnight under nitrogen. Next, crystallized polymer was filtered out of the reaction solution and dissolved in water and precipitated into cold methanol, centrifuged, and dried. Dialysis was performed using Slide-A-lyzer® dialysis cassette with a 3,500 molecular weight cutoff (MWCO) (Thermo Scientific, Waltham, MA) in water in order to remove unreacted monomer, copper (I) and (II) bromide, and Bpy ligand. Polymers were then lyophilized and analyzed by GPC to determine the molecular weight.

Gel permeation chromatography (GPC) samples were run on an Agilent 1200 Infinity Series (Agilent Technologies, Santa Clara, CA) connected to either an Agilent PL Aquagel-OH column (Agilent Technologies, Santa Clara, CA) or a Waters Ultrahydrogel column (Waters, Milford, MA) at 1 mL/min in PBS with 0.02% azide (w/v). Samples were monitored with a Mini Dawn Treos light scattering detector and an Optilab T-rex refractive index detector (Wyatt Technology, Santa Barbara, CA).

6.2.4 Graft-To Modification of Fluorescent Latex Beads

To prepare CBAA-PS beads, carboxylate-modified fluorescent latex particles (2 w/v%) were diluted in half with a 100 mM MES buffer, pH 6. An equal volume of a 50 mM MES, pH 6 solution containing five times molar excess of EDC/sulfoNHS was then added. Beads were allowed to activate for 20 minutes. Beads were then be purified with an Amicon Ultra Centrifugal Filter Unit with a molecular weight cut-off (MWCO) of 100 kDa (Millipore, Billerica, MA) at least three times to remove any excess EDC/sulfoNHS. Next, a five time molar excess of NH_2-CBAA polymer solution was added in 100 mM PBS, pH 7.4. Beads were reacted overnight and then underwent extensive dialysis in PBS using Float-A-Lyzer G2 dialysis devices with a MWCO of 100 kDa (Spectrum Laboratories, Rancho Dominguez, CA).

To prepare SBMA-PS and PEG-PS beads, carboxylate-modified fluorescent latex particles (2 w/v%) were diluted fourfould in Millipore water. A ten time molar excess of NH_2-SBMA or NH_2-PEG polymer was then added to the solution. Sulfo-NHS was added to a final concentration of 7 mM and 200 mM borate buffer (pH 8.2) was added to a foufould dilution of the starting volume. EDC was added to a final concentration of 10 mM. Beads were reacted overnight at room temperature and then underwent extensive dialysis in PBS using Float-A-Lyzer G2 dialysis devices with a MWCO of 100 kDa (Spectrum Laboratories, Rancho Dominguez, CA).

6.2.5 Modification of Fluorescent Latex Beads with ATRP Initiator

Carboxylate-modified fluorescent latex particles (2 w/v%) were placed in 100 mM MES buffer at pH 6. Varying amounts of EDC and sulfo-NHS were weighed out and dissolved in MES, pH 6 buffer. The EDC/sulfo-NHS solution was added to the beads and activated for 15 minutes at room temperature. In the meantime, a stock solution of amine-terminated ATRP initiator was

prepared (62.5 mg in 2mL) in PBS with 0.1% Tween20 by volume. The pH of the solution was adjusted to 7.4 with NaOH. ATRP initiator was added to the beads in varying ratios and the latex particles were allowed to react overnight while being rotated and covered with aluminum foil. Particles were characterized before and after ATRP initiator conjugation with dynamic light scattering (DLS) and zeta potential (ZP). After conjugation was complete the particles were dialyzed in a 0.1% Tween20 solution to remove any remaining free initiator and to stabilize the particles with detergent before polymerization.

6.2.6 Graft-From ATRP from Fluorescent Latex Beads

ATRP conditions with ratios of 1:100:1:0.25:2.5 of initiator to monomer to copper I to copper II to ligand were used. Cu(I)Br (5.02 mg, 0.035 mmol), Cu(II)Br_2 (1.95 mg, 0.0088 mmol), and BPY (32.8 mg, 0.21 mmol) were placed in a small test tube under nitrogen protection and sealed with a rubber septum. CBAA monomer (877.8 mg, 3.85 mmol) and Tween20 (0.1 vol%) were placed in a large test tube, also under nitrogen protection and sealed with a rubber septum. Finally, 300 μL of initiator containing particles were placed in a test tube under nitrogen protection and sealed with a rubber septum. All test tubes were deoxygenated by five repetitions of a strong vacuum followed by nitrogen backfill. Deoxygenated water (bubbled with nitrogen gas) was then added to the test tube containing Cu(I)Br/Cu(II)Br_2/BPY (2.45 mL) and to the test tube containing CBAA monomer/Tween20 (1.75 mL). The test tube containing BPY ligand was stirred for 20 minutes to allow for ligand-copper complex formation. To initiate polymerization, 0.5 mL of CBAA monomer/Tween 20 followed by 0.7 mL of Cu(I)Br/Cu(II)Br_2/BPY was added to the initiator containing latex particles. Polymerization was allowed to proceed overnight. Following completion of the polymerization reaction CBAA particles were dialyzed in PBS.

6.2.7 Stability Testing of CBAA-PS Beads in PBS and Single Protein Solutions

To evaluate the stability of CBAA-PS, particles were concentrated using an Amicon Ultra Centrifugal Filter Unit with a MWCO of 100 kDa (Millipore, Billerica, MA) and resuspended in either PBS, 1 mg/mL fibrinogen, or 1 mg/mL lysozyme. Stability tests in PBS and single protein solutions were conducted for 1 hour. After the allotted exposure time, samples were analyzed via dynamic light scattering (DLS) (Malvern, Worcestershire, UK) to measure the hydrodynamic radius and via zeta potential (ZP) to measure the surface charge.

6.2.8 Synthetic Cervical Mucus Formulation

Preservatives (0.6 g imidurea, 0.3 g methylparaben, 0.04 g propylparaben) were dissolved in 90% of the water (173 mL) and stirred by an Arrow 6000 electric lab stirrer (Arrow Engineering, Hillside, NJ) at high speed for five minutes. A total of 2 g of guar gum was slowly added to this mixture into the vortex. The solution was then mixed for twenty minutes. Complete hydration was marked by a visual increase in the viscosity of the dispersion. A solution containing 1 g of dried porcine gastric mucin type III, 0.52 g of dibasic potassium phosphate, and 3.14 g of monobasic potassium phosphate dissolved in the remaining 10% of water (19 mL) were then added. Finally, at the end 0.5 mL of a 0.1 M sodium borate solution was added and the contents were shaken thoroughly.

6.2.9 Rheology Measurements of Synthetic Cervical Mucus

Rheology measurements were performed on an Anton Paar MCR301 model rheometer (Österreich, Austria). A stainless steel cone and plate were used with a diameter of 49.963 mm, an angle of 1.008˚, and a truncation of 49 μm. A shear rate from 0 to 20 (1/s) was applied and the shear stress was recorded.

6.2.10 Particle Tracking Experiments

Particle tracking experiments were performed in synthetic mucus formulations to determine diffusive properties of COO-PS, PEG-PS, and SBMA-PS particles. Particle transport rates were measured by analyzing trajectories of yellow-green fluorescent particles, recorded using a CCD Cool Snap cf Color Camera (Photometrics, Tucson, AZ) mounted on an inverted epifluorescence Nikon Eclipse TE2000-U microscope (Nikon, Tokyo, Japan) equipped with a 100x oil immersion objective and the appropriate filters. Experiments were carried out in glass bottom 24 well plates (MatTek Corporation, Ashland, MA), where diluted particle solutions (0.0082% wt/vol) were added to 1 mL of synthetic mucus to a final concentration of 3% (v/v) (final particle concentration, 8.25 x 10^{-7}% wt/vol) and incubated for 2 hours before microscopy. Movies were captured with the camera at a temporal resolution of 181.8 ms for 20 s. A software plugin from Image J was used to analyze the positional data in the x and y direction for individual particles. The coordinates of nanoparticle centroids were transformed into a time-averaged mean square displacement (MSD), calculated as $\langle \Delta r^2(\tau) \rangle = [x(t+\tau) - x(t)]^2 + [y(t+\tau) - y(t)]^2$, where x and y represent the nanoparticle coordinates at a given time and τ is the time scale or time lag. The effective diffusivites (D_{mucus}) of particles in mucus can be calculated from $MSD = 4D_{mucus}\,\tau$, where τ is the time scale. All effective diffusivities in mucus were calculated at a time scale of 1 second. Theoretical diffusion coefficients in water (D_{water}) are calculated based on the Stokes-Einstein equation, $D_{water} = kT/6\pi\mu a$, where k is the Boltzmann's constant, T is temperature, μ is the viscosity of the medium, and a is the particle radius.

6.3 Results and Discussion

Graft-to and graft-from methods were considered for the formation of zwitterionic coated particles to demonstrate mucus-penetrating capabilities (Figure 6-1). Graft-to methods allow for

facile conjugation of polymers to the surface and allow for better control over polymer size. Polymers are first synthesized via atom transfer radical polymerization (ATRP) and then attached to a particle surface utilizing conjugation chemistries. Conversely, graft-from methods allow for a higher density of ligands on the surface and allow for greater control over grafting density[193]. To perform graft-from polymerization on beads an appropriate initiator needs to be added to the surface. Following functionalization with an initiator, particles are grafted with zwitterionic polymer via atom transfer radical polymerization (ARTP). In this work, we modify carboxylate coated polystyrene particles that have a fluorescent dye incorporated inside the core to enable particle tracking experiments. Carboxylate modified polystyrene particles are convenient since they are amenable to EDC/sulfo-NHS functionalization.

a)

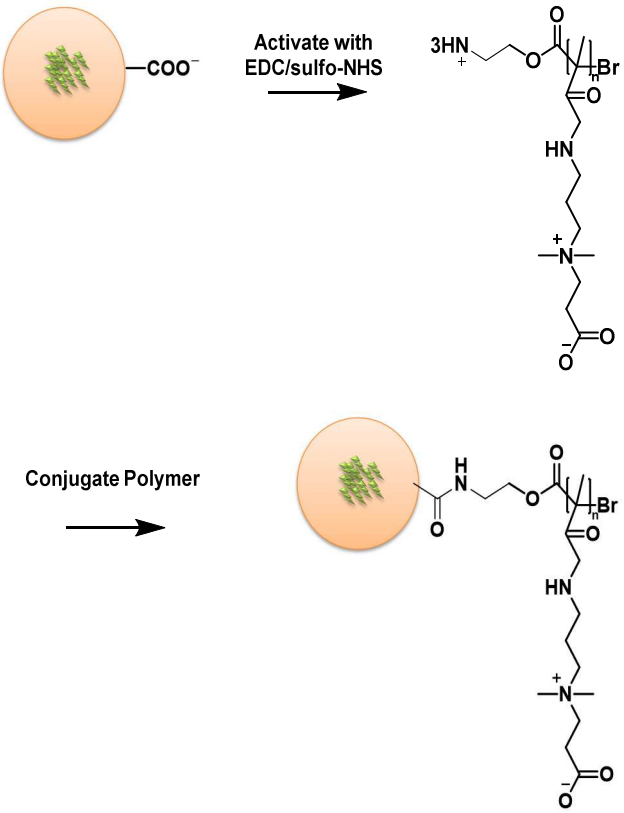

b)

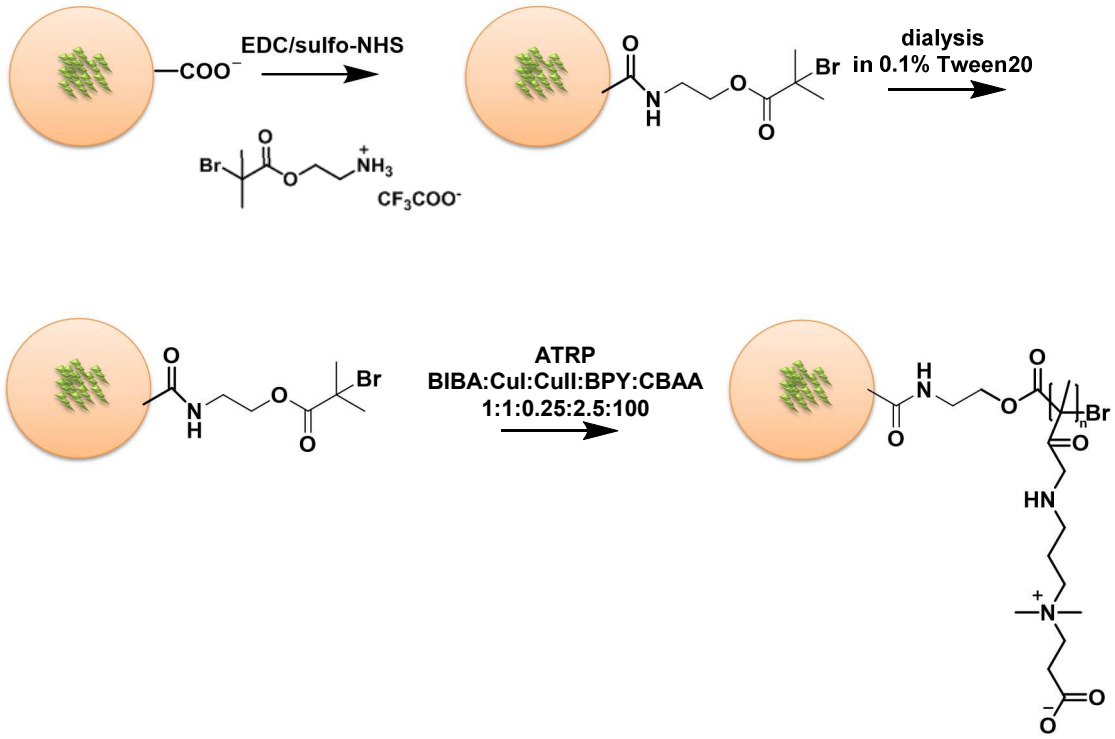

Figure 6-1. Scheme showing graft-to and graft-from approach to form zwitterionic particles.
(a) Graft-to approach. (b) Graft-from approach.

6.3.1 Polymer Synthesis of CBAA and SBMA

To prepare graft-to polystyrene particles amine-terminated polymers of varying sizes were synthesized. ATRP was performed in solution to obtain zwitterionic polymers of poly(carboxybetaine acrylamide) (polyCBAA) and poly(sulfobetaine) methacrylate (polySBMA). All polymers were evaluated by gel permeation chromatography (GPC) to determine the hydrodynamic size comparable to PEG standards. Two polymers were synthesized via ATRP: CBAA-NH_2 (MW: 25,145 Da, PDI: 1.23) and SBMA-NH_2 (MW: 3,813 Da, PDI: 1.17).

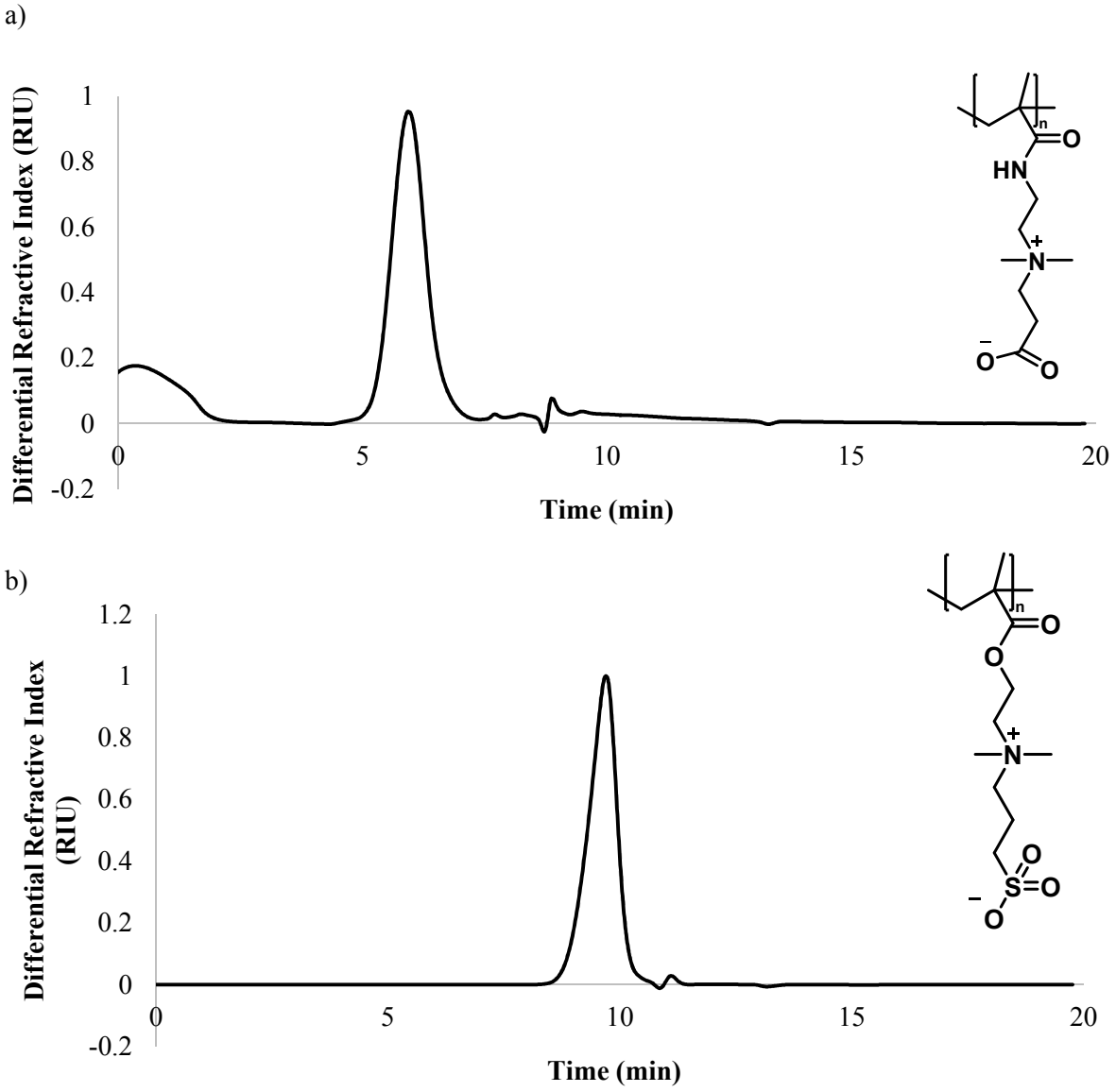

Figure 6-2. GPC Chromatograms for CBAA-NH_2 and SBMA-NH_2.
GPC chromatograms for (a) CBAA-NH_2 and (b) SBMA-NH_2. CBAA-NH_2 samples were analyzed on an Agilent PL Aquagel-OH column at a flow rate of 1 mL/min in PBS. SBMA-NH_2 samples were analyzed on a Waters Ultrahydrogel column at a flow rate of 1 mL/min in PBS. Molecular weights were determined based on a series of PEG standards.

6.3.2 Graft-To Modification of COO-PS Particles

Carboxylate modified polystyrene latex particles having a diameter of 100 nm were modified with either CBAA-NH_2, SBMA-NH_2, or PEG-NH_2 utilizing a graft-to technique in combination with

EDC/sulfo-NHS chemistry. If particles were going to be conjugated with CBAA-NH_2 polymers, the activated particles were purified by ultracentrifugation to remove any unreacted EDC/sulfo-NHS which may react with the carboxylate group on the polymer side chain. Conjugated particles underwent extensive dialysis in PBS and were then characterized by DLS for size and zeta potential. Bare carboxylate particles (COO-PS) were prepared as a negative control.

The hydrodynamic size (nm), PDI, and zeta potential (mV) of all graft-to particles are summarized in Table 6-1. All particles displayed very low PDI values less than 0.1 indicating monodispersity after polymer conjugation. Bare COO-PS beads have a highly negative charge at almost -49.1 ± 1.8 mV. A shift towards a more neutral charge would be expected upon polymer addition. This is the case with PEG-PS particles which decrease in zeta potential to -1.5 ± 0.1 mV after polymer conjugation. Likewise, SBMA-PS particles decrease in zeta potential to -25.2 ± 0.7 mV. The negative charge remaining is most likely due to poor surface grafting of the SBMA polymer leaving unreacted carboxylate groups. PEG is able to achieve a zeta potential closer to neutral since it is a linear polymer and can pack more tightly on the surface.

Table 6-1. DLS of graft-to particles for COO-PS, PEG-PS, SBMA-PS, and CBAA-PS.

Graft-to Particle	Polymer Size (Da)	Hydrodynamic Size (nm)	PDI	Zeta Potential (mV)
COO-PS	none	123.4 ± 1.0	0.03 ± 0.01	-49.1 ± 1.8
PEG-PS	5,000	153.1 ± 1.4	0.06 ± 0.03	-1.5 ± 0.1
SBMA-PS	3,813	133.3 ± 0.6	0.02 ± 0.01	-25.2 ± 0.7
CBAA-PS	25,145	212.1 ± 1.5	0.07 ± 0.05	19.15 ± 1.3

On the other hand, CBAA-PS particles possess a positive charge after surface modification. This is an unexpected result and is most likely due to the CBAA polymer salting out inside the polystyrene particle and becoming trapped. In fact, even when no EDC/sulfo-NHS is added to the polymer conjugation solution, the zeta potential of particles becomes positive and remains positive

even after extensive dialysis in PBS. Conversely, when SBMA polymer is added to the conjugation solution with no EDC/sulfo-NHS the zeta potential of the COO-PS particles returns to -49.1 ± 1.8 mV after rinsing in PBS. Carboxybetaine polymers are more highly hydrated than sulfobetaine polymers making them more sensitive to salting-out effects.

6.3.3 Formation of Initiator Coated PS Particles

In addition to utilizing graft-to techniques to form CBAA-PS particles, graft-from techniques were also explored for particle synthesis. Carboxylate modified polystyrene latex particles having a diameter of 100 nm were reacted with an amine terminating ATRP initiator through EDC/sulfoNHS chemistry. The addition of the initiator to the surface can be indirectly monitored by tracking the zeta potential of particles before and after the reaction. Unmodified particles have a zeta potential of -49.1 ± 1.8 mV. A range of initiator concentrations from 3 mM to 100 mM (final concentration in reaction) were tested in order to determine the optimal concentration that allows addition of initiator without aggregation of particles. Figure 6-3 indicates that as the concentration of initiator increases the zeta potential of the particles decreases. This is in agreement with the conjugation of initiator to carboxylate groups on the surface which would replace a negatively charged carboxylate group with a neutrally charged *tert*-butyl bromide group. A value of 37 mM ATRP initiator was selected as optimal for all experiments based on a balance between addition of initiator and size stability of the initiator coated particle. It was found that it was necessary to include a 0.1% Tween detergent solution to stabilize the initiator-coated particles from aggregating during dialysis. Following the addition of initiator, a dialysis was performed in order to remove any unreacted free initiator from the system.

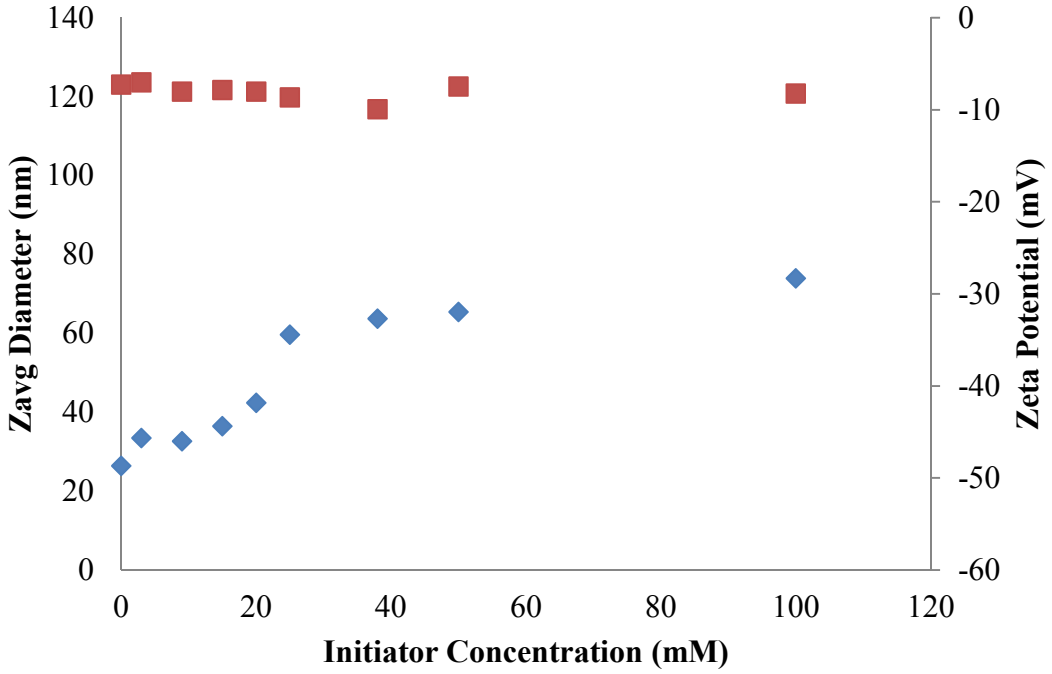

Figure 6-3. Modification of COO-PS latex particles with ATRP initiator.
Measurement of hydrodynamic diameter (nm) (left axis, red squares) and zeta potential (mV) (right axis, blue diamonds) for varying amounts of ATRP initiator in solution (mM) during functionalization of the carboxylate-modified polystyrene particles.

6.3.4 ATRP Polymerization to Form Graft-From CBAA-PS Particles

Atom transfer radical polymerization of particles was performed to grow poly(carboxybetaine acrylamide) from the surface. A ratio of 1:1:0.25:2.5 of initiator to copper I to copper II to ligand were used. Varying amounts of monomer were added in 10 and 20 times excess of the initiator. Reactions were performed under oxygen-free environments and in the presence of 0.1% Tween detergent overnight.

Particles undergoing ATRP polymerization were evaluated using dynamic light scattering (DLS) and zeta potential (ZP) in PBS after ultracentrifugation through 30 kDa Amicon molecular weight cut-off filters to remove unreacted monomer from the solution (

Figure 6-4). Relatively monodisperse particles were formed from ATRP conditions containing 10:1 and 20:1 monomer to initiator ratios. The average hydrodynamic size of particles under 10:1 conditions was 260.6 ± 0.9 nm with a PDI of 0.14 ± 0.01 and the average hydrodynamic size of particles under 20:1 conditions was 291.1 ± 1.3 nm with a PDI of 0.14 ± 0.02.

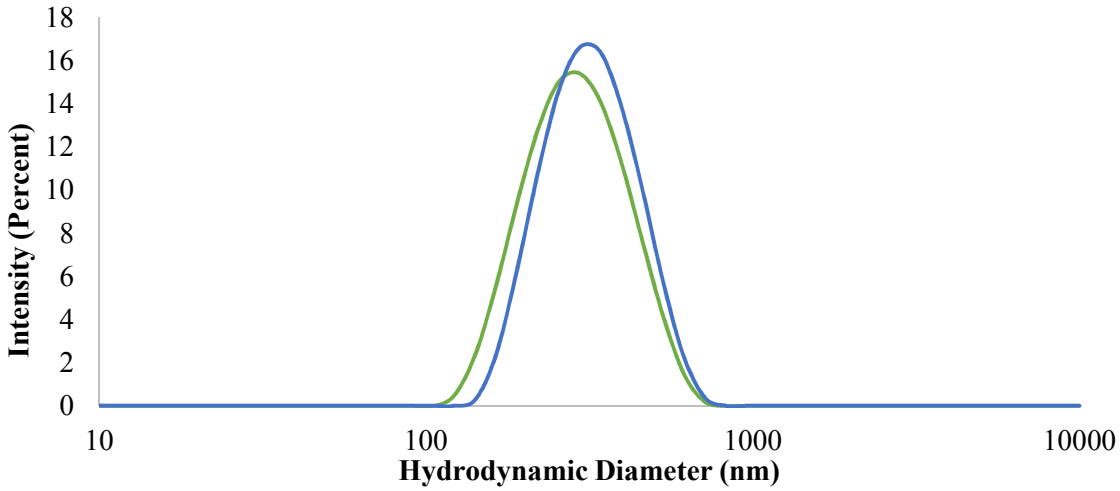

Figure 6-4. Hydrodynamic size comparison of CBAA-PS after ATRP.
Intensity data from dynamic light scattering of particles in PBS after ATRP with monomer to initiator ratios of 10:1 (green line) and 20:1 (blue line).

In addition to evidence that polymerization is occurring from dynamic light scattering data, zeta potential measurements provide further confirmation. As seen in Table 6-2, the zeta potential of CBAA-PS particles is around 5 mV after final purification into PBS.

Table 6-2. Zeta potential comparison of CBAA-PS to control particles after ATRP.

Monomer to Initiator Ratio	Zeta Potential (mV)
10:1	4.9 ± 0.1
20:1	4.4 ± 0.2

6.3.5 Further Development of CBAA Coated Particle

Both CBAA-PS graft-to and CBAA-PS graft-from particles displayed aggregation upon introduction into synthetic mucus. CBAA-PS graft-to particles possessed a positive charge due to

salting-out of polymer inside the latex beads. CBAA-PS graft-from particles had a nearly neutral charge, but needed the addition of Tween 20 detergent for stabilization during ATRP. It is likely that all of the Tween 20 detergent was not removed by dialysis and may cause aggregation of particles in mucus. The formation of CBAA-PS particles needs to be optimized to form particles with a neutral charge and an appropriate detergent to be able to accurately assess the stability of these particles in mucus.

In addition to the development of CBAA-PS particles, diblock polymers consisting of CBAA-PLGA can be tested as potential candidates for mucus-penetrating particles. These polymers can be assembled into spherical structures and loaded with a fluorescent dye using nanoprecipitation methods[126]. The block lengths of hydrophilic polymer (CBAA) and hydrophobic polymer (PLGA) can be varied to adjust the size and morphology of structures formed. CBAA-PLGA particles loaded with fluorescent dye can be evaluated via multiple particle tracking for mucus-penetrating applications identically to CBAA-PS particles.

6.3.6 Stability of Particles in Protein Solutions

Since, CBAA-PS particle formation was not able to be optimized we decided to proceed with further testing of SBMA-PS particles. In addition to testing stability in PBS, SBMA-PS and PEG-PS particles were tested in single protein solutions of 1 mg/mL fibrinogen and 1 mg/mL lysozyme in PBS. COO-PS particles were evaluated as a control. Particles were concentrated using ultra-centrifugation filters with a molecular weight cut-off of 100 kDa and then resuspended in protein solutions. After one hour particle size was assessed using DLS. There was no aggregation observed for particles after exposure to lysozyme proteins solutions and a slight increase in size after exposure to fibrinogen proteins (Figure 6-5) for SBMA-PS and PEG-PS particles. The hydrodynamic diameter

of SBMA-PS particles was 133.3 ± 0.6 nm for PBS, 143.4 ± 0.8 nm for fibrinogen, and 135.7 ± 1.2 for lysozyme. For PEG-PS, the hydrodynamic diameter was 153.1 ± 1.4 nm for PBS, 171.2 ± 0.4 nm for fibrinogen, and 155.6 ± 2.0 nm for lysozyme. Finally, for control COO-PS particles the hydrodynamic diameter was 123.4 ± 1.0 nm for PBS, 164.1 ± 1.0 nm for fibrinogen, and 2,135.3 ± 122.3 nm for lysozyme.

a)

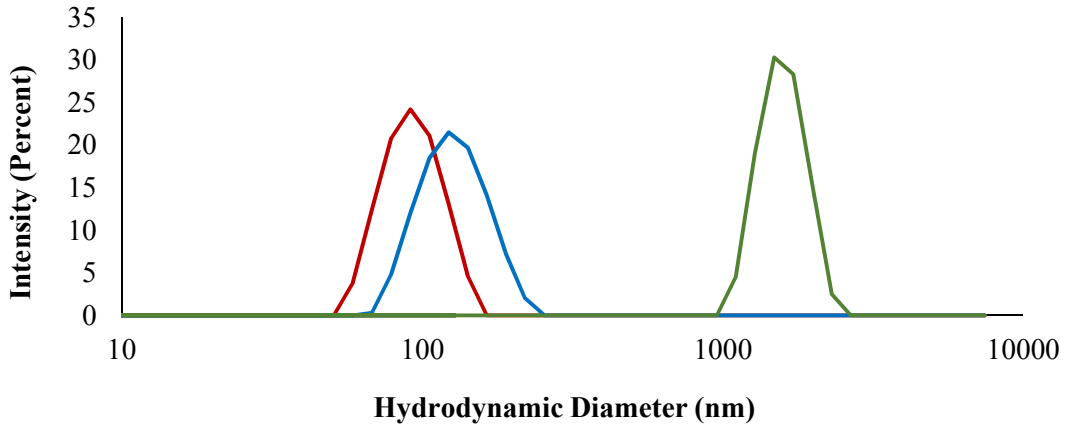

b)

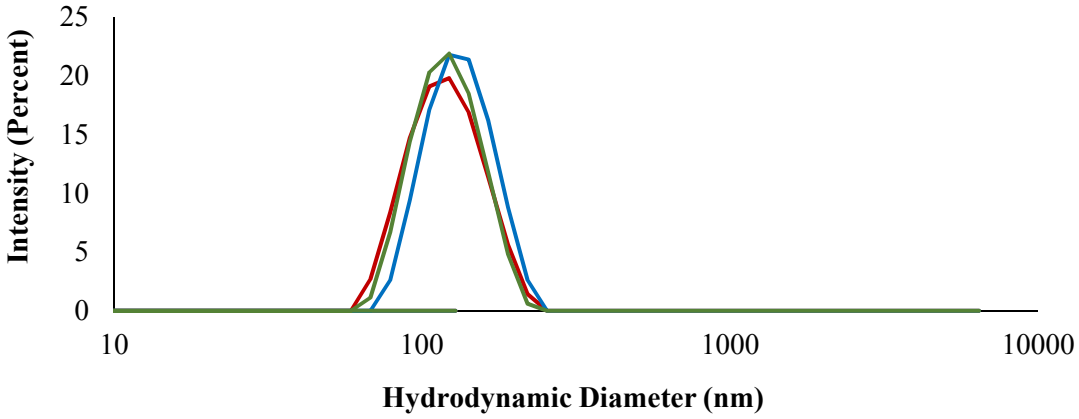

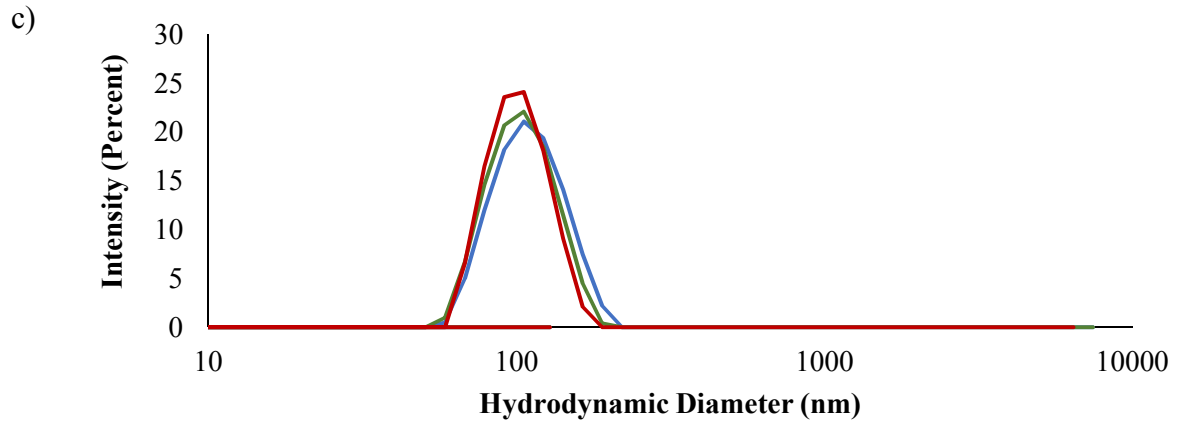

Figure 6-5. Hydrodynamic size of COO-PS, PEG-PS, and SBMA-PS after exposure to protein solutions.
Intensity data from dynamic light scattering of particles in the control PBS solution (red line) and after exposure to 1 mg/mL fibrinogen in PBS (blue line) and 1 mg/mL lysozyme in PBS (green line) for one hour. (a) COO-PS (b) PEG-PS and (c) SBMA-PS.

6.3.7 Particle Tracking Experiments

Although preliminary stability tests can give an indication of whether particles will be viable candidates for containing mucus-penetrating properties, it is best to test particles directly in mucus. A synthetic cervical mucus formulation was prepared for preliminary testing[194]. This synthetic formulation contains 1% (w/w) guar gum cross-linked with borate ion and 0.5% (w/w) dried porcine gastric mucin (type III). Natural mucus has varying ranges of viscosity reported in the literature ranging from 2,840 cp to 10,000 cp for mid-cycle human cervical mucus[195,196]. Rheology measurements were performed on the synthetic mucus sample in order to ensure the viscosity falls within the range for natural mucus. The shear rate vs shear stress were measured at 23 ˚C and 37 ˚C and the apparent viscosity was calculated by averaging the individual viscosities at each time point measured (Figure 6-6). The apparent viscosity was 3,565.2 cp at 23 ˚C and 2,474.1 cp at 37 ˚C. The apparent viscosities are slightly low compared to the average of natural cervical mucus which falls around 5,000 cp.

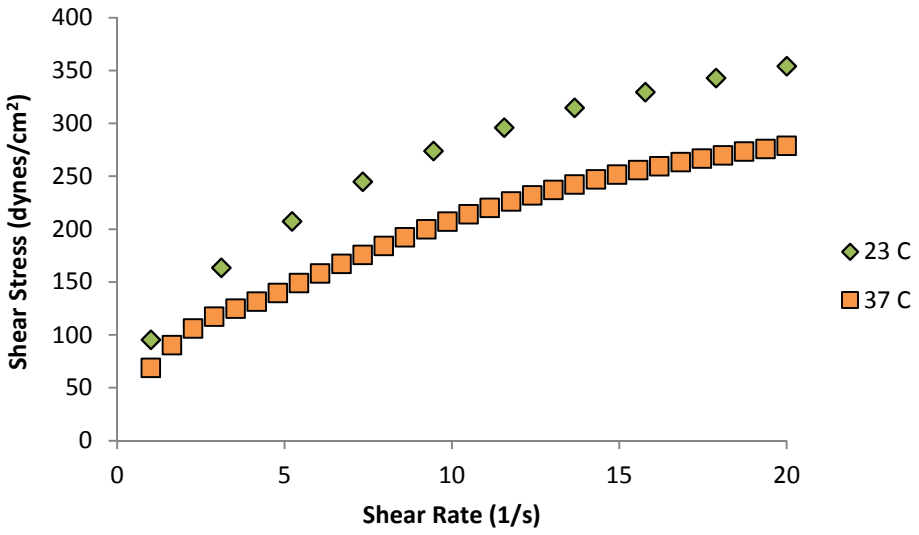

Figure 6-6. Rheology measurement of synthetic mucus formulation at varying temperatures.
Plot of shear stress (dynes/cm^2) vs shear rate (1/s) for synthetic mucus formulation at 23 ˚C (green triangles) and 37 ˚C (orange squares).

The synthetic mucus formulation can be used to perform fluorescent multiple particle tracking experiments to determine individual and ensemble transport properties[197,198]. Two dimensional tracking can provide accurate information on particle behavior if the environment is locally isotropic. By tracking the x and y positional data of the transporting particles over time, the mean square displacement can be calculated, in two dimensions, of each particle. This value can then be used to obtain the effective diffusivity. The values for individual particles can be averaged to obtain ensemble values.

Particle tracking measurements were performed in synthetic mucus for COO-PS, PEG-PS, and SBMA-PS particles. Ensemble-averaged geometric mean square displacements (<MSD>) as a function of time scale are shown in Figure 6-7. Preliminary results indicate that particles coated with SBMA-PS displayed slightly faster penetration than particles coated with PEG-PS. To further confirm these results larger sample sizes need to be analyzed to obtain statistical significance (at least n = 90).

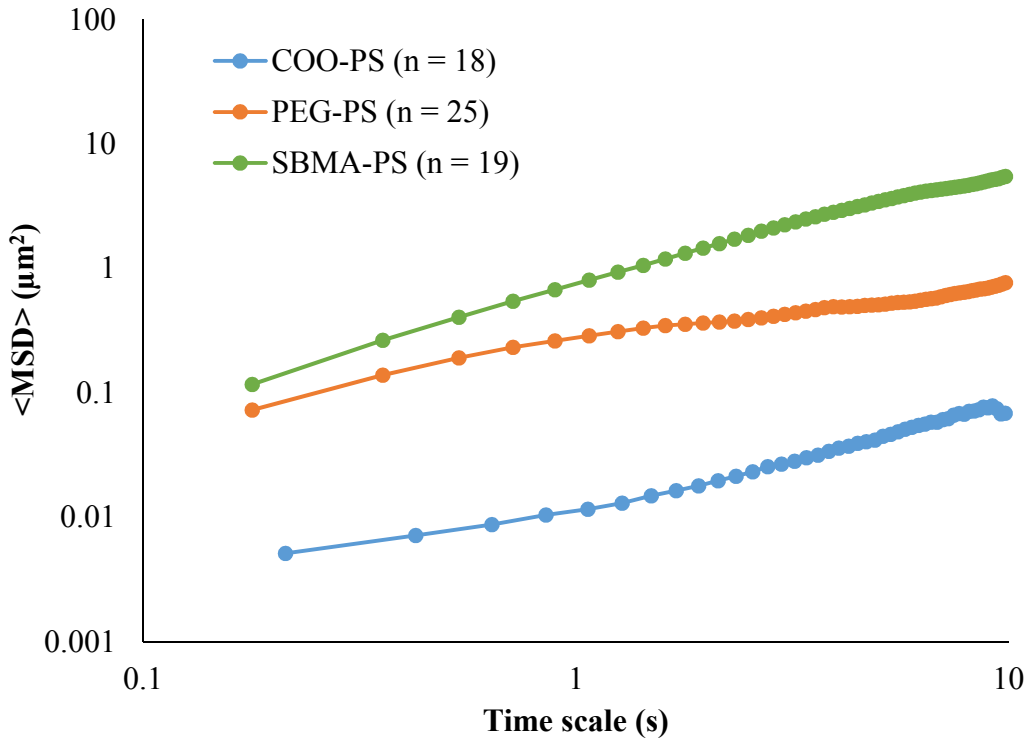

Figure 6-7. Ensemble-averaged geometric mean square displacements as a function of time scale. Transport rates of 100 nm modified PS particles in synthetic mucus. Ensemble-averaged geometric mean square displacements as a function of time scale for COO-PS (blue line), PEG-PS (orange line), and SBMA-PS (green line).

In addition to calculating the MSD value, the effective diffusivity values in mucus (D_m) can be calculated at a selected time scale and compared to the theoretical diffusivity in water (D_w). The theoretical diffusivity in water (D_w) can be calculated from the Stokes-Einstein equation. The value of D_m/D_w can then be compared to reported literature values for PEG-PS particles[199]. Results for the calculation of D_m/D_w are found in Table 6-3. Effective diffusivity values were calculated at a time scale of 1 second. COO-PS particles do not penetrate mucus and have a diffusion rate 1,300 times slower in mucus compared to their diffusion in water. PEG-PS particles have a diffusion rate 48 times slower in mucus and SBMA-PS particles have a diffusion rate 18 times slower in mucus compared to water. Literature values report that PEG-PS particles can have diffusion times that are 4-6 times slower than water[199]. The slower values reported for diffusion here may be due to

insufficient sample size. These results should be considered preliminary and a larger sample size needs to be evaluated to confirm the results. Zwitterionic coated SBMA-PS particles show promise as effective mucus-penetrating particles. In the future, particle optimization to achieve a higher polymer graft density of SBMA and to obtain a zeta potential closer to neutral should be performed.

Table 6-3. Characterization of COO-PS, PEG-PS, and SBMA-PS and their diffusion values.
Hydrodynamic size and the ensemble average diffusion coefficients in mucus (D_{mucus}) compared to in water (D_w). Effective diffusivity values were calculated at a time scale of 1 s. D_{water} was calculated from the Stokes-Einstein equation.

Particle	Diameter (nm)	MSD (μm^2)	D_{mucus} ($\mu m^2/s$)	D_{water} ($\mu m^2/s$)	D_{mucus}/D_{water}	Times slower in water
COO-PS	122.3	0.012	2.73×10^{-15}	3.57×10^{-12}	0.0008	1300
PEG-PS	133.7	0.288	6.75×10^{-14}	3.27×10^{-12}	0.0207	48
SBMA-PS	129.8	0.807	1.88×10^{-13}	3.36×10^{-12}	0.0560	18

6.4 Conclusions

The use of zwitterionic polymers is considered as a potential material for mucus-penetrating particles. Delivering particles through mucosal barriers is a challenging task due to its sticky, hydrophobic nature and its continual clearance from the body. Zwitterionic polymers have already proven versatile for many applications where nonspecific adsorption needs to be avoided and is a promising candidate for mucus penetration. Graft-to and graft-from methods were explored to modify a fluorescent polystyrene based particle with zwitterionic polymers. The SBMA-PS particles were shown to be stable in PBS and single protein solutions of fibrinogen and lysozyme. In addition, SBMA-PS particles were shown to display mucus-penetrating properites. Future work will involve optimizing the formation of CBAA-PS particles. CBAA polymers should work very well for mucus penetration when high surface packing densities are achieved. Particles possessing different polymer

densities and different sizes can be evaluated to determine the optimal coatings for mucus penetration.

Chapter 7: Conclusions

This work has discussed the importance of the continued expansion of low fouling materials for biomedical applications. Rational and combinatorial design approaches to develop peptides as a new low fouling material are described. Several applications of low fouling peptide sequences are presented. In addition, the utilization of zwitterionic polymers is applied to improve the properties of mucus-penetrating particles.

In Chapter 2, zwitterionic principles were used to rationally design a low fouling peptide sequence composed of alternating charged residues of glutamic acid and lysine (EK). In addition, the surfaces of human proteins were analyzed to biomimetically design peptide sequences inspired by nature. The sequence EK was again identified as a prime candidate, in addition to neutrally charged asparagine (N). These sequences were evaluated for nonspecific protein adsorption by forming them into peptide self-assembled monolayers on a surface. It was discerned that simply using a cysteine residue for surface anchoring does not provide a peptide capable of self-assembly into an ultra-low fouling monolayer on gold surfaces. We identified that inclusion of a rigid, hydrophobic linker is necessary to allow close-packing of chains. The inclusion of a four residue proline linker in addition to cysteine (-PPPPC) provides a well-defined secondary structure determined by circular dichroism, molecular simulations, ATR-FTIR, and XPS. The cell recognition sequence RGD was added as an example of specific recognition, while maintaining a nonfouling background.

The concept of an all-in-one natural peptide possessing biomolecular recognition, ultra-low fouling, and surface anchoring functions was applied to a gold nanoparticle system in Chapter 3. Developing stealth applications for circulating nanoparticles is challenging due to rapid clearance and potential aggregation upon introduction into the human blood stream. EK-GNPs displayed stability in high salt, single protein solutions, and undiluted human serum at 37˚C for 24 hours. *In*

vitro cell studies show low macrophage cell uptake suggesting EK-GNPs could achieve long blood circulation half-life *in vivo.* Importantly, the particles can be functionalized without the need for chemical conjugation by simply extending the peptide sequence with a specific targeting moiety. Specific cell uptake is demonstrated by including a cyclic RGD targeting sequence in addition to the low fouling EK background.

In addition to the development of low fouling peptide-self assembled monolayers and stealth gold nanoparticles, Chapter 4 proposes the design of an EK-PLGA diblock polymer that can be assembled to form micelle drug delivery nanocarriers. This platform capitalizes on the complete biodegradability of poly(amino acids) adding advantages such as low toxicity, easily metabolized degradation products, and potentially lower immunogenicity as compared to non-biodegradable stealth polymer systems such as poly(ethylene glycol) (PEG). Several synthesis routes were explored for EK-PLGA polymer synthesis and nanoprecipitation methods were used to form micelles.

Chapters 2 through 4 exemplify relevant biomedical applications of the rationally designed EK low fouling peptide sequence. While designing low fouling sequences based on known zwitterionic principles and inspiration from nature can be successful, these methods are limited to the analysis of tens of sequences. In Chapter 5 we explore the development of a new combinatorial screening method to identify novel low fouling peptide sequences. Traditional display technologies could not be employed due to the interference of nonspecific background binding, so an amine-modified controlled pore glass substrate platform was developed. Thousands of peptide sequences can be screened using fluorescently labeled protein followed by confocal microscope evaluation. A combination of PED and MALDI-TOF can be used to recover the peptide sequences of low fouling beads. The identification of new low fouling sequences can provide novel insights into the

fundamental understanding of molecular-level nonfouling mechanisms and the development of new nonfouling materials.

Finally, in Chapter 6 zwitterionic polymers were considered as a potential material for mucus-penetrating particles since they have already proven versatile for many applications where nonspecific adsorption needs to be avoided. Delivering particles through mucosal barriers is a challenging task due to its hydrophobic nature, densely cross-linked network, and continual clearance from the body. Preliminary results for poly(sulfobetaine methacrylate) coated polystyrene particles (SBMA-PS) are presented. The SBMA-PS particles were shown to be stable in PBS and single protein solutions of fibrinogen and lysozyme. Preliminary particle tracking experiments indicate that SB-PS can successfully penetrate mucus.

The continual development of new low fouling materials, such as peptides, can provide attractive alternatives to traditionally used stealth materials such as PEG. Peptides offer advantages such as well-defined structure, biocompatibility, chemical diversity, and biodegradability. In addition, zwitterionic polymers can find utility in many fields where the resistance of non-specific adsorption is necessary, such as in mucus-penetrating particles.

References

(1) Tsai, W. B.; Grunkemeier, J. M.; Horbett, T. A. Human Plasma Fibrinogen Adsorption and Platelet Adhesion to Polystyrene. *J. Biomed. Mater. Res.* **1999**, *44*, 130–139.

(2) Guiton, P. S.; Hung, C. S.; Hancock, L. E.; Caparon, M. G.; Hultgren, S. J. Enterococcal Biofilm Formation and Virulence in an Optimized Murine Model of Foreign Body-Associated Urinary Tract Infections. *Infect. Immun.* **2010**, *78*, 4166–75.

(3) Tambyah, P. A.; Knasinski, V.; Maki, D. G. The Direct Costs of Nosocomial Catheter-Associated Urinary Tract Infection in the Era of Managed Care. *Infect. Control Hosp. Epidemiol.* **2002**, *23*, 27–31.

(4) Jarvis, W. R. Selected Aspects of the Socioeconomic Impact of Nosocomial Infections: Morbidity, Mortality, Cost, and Prevention. *Infect. Control Hosp. Epidemiol.* **1996**, *17*, 552–557.

(5) Anderson, J. M.; Rodriguez, A.; Chagn, D. T. Foreign Body Reaction to Biomaterials. *Semin. Immunol.* **2009**, *20*, 86–100.

(6) Moghimi, S. M.; Hunter, A. C.; Andresen, T. L. Factors Controlling Nanoparticle Pharmacokinetics: An Integrated Analysis and Perspective. *Annu. Rev. Pharmacol. Toxicol.* **2012**, *52*, 481–503.

(7) Bixler, G. D.; Bhushan, B. Biofouling : Lessons from Nature. *Philos. Trans. R. Soc. Ser. A* **2012**, *370*, 2381–2417.

(8) Harder, P.; Grunze, M.; Dahint, R. Molecular Conformation in Oligo (ethylene Glycol)-Terminated Self-Assembled Monolayers on Gold and Silver Surfaces Determines Their Ability to Resist Protein Adsorption. *J. Phys. Chem. B* **1998**, *102*, 426–436.

(9) Holland, N. B.; Qiu, Y.; Ruegsegger, M.; Marchant, R. E. Biomimetic Engineering of Non-Adhesive Glycocalyx-like Surfaces Using Oligosaccharide Surfactant Polymers. *Nature* **1998**, *392*, 799–802.

(10) Pidhatika, B.; Möller, J.; Vogel, V.; Konradi, R. Nonfouling Surface Coatings Based on Poly(2-Methyl-2-Oxazoline). *Chim. Int. J. Chem.* **2008**, *62*, 264–269.

(11) Bernards, M. T.; Cheng, G.; Zhang, Z.; Chen, S.; Jiang, S. Nonfouling Polymer Brushes via Surface-Initiated , Two-Component Atom Transfer Radical Polymerization. *Macromolecules* **2008**, *41*, 4216–4219.

(12) Holmlin, R. E.; Chen, X.; Chapman, R. G.; Takayama, S.; Whitesides, G. M. Zwitterionic SAMs That Resist Nonspecific Adsorption of Protein from Aqueous Buffer. *Langmuir* **2001**, *17*, 2841–2850.

(13) Chen, S.; Cao, Z.; Jiang, S. Ultra-Low Fouling Peptide Surfaces Derived from Natural Amino Acids. *Biomaterials* **2009**, *30*, 5892–5896.

(14) Bolduc, O. R.; Pelletier, J. N.; Masson, J.-F. SPR Biosensing in Crude Serum Using Ultralow Fouling Binary Patterned Peptide SAM. *Anal. Chem.* **2010**, *82*, 3699–3706.

(15) Jiang, S.; Cao, Z. Ultralow-Fouling, Functionalizable, and Hydrolyzable Zwitterionic Materials and Their Derivatives for Biological Applications. *Adv. Mater.* **2010**, *22*, 920–932.

(16) Knop, K.; Hoogenboom, R.; Fischer, D.; Schubert, U. S. Poly(Ethylene Glycol) in Drug Delivery: Pros and Cons as Well as Potential Alternatives. *Angew. Chem. Int. Ed.* **2010**, *49*, 6288–6308.

(17) Kaatze, U.; Göttmann, O.; Podbielski, R.; Pottel, R.; Terveer, U. Dielectric Relaxation in Aqueous Solutions of Some Oxygen-Containing Linear Hydrocarbon Polymers. *J. Phys. Chem.* **1978**, *82*, 112-120.

(18) Keefe, A. J.; Jiang, S. Poly(zwitterionic) Protein Conjugates Offer Increased Stability without Sacrificing Binding Affinity or Bioactivity. *Nat. Chem.* **2012**, *4*, 59–63.

(19) Ostuni, E.; Chapman, R. G.; Holmlin, R. E.; Takayama, S.; Whitesides, G. M. A Survey of Structure−Property Relationships of Surfaces That Resist the Adsorption of Protein. *Langmuir* **2001**, *17*, 5605–5620.

(20) Herold, D. A.; Keik, K.; Bruns, D. E. Oxidation of Polyethylene Glycols by Alcohol Dehydrogenase. *Biochem. Pharmacol.* **1989**, *38*, 73–76.

(21) Zhang, Z.; Finlay, J. A.; Wang, L.; Gao, Y.; Callow, J. A.; Callow, M. E.; Jiang, S. Polysulfobetaine-Grafted Surfaces as Environmentally Benign Ultralow Fouling Marine Coatings. *Langmuir* **2009**, *25*, 13516–13521.

(22) Iwasaki, Y.; Ishihara, K. Cell Membrane-Inspired Phospholipid Polymers for Developing Medical Devices with Excellent Biointerfaces. *Sci. Technol. Adv. Mater.* **2012**, *13*, 064101.

(23) Chen, S.; Li, L.; Zhao, C.; Zheng, J. Surface Hydration: Principles and Applications toward Low-Fouling/Nonfouling Biomaterials. *Polymer* **2010**, *51*, 5283–5293.

(24) Cheng, G.; Li, G.; Xue, H.; Chen, S.; Bryers, J. D.; Jiang, S. Zwitterionic Carboxybetaine Polymer Surfaces and Their Resistance to Long-Term Biofilm Formation. *Biomaterials* **2009**, *30*, 5234–5240.

(25) Carr, L. R.; Jiang, S. Mediating High Levels of Gene Transfer without Cytotoxicity via Hydrolytic Cationic Ester Polymers. *Biomaterials* **2010**, *31*, 4186–4193.

(26) Chien, H.-W.; Xu, X.; Ella-Menye, J.-R.; Tsai, W.-B.; Jiang, S. High Viability of Cells Encapsulated in Degradable Poly(Carboxybetaine) Hydrogels. *Langmuir* **2012**, *28*, 17778–17784.

(27) Cheng, G.; Xue, H.; Li, G.; Jiang, S. Integrated Antimicrobial and Nonfouling Hydrogels to Inhibit the Growth of Planktonic Bacterial Cells and Keep the Surface Clean. *Langmuir* **2010**, *26*, 10425–10428.

(28) Taylor, A. D.; Ladd, J.; Yu, Q.; Chen, S.; Homola, J.; Jiang, S. Quantitative and Simultaneous Detection of Four Foodborne Bacterial Pathogens with a Multi-Channel SPR Sensor. *Biosens. Bioelectron.* **2006**, *22*, 752–758.

(29) Zhang, L.; Xue, H.; Gao, C.; Carr, L.; Wang, J.; Chu, B.; Jiang, S. Imaging and Cell Targeting Characteristics of Magnetic Nanoparticles Modified by a Functionalizable Zwitterionic Polymer with Adhesive 3,4-Dihydroxyphenyl-$_L$-Alanine Linkages. *Biomaterials* **2010**, *31*, 6582–6588.

(30) Merrifield, R. B. Solid Phase Peptide Synthesis. I. The Synthesis of a Tetrapeptide. *J. Am. Chem. Soc.* **1963**, *85*, 2149–2154.

(31) Johnson, I. S. Human Insulin from Recombinant DNA Technology. *Science* **1983**, *219*, 632–637.

(32) Veronese, F. M. Peptide and Protein PEGylation: A Review of Problems and Solutions. *Biomaterials* **2001**, *22*, 405–417.

(33) Collier, J. H.; Segura, T. Evolving the Use of Peptides as Components of Biomaterials. *Biomaterials* **2011**, *32*, 4198–4204.

(34) Sun, H.; Meng, F.; Dias, A. A.; Hendriks, M.; Feijen, J.; Zhong, Z. α-Amino Acid Containing Degradable Polymers as Functional Biomaterials: Rational Design, Synthetic Pathway, and Biomedical Applications. *Biomacromolecules* **2011**, *12*, 1937–1955.

(35) White, A. D.; Keefe, A. J.; Ella-Menye, J.-R.; Nowinski, A. K.; Shao, Q.; Pfaendtner, J.; Jiang, S. Free Energy of Solvated Salt Bridges: A Simulation and Experimental Study. *J. Phys. Chem. B* **2013**, *117*, 7254–7259.

(36) Lancelot, G.; Mayer, R.; Helene, C. Conformational Study of the Dipeptide Arginylglutamic Acid and of Its Complex with Nucleic Bases. *J. Am. Chem. Soc.* **1979**, *101*, 1569–1576.

(37) Mason, P. E.; Neilson, G. W.; Dempsey, C. E.; Barnes, A. C.; Cruickshank, J. M. The Hydration Structure of Guanidinium and Thiocyanate Ions : Implications for Protein Stability in Aqueous Solution. *Proc. Natl. Acad. Sci. U. S. A.* **2003**, *100*, 4557–4561.

(38) Arakawa, T.; Ejima, D.; Tsumoto, K.; Obeyama, N.; Tanaka, Y.; Kita, Y.; Timasheff, S. N. Suppression of Protein Interactions by Arginine: A Proposed Mechanism of the Arginine Effects. *Biophys. Chem.* **2007**, *127*, 1–8.

(39) Anderson, N. L.; Anderson, N. G. The Human Plasma Proteome: History, Character, and Diagnostic Prospects. *Mol. Cell. Proteomics* **2002**, *1*, 845–867.

(40) White, A. D.; Nowinski, A. K.; Huang, W.; Keefe, A. J.; Sun, F.; Jiang, S. Decoding Nonspecific Interactions from Nature. *Chem. Sci.* **2012**, *3*, 3488.

(41) White, A. D.; Huang, W.; Jiang, S. Role of Nonspecific Interactions in Molecular Chaperones through Model-Based Bioinformatics. *Biophys. J.* **2012**, *103*, 2484–2491.

(42) Potyrailo, R.; Rajan, K.; Stoewe, K.; Takeuchi, I.; Chisholm, B.; Lam, H. Combinatorial and High-Throughput Screening of Materials Libraries: Review of State of the Art. *ACS Comb. Sci.* **2011**, *13*, 579–633.

(43) Molek, P.; Strukelj, B.; Bratkovic, T. Peptide Phage Display as a Tool for Drug Discovery: Targeting Membrane Receptors. *Molecules* **2011**, *16*, 857–887.

(44) Szent-Gyorgyi, C.; Schmidt, B. F.; Creeger, Y.; Fisher, G. W.; Zakel, K. L.; Adler, S.; Fitzpatrick, J. A. J.; Woolford, C. A.; Yan, Q.; Vasilev, K. V.; Berget, P. B.; Bruchez, M. P.; Jarvik, J. W.; Waggoner, A. Fluorogen-Activating Single-Chain Antibodies for Imaging Cell Surface Proteins. *Nat. Biotechnol.* **2008**, *26*, 235–240.

(45) Adams, B. L.; Finch, A. S.; Hurley, M. M.; Sarkes, D. A.; Stratis-Cullum, D. N. Genetically Engineered Peptides for Inorganics : Study of an Unconstrained Bacterial Display Technology and Bulk Aluminum Alloy. *Adv. Mater.* **2013**, *25*, 4585–4591.

(46) Wavreille, A.; Garaud, M.; Zhang, Y.; Pei, D. Defining SH2 Domain and PTP Specificity by Screening Combinatorial Peptide Libraries. *Methods* **2007**, *42*, 207–219.

(47) Keefe, A. J.; Caldwell, K. B.; Nowinski, A. K.; White, A. D.; Thakkar, A.; Jiang, S. Screening Nonspecific Interactions of Peptides without Background Interference. *Biomaterials* **2013**, *34*, 1871–1877.

(48) Lai, S. K.; Wang, Y.-Y.; Hanes, J. Mucus-Penetrating Nanoparticles for Drug and Gene Delivery to Mucosal Tissues. *Adv. Drug Deliv. Rev.* **2009**, *61*, 158–171.

(49) Ensign, L. M.; Tang, B. C.; Wang, Y.-Y.; Tse, T. A.; Hoen, T.; Cone, R.; Hanes, J. Mucus-Penetrating Nanoparticles for Vaginal Drug Delivery Protect against Herpes Simplex Virus. *Sci. Transl. Med.* **2012**, *4*, 138ra79.

(50) Griesenbach, U.; Alton, E. W. F. W. Moving Forward: Cystic Fibrosis Gene Therapy. *Hum. Mol. Genet.* **2013**, *22*, R52–R58.

(51) Woodrow, K. A.; Bennett, K. M.; Lo, D. D. Mucosal Vaccine Design and Delivery. *Annu. Rev. Biomed. Eng.* **2012**, *14*, 17–46.

(52) Chen, S.; Zheng, J.; Li, L.; Jiang, S. Strong Resistance of Phosphorylcholine Self-Assembled Monolayers to Protein Adsorption: Insights into Nonfouling Properties of Zwitterionic Materials. *J. Am. Chem. Soc.* **2005**, *127*, 14473–14478.

(53) Chelmowski, R.; Köster, S. D.; Kerstan, A.; Prekelt, A.; Grunwald, C.; Winkler, T.; Metzler-Nolte, N.; Terfort, A.; Wöll, C. Peptide-Based SAMs That Resist the Adsorption of Proteins. **2008**, *130*, 14952–14953.

(54) Statz, A. R.; Meagher, R. J.; Barron, A. E.; Messersmith, P. B. New Peptidomimetic Polymers for Antifouling Surfaces. *J. Am. Chem. Soc.* **2005**, *127*, 7972–7973.

(55) Boncheva, M.; Vogel, H. Formation of Stable Polypeptide Monolayers at Interfaces: Controlling Molecular Conformation and Orientation. *Biophys. J.* **1997**, *73*, 1056–1072.

(56) Hynes, R. O. Integrins: Bidirectional, Allosteric Signaling Machines. *Cell* **2002**, *110*, 673–687.

(57) VandeVondele, S.; Vörös, J.; Hubbell, J. A. RGD-Grafted Poly-L-Lysine-Graft-(Polyethylene Glycol) Copolymers Block Non-Specific Protein Adsorption While Promoting Cell Adhesion. *Biotechnol. Bioeng.* **2003**, *82*, 784–790.

(58) Perlin, L.; MacNeil, S.; Rimmer, S. Production and Performance of Biomaterials Containing RGD Peptides. *Soft Matter* **2008**, *4*, 2331-2349.

(59) Niu, X.; Wang, Y.; Luo, Y.; Xin, J.; Li, Y. Arg-Gly-Asp (RGD) Modified Biomimetic Polymeric Materials. *J. Mater. Sci. Technol.* **2005**, *21*, 571–576.

(60) *Surface Plasmon Resonance Based Sensors*; Wolfbeis, O.S.; Homola, J., Eds.; Springer Series on Chemical Sensors and Biosensors; Springer: New York, U.S. **2006**; Vol. 4.

(61) Rohl, C. A.; Strauss, C. E.; Misura, K. M.; Baker, D. Protein Structure Prediction Using Rosetta. *Methods Enzymol.* **2004**, *383*, 66–93.

(62) Hess, B.; Kutzner, C.; van der Spoel, D.; Lindahl, E. GROMACS 4 : Algorithms for Highly Efficient, Load-Balanced, and Scalable Molecular Simulation. *J. Chem. Theory Comput.* **2008**, *4*, 435–47.

(63) Lindorff-Larsen, K.; Piana, S.; Palmo, K.; Maragakis, P.; Klepeis, J. L.; Dror, R. O.; Shaw, D. E. Improved Side-Chain Torsion Potentials for the Amber ff99SB Protein Force Field. *Proteins* **2010**, *78*, 1950–1958.

(64) Dunbrack, R. L.; Cohen, F. E. Bayesian Statistical Analysis of Protein Side-Chain Rotamer Preferences. *Protein Sci.* **1997**, *6*, 1661–1681.

(65) Essmann, U.; Perera, L.; Berkowitz, M. L.; Darden, T.; Lee, H.; Pedersen, L. G. A Smooth Particle Mesh Ewald Method. *J. Chem. Phys.* **1995**, *103*, 8577-8593.

(66) Bussi, G.; Donadio, D.; Parrinello, M. Canonical Sampling through Velocity Rescaling. *J. Chem. Phys.* **2007**, *126*, 014101.

(67) Kabsch, W.; Sander, C. Dictionary of Protein Secondary Structure: Pattern Recognition of Hydrogen-Bonded and Geometrical Features. *Biopolymers* **1983**, *22*, 2577–2637.

(68) MacArthur, M. W.; Thornton, J. M. Influence of Proline Residues on Protein Conformation. *J. Mol. Biol.* **1991**, *218*, 397–412.

(69) Fasman, G. D. Ed. Prediction of Protein Structure and the Principles of Protein Conformation; Plenum Press: New York, U.S. **1989**. Volume XIV.

(70) Zhang, S.; Yan, L.; Altman, M.; Lässle, M.; Nugent, H.; Frankel, F.; Lauffenburger, D. A.; Whitesides, G. M.; Rich, A. Biological Surface Engineering: A Simple System for Cell Pattern Formation. *Biomaterials* **1999**, *20*, 1213–1220.

(71) Lévy, R.; Thanh, N. T. K.; Doty, R. C.; Hussain, I.; Nichols, R. J.; Schiffrin, D. J.; Brust, M.; Fernig, D. G. Rational and Combinatorial Design of Peptide Capping Ligands for Gold Nanoparticles. *J. Am. Chem. Soc.* **2004**, *126*, 10076–10084.

(72) Nam, K. T.; Shelby, S. A; Choi, P. H.; Marciel, A. B.; Chen, R.; Tan, L.; Chu, T. K.; Mesch, R. A.; Lee, B.-C.; Connolly, M. D.; et al. Free-Floating Ultrathin Two-Dimensional Crystals from Sequence-Specific Peptoid Polymers. *Nat. Mater.* **2010**, *9*, 454–460.

(73) Greenfield, N. J. Using Circular Dichroism to Estimate Protein Secondary Structure. *Nat. Protoc.* **2006**, *1*, 2876–2890.

(74) Woody, R. W. Circular Dichroism Spectrum of Peptides in the Poly(Pro)II Conformation. *J. Am. Chem. Soc.* **2009**, *131*, 8234–8245.

(75) Surewicz, W. K.; Mantsch, H. H.; Chapman, D. Perspectives in Biochemistry Determination of Protein Secondary Structure by Fourier Transform Infrared Spectroscopy : A Critical Assessment *Biochemistry* **1993**, *32*, 389–394.

(76) Sakurai, T.; Oka, S.; Kubo, A.; Nishiyama, K.; Taniguchi, I. Formation of Oriented Polypeptides on Au(111) Surface Depends on the Secondary Structure Controlled by Peptide Length. *J. Pept. Sci.* **2006**, *12*, 396–402.

(77) Infrared Analysis of Peptides and Proteins Principles and Applications. In *ACS Symposium Series 750*; Singh, B. R., Ed.; American Chemical Society: Washington, DC, **2000**; p. 190.

(78) Castner, D. G.; Hinds, K.; Grainger, D. W. X-Ray Photoelectron Spectroscopy Sulfur 2p Study of Organic Thiol and Disulfide Binding Interactions with Gold Surfaces. *Langmuir* **1996**, *12*, 5083–5086.

(79) Herrwerth, S.; Eck, W.; Reinhardt, S.; Grunze, M. Factors That Determine the Protein Resistance of Oligoether Self-Assembled Monolayers --Internal Hydrophilicity, Terminal Hydrophilicity, and Lateral Packing Density. *J. Am. Chem. Soc.* **2003**, *125*, 9359–9366.

(80) Glaser, F.; Steinberg, D. M.; Vakser, I. A.; Ben-tal, N. Residue Frequencies and Pairing Preferences at Protein – Protein Interfaces. *Proteins* **2001**, *43*, 89–102.

(81) Yeh, Y.-C.; Creran, B.; Rotello, V. M. Gold Nanoparticles: Preparation, Properties, and Applications in Bionanotechnology. *Nanoscale* **2012**, *4*, 1871–1880.

(82) Baptista, P.; Pereira, E.; Eaton, P.; Doria, G.; Miranda, A.; Gomes, I.; Quaresma, P.; Franco, R. Gold Nanoparticles for the Development of Clinical Diagnosis Methods. *Anal. Bioanal. Chem.* **2008**, *391*, 943–950.

(83) Dykman, L. A.; Khlebtsov, N. G. Gold Nanoparticles in Biology and Medicine: Recent Advances and Prospects. *Acta Naturae* **2011**, *3*, 34–55.

(84) Vigderman, L.; Zubarev, E. R. Therapeutic Platforms Based on Gold Nanoparticles and Their Covalent Conjugates with Drug Molecules. *Adv. Drug Deliv. Rev.* **2013**, *65*, 663–676.

(85) Choi, C. H. J.; Zuckerman, J. E.; Webster, P.; Davis, M. E. Targeting Kidney Mesangium by Nanoparticles of Defined Size. *Proc. Natl. Acad. Sci. U. S. A.* **2011**, *108*, 6656–6661.

(86) Melancon, M. P.; Lu, W.; Li, C. Gold-Based Magneto/Optical Nanostructures: Challenges for *In Vivo* Applications in Cancer Diagnostics and Therapy. *Mater. Res. Bull.* **2009**, *34*, 415–421.

(87) Owens III, D. E.; Peppas, N. A. Opsonization, Biodistribution, and Pharmacokinetics of Polymeric Nanoparticles. *Int. J. Pharm.* **2006**, *307*, 93–102.

(88) Albanese, A.; Tang, P. S.; Chan, W. C. The Effect of Nanoparticle Size, Shape, and Surface Chemistry on Biological Systems. *Annu. Rev. Biomed. Eng.* **2012**, *14*, 1–16.

(89) Karmali, P. P.; Simberg, D. Interactions of Nanoparticles with Plasma Proteins: Implication on Clearance and Toxicity of Drug Delivery Systems. *Expert Opin. Drug Deliv.* **2011**, *8*, 343–357.

(90) Larson, T. A.; Joshi, P. P.; Sokolov, K. Preventing Protein Adsorption and Macrophage Uptake of Gold Nanoparticles via a Hydrophobic Shield. *ACS Nano* **2012**, *6*, 9182–9190.

(91) Kodiyan, A.; Silva, E. A.; Kim, J.; Aizenberg, M.; Mooney, D. J. Surface Modification with Alginate- Derived Polymers for Stable, Protein-Repellant, Long-Circulating Gold Nanoparticles. *ACS Nano* **2012**, 4796–4805.

(92) Liu, X.; Chen, Y.; Li, H.; Huang, N.; Jin, Q.; Ren, K.; Ji, J. Enhanced Retention and Cellular Uptake of Nanoparticles in Tumors by Controlling Their Aggregation Behavior. *ACS Nano* **2013**, *7*, 6244–6257.

(93) Yang, W.; Zhang, L.; Wang, S.; White, A. D.; Jiang, S. Functionalizable and Ultra Stable Nanoparticles Coated with Zwitterionic Poly(Carboxybetaine) in Undiluted Blood Serum. *Biomaterials* **2009**, *30*, 5617–5621.

(94) Zhang, L.; Xue, H.; Gao, C.; Carr, L.; Wang, J.; Chu, B.; Jiang, S. Imaging and Cell Targeting Characteristics of Magnetic Nanoparticles Modified by a Functionalizable Zwitterionic Polymer with Adhesive 3,4-Dihydroxyphenyl-$_L$-Alanine Linkages. *Biomaterials* **2010**, *31*, 6582–6588.

(95) Lévy, R.; Thanh, N. T. K.; Doty, R. C.; Hussain, I.; Nichols, R. J.; Schiffrin, D. J.; Brust, M.; Fernig, D. G. Rational and Combinatorial Design of Peptide Capping Ligands for Gold Nanoparticles. *J. Am. Chem. Soc.* **2004**, *126*, 10076–10084.

(96) Olmedo, I.; Araya, E.; Sanz, F.; Medina, E.; Arbiol, J.; Toledo, P.; Álvarez-Lueje, A.; Giralt, E.; Kogan, M. J. How Changes in the Sequence of the Peptide CLPFFD-NH_2 Can Modify the Conjugation and Stability of Gold Nanoparticles and Their Affinity for β-Amyloid Fibrils. *Bioconjug. Chem.* **2008**, *19*, 1154–1163.

(97) Morais, T.; Soares, M. E.; Duarte, J. A.; Soares, L.; Maia, S.; Gomes, P.; Pereira, E.; Fraga, S.; Carmo, H.; Bastos, M. L. Effect of Surface Coating on the Biodistribution Profile of Gold Nanoparticles in the Rat. *Eur. J. Pharm. Biopharm.* **2012**, *80*, 185–193.

(98) Prades, R.; Guerrero, S.; Araya, E.; Molina, C.; Salas, E.; Zurita, E.; Selva, J.; Egea, G.; López-Iglesias, C.; Teixidó, M.; et al. Delivery of Gold Nanoparticles to the Brain by Conjugation with a Peptide That Recognizes the Transferrin Receptor. *Biomaterials* **2012**, *33*, 7194–7205.

(99) Ferro-Flores, G.; Ocampo-García, B. E.; Ramírez, F. M.; Gutierrez-Wing, C. E.; Murphy C. A.; Santos-Cuevas, C. L. Gold Nanoparticles Conjugated to Peptides. *Colloids in Biotechnology* **2010**, *152,* 231-252.

(100) Arosio, D.; Manzoni, L.; Araldi, E. M.; Scolastico, C. Cyclic RGD Functionalized Gold Nanoparticles for Tumor Targeting. *Bioconjug. Chem.* **2011**, *22*, 664–672.

(101) Kim, Y.-H.; Jeon, J.; Hong, S. H.; Rhim, W.-K.; Lee, Y.-S.; Youn, H.; Chung, J.-K.; Lee, M. C.; Lee, D. S.; Kang, K. W.; et al. Tumor Targeting and Imaging Using Cyclic RGD-PEGylated Gold Nanoparticle Probes with Directly Conjugated Iodine-125. *Small* **2011**, *7*, 2052–2060.

(102) Scarì, G.; Porta, F.; Fascio, U.; Avvakumova, S.; Dal Santo, V.; De Simone, M.; Saviano, M.; Leone, M.; Del Gatto, A.; Pedone, C.; et al. Gold Nanoparticles Capped by a GC-Containing Peptide Functionalized with an RGD Motif for Integrin Targeting. *Bioconjug. Chem.* **2012**, *23*, 340–349.

(103) Sun, L.; Liu, D.; Wang, Z. Functional Gold Nanoparticle-Peptide Complexes as Cell-Targeting Agents. *Langmuir* **2008**, *24*, 10293–10297.

(104) Nowinski, A. K.; Sun, F.; White, A. D.; Keefe, A. J.; Jiang, S. Sequence, Structure, and Function of Peptide Self-Assembled Monolayers. *J. Am. Chem. Soc.* **2012**, *134*, 6000–6005.

(105) Zhu, J.; Marchant, R. E. Solid-Phase Synthesis of Tailed Cyclic RGD Peptides Using Glutamic Acid : Unexpected Glutarimide Formation. *J. Pept. Sci.* **2008**, *14*, 690–696.

(106) Frens, G. Controlled Nucleation for the Regulation of the Particle Size in Monodisperse Gold Suspensions. *Nat. Phys. Sci.* **1973**, *241*, 20–22.

(107) Turkevich, J.; Stevenson, P. C.; Hillier J. A Study of the Nucleation and Growth Processes in the Synthesis of Colloidal Gold. *Discuss. Faraday Soc.* **1951**, *11*, 55-75.

(108) Bellino, M.G.; Calvo, E. J.; Gordillo, G. Adsorption Kinetics of Charged Thiols on Gold Nanoparticles. *Phys. Chem. Chem. Phys.* **2004**, *6*, 424–28.

(109) Haiss, W.; Thanh, N. T. K.; Aveyard, J.; Fernig, D. G. Determination of Size and Concentration of Gold Nanoparticles from UV-Vis Spectra. *Anal. Chem.* **2007**, *79*, 4215–4221.

(110) Manciu, M.; Ruckenstein, E. Role of the Hydration Force in the Stability of Colloids at High Ionic Strengths. *Langmuir* **2001**, *17*, 7061–7070.

(111) Bartneck, M.; Keul, H. A.; Singh, S.; Czaja, K.; Bornemann, J.; Bockstaller, M.; Moeller, M.; Zwadlo-Klarwasser, G. Rapid Uptake of Gold Nanorods by Primary Human Blood Phagocytes and Immunomodulatory Effects of Surface Chemistry. *ACS Nano* **2010**, *4*, 3073–3086.

(112) Chithrani, B. D.; Ghazani, A. A.; Chan, W. C. W. Determining the Size and Shape Dependence of Gold Nanoparticle Uptake into Mammalian Cells. *Nano Lett.* **2006**, *6*, 662–668.

(113) Temming, K.; Schiffelers, R. M.; Molema, G.; Kok, R. J. RGD-Based Strategies for Selective Delivery of Therapeutics and Imaging Agents to the Tumour Vasculature. *Drug Resist. Updat.* **2005**, *8*, 381–402.

(114) Thorley, A. J.; Tetley, T. D. New Perspectives in Nanomedicine. *Pharmacol. Ther.* **2013**, *140*, 176–185.

(115) Danhier, F.; Ansorena, E.; Silva, J. M.; Coco, R.; Le Breton, A.; Préat, V. PLGA-Based Nanoparticles: An Overview of Biomedical Applications. *J. Control. Release* **2012**, *161*, 505–522.

(116) Wacker, M. Nanocarriers for Intravenous Injection-The Long Hard Road to the Market. *Int. J. Pharm.* **2013**, *457*, 50–62.

(117) Sah, H.; Thoma, L. A.; Desu, H. R.; Sah, E.; Wood, G. C. Concepts and Practices Used to Develop Functional PLGA-Based Nanoparticulate Systems. *Int. J. Nanomedicine* **2013**, *8*, 747–765.

(118) Makadia, H. K.; Siegel, S. J. Poly Lactic-*co*-Glycolic Acid (PLGA) as Biodegradable Controlled Drug Delivery Carrier. *Polymers.* **2011**, *3*, 1377–1397.

(119) Ratner, B. D.; Hoffman, A. S.; Schoen, F. J.; Lemons, J. E. *Biomaterials Science: An Introduction to Materials in Medicine*; Elsevier Academic Press: Boston, 2004; pp. 67–69, 115–126.

(120) Cheng, J.; Teply, B. A.; Sherifi, I.; Sung, J.; Luther, G.; Gu, F. X.; Levy-Nissenbaum, E.; Radovic-Moreno, A. F.; Langer, R.; Farokhzad, O. C. Formulation of Functionalized PLGA-PEG Nanoparticles for *In Vivo* Targeted Drug Delivery. *Biomaterials* **2007**, *28*, 869–876.

(121) Li, Y.; Pei, Y.; Zhang, X.; Gu, Z.; Zhou, Z.; Yuan, W.; Zhou, J.; Zhu, J.; Gao, X. PEGylated PLGA Nanoparticles as Protein Carriers: Synthesis, Preparation and Biodistribution in Rats. *J. Control. Release* **2001**, *71*, 203–211.

(122) Yasugi, K.; Nagasaki, Y.; Kato, M.; Kataoka, K. Preparation and Characterization of Polymer Micelles from Poly(Ethylene Glycol)-poly($_{D,L}$-Lactide) Block Copolymers as Potential Drug Carrier. *J. Control. Release* **1999**, *62*, 89–100.

(123) Schlaad, H.; Diehl, C.; Gress, A.; Meyer, M.; Demirel, A. L.; Nur, Y.; Bertin, A. Poly(2-Oxazoline)s as Smart Bioinspired Polymers. *Macromol. Rapid Commun.* **2010**, *31*, 511–525.

(124) Říhová, B.; Etrych, T.; Sírová, M.; Kovár, L.; Hovorka, O.; Kovár, M.; Benda, A.; Ulbrich, K. Synergistic Action of Doxorubicin Bound to the Polymeric Carrier Based on N-(2-Hydroxypropyl)Methacrylamide Copolymers through an Amide or Hydrazone Bond. *Mol. Pharm.* **2010**, *7*, 1027–40.

(125) Kainthan, R. K.; Brooks, D. E. *In Vivo* Biological Evaluation of High Molecular Weight Hyperbranched Polyglycerols. *Biomaterials* **2007**, *28*, 4779–4787.

(126) Cao, Z.; Yu, Q.; Xue, H.; Cheng, G.; Jiang, S. Nanoparticles for Drug Delivery Prepared from Amphiphilic PLGA Zwitterionic Block Copolymers with Sharp Contrast in Polarity between Two Blocks. *Angew. Chem. Int. Ed. Engl.* **2010**, *49*, 3771–3776.

(127) Li, Y.-L.; Zhu, L.; Liu, Z.; Cheng, R.; Meng, F.; Cui, J.-H.; Ji, S.-J.; Zhong, Z. Reversibly Stabilized Multifunctional Dextran Nanoparticles Efficiently Deliver Doxorubicin into the Nuclei of Cancer Cells. *Angew. Chem. Int. Ed. Engl.* **2009**, *48*, 9914–9918.

(128) Khan, W.; Muthupandian, S.; Farah, S.; Kumar, N.; Domb, A. J. Biodegradable Polymers Derived from Amino Acids. *Macromol. Biosci.* **2011**, *11*, 1625–1636.

(129) Guo, K.; Chu, C. C. Biodegradable and Injectable Paclitaxel-Loaded Poly(ester Amide)s Microspheres: Fabrication and Characterization. *J. Biomed. Mater. Res. B. Appl. Biomater.* **2009**, *89*, 491–500.

(130) Wu, J.; Yamanouchi, D.; Liu, B.; Chu, C.-C. Biodegradable Arginine-Based Poly(Ether Ester Amide)s as a Non-Viral DNA Delivery Vector and Their Structure–Function Study. *J. Mater. Chem.* **2012**, *22*, 18983-18991.

(131) Arimura, H.; Ohya, Y.; Ouchi, T. Formation of Core-Shell Type Biodegradable Polymeric Micelles from Amphiphilic Poly(Aspartic Acid)-Block-Polylactide Diblock Copolymer. *Biomacromolecules* **2005**, *6*, 720–725.

(132) Lewitus, D.; Vogelstein, R. J.; Zhen, G.; Choi, Y.-S.; Kohn, J.; Harshbarger, S.; Jia, X. Designing Tyrosine-Derived Polycarbonate Polymers for Biodegradable Regenerative Type Neural Interface Capable of Neural Recording. *IEEE Trans. Neural Syst. Rehabil. Eng.* **2011**, *19*, 204–212.

(133) Sun, J.; Deng, C.; Chen, X.; Yu, H.; Tian, H.; Sun, J.; Jing, X. Self-Assembly of Polypeptide-Containing ABC-Type Triblock Copolymers in Aqueous Solution and Its pH Dependence. *Biomacromolecules* **2007**, *8*, 1013–1017.

(134) Zhang, W.; Shao, J. Biomedical Research of Novel Biodegradable Copoly(Amino Acid)s Based on 6-Aminocaproic Acid and L-Proline. *J. Biomed. Mater. Res. A* **2010**, *94*, 450–456.

(135) Fu, C.; Sun, X.; Liu, D.; Chen, Z.; Lu, Z.; Zhang, N. Biodegradable Tri-Block Copolymer Poly(Lactic Acid)-Poly(Ethylene Glycol)-Poly(L-Lysine)(PLA-PEG-PLL) as a Non-Viral Vector to Enhance Gene Transfection. *Int. J. Mol. Sci.* **2011**, *12*, 1371–1388.

(136) Sun, J.; Chen, X.; Lu, T.; Liu, S.; Tian, H.; Guo, Z.; Jing, X. Formation of Reversible Shell Cross-Linked Micelles from the Biodegradable Amphiphilic Diblock Copolymer Poly(L-Cysteine)-Block-Poly(L-Lactide). *Langmuir* **2008**, *24*, 10099–10106.

(137) Harre, M.; Nickisch, K.; Tilstam, U. An Efficient Method for Activation and Recycling of Trityl Resins. *React. Funct. Polym.* **1999**, *41*, 111–114.

(138) Gude, M.; Ryf, J.; White, P. D. An Accurate Method for the Quantitation of Fmoc-Derivatized Solid Phase Supports. *Lett. Pept. Sci.* **2002**, *9*, 203–206.

(139) AAPPTec. AAPPTec Technical Support Information Bulletin 1027 www.aapptec.com/custdocs/1027.pdf.

(140) Bollhagen, R.; Schmiedberger, M.; Barlos, K.; Grell, E. A New Reagent for the Cleavage of Fully Protected Peptides Synthesized on 2-Chorotrityl Chloride Resin. *J. Chem. Soc., Chem. Commun.* **1994**, 2559–2560.

(141) Javadzadeh, Y.; Ahadi, F.; Davaran, S.; Mohammadi, G.; Sabzevari, A.; Adibkia, K. Preparation and Physicochemical Characterization of Naproxen-PLGA Nanoparticles. *Colloids Surf. B. Biointerfaces* **2010**, *81*, 498–502.

(142) Jeong, J. H.; Park, T. G. Poly($_{L}$-Lysine)-g-Poly($_{D,L}$-Lactic-Co-Glycolic Acid) Micelles for Low Cytotoxic Biodegradable Gene Delivery Carriers. *J. Control. Release* **2002**, *82*, 159–166.

(143) Vilaseca, L.; Bardaji, E. Microscale Ninhydrin Test Applied to Solid-Phase Peptide Synthesis. *J. Chem. Educ.* **1995**, *72*, A99.

(144) Daly, W. H.; Poche, D. The Preparation of N-Carboxyanhydrides of α-Amino Acids Using Bis(Trichloromethyl) Carbonate. *Tetrahedron Lett.* **1988**, *29*, 5859–5862.

(145) Fan, Y.; Chen, G.; Tanaka, J.; Tateishi, T. $_{L}$-Phe End-Capped Poly($_{L}$-Lactide) as Macroinitiator for the Synthesis of Poly($_{L}$-Lactide)-b-Poly($_{L}$-Lysine) Block Copolymer. *Biomacromolecules* **2005**, *6*, 3051–3056.

(146) Dawson, P. E.; Kent, S. B. H. Synthesis of Native Proteins by Chemical Ligation. *Annu. Rev. Biochem.* **2000**, *69*, 923–960.

(147) Guzmán, F.; Barberis, S.; Illanes, A. Peptide Synthesis: Chemical or Enzymatic. *Electron. J. Biotechnol.* **2007**, 1–42.

(148) Lavik, E. B.; Hrkach, J. S.; Lotan, N.; Nazarov, R.; Langer, R. A Simple Synthetic Route to the Formation of a Block Copolymer of Poly(Lactic-Co-Glycolic Acid) and Polylysine for the Fabrication of Functionalized , Degradable Structures for Biomedical Applications. *J. Biomed. Mater. Res. (Appl. Biomater.)* **2001**, *58*, 291–294.

(149) Caillol, S.; Lecommandoux, S.; Mingotaud, A.-F.; Schappacher, M.; Soum, A.; Bryson, N.; Meyrueix, R. Synthesis and Self-Assembly Properties of Peptide-Polylactide Block Copolymers. *Macromolecules* **2003**, *36*, 1118–1124.

(150) Gotsche, M.; Keul, H.; Hocker, H. Amino-Terminated Poly($_{L}$-Lactide)s as Initiators for the Polymerization of N-Carboxyanhydrides: Synthesis of Poly($_{L}$-Lactide-Block-Poly(α-Amino Acid)s. *Macromol. Chem. Phys.* **1995**, *196*, 3891–3903.

(151) Semete, B.; Booysen, L.; Lemmer, Y.; Kalombo, L.; Katata, L.; Verschoor, J.; Swai, H. S. *In Vivo* Evaluation of the Biodistribution and Safety of PLGA Nanoparticles as Drug Delivery Systems. *Nanomedicine* **2010**, *6*, 662–671.

(152) Gu, F.; Zhang, L.; Teply, B. A.; Mann, N.; Wang, A.; Radovic-Moreno, A. F.; Langer, R.; Farokhzad, O. C. Precise Engineering of Targeted Nanoparticles by Using Self-Assembled Biointegrated Block Copolymers. *Proc. Natl. Acad. Sci. U. S. A.* **2008**, *105*, 2586–2591.

(153) Seker, U. O. S.; Demir, H. V. Material Binding Peptides for Nanotechnology. *Molecules* **2011**, *16*, 1426–1451.

(154) Silen, J. L.; Lu, A. T.; Solas, D. W.; Gore, M. A.; MacLean, D.; Shah, N. H.; Coffin, J. M.; Bhinderwala, N. S.; Wang, Y.; Tsutsui, K. T.; et al. Screening for Novel Antimicrobials from Encoded Combinatorial Libraries by Using a Two-Dimensional Agar Format. *Antimicrob. Agents Chemother.* **1998**, *42*, 1447–1453.

(155) Aina, O. H.; Liu, R.; Sutcliffe, J. L.; Marik, J.; Pan, C.-X.; Lam, K. S. From Combinatorial Chemistry to Cancer-Targeting Peptides. *Mol. Pharm.* **2007**, *4*, 631–651.

(156) Cancilla, M. T.; Leavell, M. D.; Chow, J.; Leary, J. A. Mass Spectrometry and Immobilized Enzymes for the Screening of Inhibitor Libraries. *Proc. Natl. Acad. Sci. U. S. A.* **2000**, *97*, 12008–12013.

(157) Choe, Y.; Leonetti, F.; Greenbaum, D. C.; Lecaille, F.; Bogyo, M.; Brömme, D.; Ellman, J. A.; Craik, C. S. Substrate Profiling of Cysteine Proteases Using a Combinatorial Peptide Library Identifies Functionally Unique Specificities. *J. Biol. Chem.* **2006**, *281*, 12824–12832.

(158) Sergeeva, A.; Kolonin, M. G.; Molldrem, J. J.; Pasqualini, R.; Arap, W. Display Technologies: Application for the Discovery of Drug and Gene Delivery Agents. *Adv. Drug Deliv. Rev.* **2006**, *58*, 1622–1654.

(159) Lam, K.S.; Liu, R.; Miyamoto, S.; Lehman, A. L.; Tuscano, J. M. Applications of One-Bead One-Compound Libraries and Chemical Microarrays in Signal Transduction Research. *Acc. Chem. Res.* **2003**, *36*, 370–377.

(160) Pande, J.; Szewczyk, M. M.; Grover, A. K. Phage Display: Concept, Innovations, Applications and Future. *Biotechnol. Adv.* **2010**, *28*, 849–858.

(161) Hintersteiner, M.; Kimmerlin, T.; Kalthoff, F.; Stoeckli, M.; Garavel, G.; Seifert, J.-M.; Meisner, N.-C.; Uhl, V.; Buehler, C.; Weidemann, T.; et al. Single Bead Labeling Method for Combining Confocal Fluorescence On-Bead Screening and Solution Validation of Tagged One-Bead One-Compound Libraries. *Chem. Biol.* **2009**, *16*, 724–735.

(162) Shelton, P. T.; Jensen, K. J. Linkers, Resins, and General Procedures for Solid-Phase Peptide Synthesis. In *Peptide Synthesis and Applications, Methods in Molecular Biology*; Springer Science + Business Media: New York, 2013; Vol. 1047, pp. 23–42.

(163) Arakawa, T.; Timasheff, S. N. Mechanism of Protein Salting In and Salting Out by Divalent Cation Salts : Balance between Hydration and Salt Binding. *Biochemistry* **1984**, *23*, 5912–5923.

(164) Richards, M. M. The Effect of Glycine Upon the Activity Coefficient of Glycine, Egg Albumin, and Carboxyhemoglobin. *J. Biol. Chem.* **1937**, *122*, 727–743.

(165) Straughn III, W.; Wagner, R. H. A Simple Method for Preparing Fibrinogen. *Thromb. Diath. Haemorrh.* **1966**, *16*, 198–206.

(166) Kazal, L. A.; Amsel, S.; Miller, O. P.; Tocantins, L. M. The Preparation and Some Properties of Fibrinogen Precipitated From Human Plasma by Glycine. *Proc. Soc. Exp. Biol. Med.* **1963**, *113*, 989–994.

(167) Wagner, B. H.; McLester, W. D.; Smith, M.; Brinkhous, K. M. Purification of Antihemophilic Factor (Factor VIII) by Amino Acid Precipitation. *Thromb. Diath. Haemorrh.* **1964**, *11*, 64–74.

(168) Auzanneau, F. I.; Meldal, M.; Bock, K. Synthesis, Characterization, and Biocompatibility of PEGA Resins. *J. Pept. Sci.* **1995**, *1*, 31–44.

(169) Kim, D. H.; Shin, D. S.; Lee, Y. S. Spot Arrays on Modified Glass Surfaces for Efficient SPOT Synthesis and On-Chip Bioassay of Peptides. *J. Pept. Sci.* **2007**, 625–633.

(170) Smith, B. J. Chemical Cleavage of Proteins at Methionyl Residues. In *The Protein Protocols Handbook*; Walker, J. M., Ed.; Humana Press: Totowa, NJ, 1996; pp. 369–373.

(171) Kaiser, R.; Metzka, L. Enhancement of Cyanogen Bromide Cleavage Yields for Methionyl-Serine and Methionyl-Threonine Peptide Bonds. *Anal. Biochem.* **1999**, *266*, 1–8.

(172) Han, K.; Belaiche, D.; Moreau, O.; Briakd, G. Current Developments in Stepwise Edman Degradation of Peptides and Proteins. *Int. J. Biochem.* **1985**, *17*, 429–445.

(173) Thakkar, A.; Cohen, A. S.; Connolly, M. D.; Zuckermann, R. N.; Pei, D. High-Throughput Sequencing of Peptoids and Peptide-Peptoid Hybrids by Partial Edman Degradation and Mass Spectrometry. *J. Comb. Chem.* **2009**, *11*, 294–302.

(174) Thakkar, A.; Wavreille, A.-S.; Pei, D. Traceless Capping Agent for Peptide Sequencing by Partial Edman Degradation and Mass Spectrometry. *Anal. Chem.* **2006**, *78*, 5935–5939.

(175) Kussmann, M.; Nordhoff, E.; Rahbek-Nielsen, H.; Haebel, S.; Rossel-Larsen, M.; Jakobsen, L.; Gobom, J.; Mirgorodskaya, E.; Kroll-Kristensen, A.; Palm, L.; et al. Matrix-Assisted Laser Desorption/Ionization Mass Spectrometry Sample Preparation Techniques Designed for Various Peptide and Protein Analytes. *J. Mass Spectrom.* **1997**, *32*, 593–601.

(176) Cohen, S. L.; Chait, B. T. Influence of Matrix Solution Conditions on the MALDI-MS Analysis of Peptides and Proteins. *Anal. Chem.* **1996**, *68*, 31–37.

(177) Trauger, S. A.; Webb, W.; Siuzdak, G. Peptide and Protein Analysis with Mass Spectrometry. *Spectroscopy* **2002**, *16*, 15–28.

(178) Knowles, M. R.; Boucher, R. C. Mucus Clearance as a Primary Innate Defense Mechanism for Mammalian Airways. *J. Clin. Invest.* **2002**, *109*, 571–577.

(179) *Mucosal Immunology*; Mestecky, J.; Lamm, M. F.; Strober, W.; Bienenstock, J.; McGhee, J. R.; Mayer, L., Eds.; 3rd ed.; Elsevier Inc.: Burlington, MA, 2005.

(180) Cone, R. A. Barrier Properties of Mucus. *Adv. Drug Deliv. Rev.* **2009**, *61*, 75–85.

(181) Woodley, J. Bioadhesion:New Possibilities for Drug Administration *Clin. Pharmacokinet.* **2001**, *40*, 77–84.

(182) Takeuchi, H.; Yamamoto, H.; Kawashima, Y. Mucoadhesive Nanoparticulate Systems for Peptide Drug Delivery. *Adv. Drug Deliv. Rev.* **2001**, *47*, 39–54.

(183) Serra, L.; Doménech, J.; Peppas, N. A. Design of Poly(Ethylene Glycol)-Tethered Copolymers as Novel Mucoadhesive Drug Delivery Systems. *Eur. J. Pharm. Biopharm.* **2006**, *63*, 11–18.

(184) Luelen, H. L.; Rentel, C.; Kotzé, A. F.; Lehr, C.; de Boer, A. G. ; Verhoef, J. C.; Junginger, H. E. Mucoadhesive Polymers in Peroral Peptide Drug Delivery. IV. Polycarbophil and Chitosan Are Potent Enhancers of Peptide Transport Across Intestinal Mucosae *In Vitro*. *J. Control. Release* **1997**, *45*, 15–23.

(185) Quintanar-Guerrero, D.; Villalobos-García, R.; Alvarez-Colín, E.; Cornejo-Bravo, J. M. *In Vitro* Evaluation of the Bioadhesive Properties of Hydrophobic Polybasic Gels Containing N,N-Dimethylaminoethyl Methacrylate-Co-Methyl Methacrylate. *Biomaterials* **2001**, *22*, 957–961.

(186) Furtado, S.; Abramson, D.; Burrill, R.; Olivier, G.; Gourd, C.; Bubbers, E.; Mathiowitz, E. Oral Delivery of Insulin Loaded Poly(Fumaric-Co-Sebacic) Anhydride Microspheres. *Int. J. Pharm.* **2008**, *347*, 149–155.

(187) Norris, D. A.; Sinko, P. J. Effect of Size, Surface Charge, and Hydrophobicity on the Translocation of Polystyrene Microspheres Through Gastrointestinal Mucin. *J. Appl. Polym. Sci.* **1997**, *11*, 1481–1492.

(188) Sakuma, S.; Sudo, R.; Suzuki, N.; Kikuchi, H.; Akashi, M.; Ishida, Y.; Hayashi, M. Behavior of Mucoadhesive Nanoparticles Having Hydrophilic Polymeric Chains in the Intestine. *J. Control. Release* **2002**, *81*, 281–290.

(189) Lai, S. K.; O'Hanlon, D. E.; Harrold, S.; Man, S. T.; Wang, Y.-Y.; Cone, R.; Hanes, J. Rapid Transport of Large Polymeric Nanoparticles in Fresh Undiluted Human Mucus. *Proc. Natl. Acad. Sci. U. S. A.* **2007**, *104*, 1482–1487.

(190) Li, L. D.; Crouzier, T.; Sarkar, A.; Dunphy, L.; Han, J.; Ribbeck, K. Spatial Configuration and Composition of Charge Modulates Transport into a Mucin Hydrogel Barrier. *Biophys. J.* **2013**, *105*, 1357–1365.

(191) Laffleur, F.; Hintzen, F.; Shahnaz, G.; Rahmat, D.; Leithner, K.; Bernkop-Schnurch, A. Development and *In Vitro* Evaluation of Slippery Nanoparticles for Enhanced Diffusion Through Native Mucus. *Nanomedicine* **2014**, *9*, 387–396.

(192) Olmsted, S. S.; Padgett, J. L.; Yudin, A. I.; Whaley, K. J.; Moench, T. R.; Cone, R. A. Diffusion of Macromolecules and Virus-like Particles in Human Cervical Mucus. *Biophys. J.* **2001**, *81*, 1930–1937.

(193) Olivier, A.; Meyer, F.; Raquez, J.-M.; Damman, P.; Dubois, P. Surface-Initiated Controlled Polymerization as a Convenient Method for Designing Functional Polymer Brushes: From Self-Assembled Monolayers to Patterned Surfaces. *Prog. Polym. Sci.* **2012**, *37*, 157–181.

(194) Burruano, B. T.; Schnaare, R. L.; Malamud, D. Synthetic Cervical Mucus Formulation. *Contraception* **2002**, *66*, 137–140.

(195) Karni, Z.; Polishuk, W. Z.; Adoni, A.; Diamant, Y. Newtonian Viscosity of the Human Cervical Mucus during the Menstrual Cycle. *Int. J. Fertil.* **1971**, *16*, 185–188.

(196) Ishijima, S.; Oshio, S.; Mohri, H. Flagellar Movement of Human Spermatozoa. *Gamete Res.* **1986**, *13*, 185–197.

(197) Suh, J.; Dawson, M.; Hanes, J. Real-Time Multiple-Particle Tracking: Applications to Drug and Gene Delivery. *Adv. Drug Deliv. Rev.* **2005**, *57*, 63–78.

(198) Lai, S. K.; Hanes, J. Real-Time Multiple Particle Tracking of Gene Nanocarriers in Complex Biological Environments. *Methods Mol. Biol.* **2008**, *434*, 81–97.

(199) Wang, Y.-Y.; Lai, S. K.; Suk, J. S.; Pace, A.; Cone, R.; Hanes, J. Addressing the PEG Mucoadhesivity Paradox to Engineer Nanoparticles That "Slip" through the Human Mucus Barrier. *Angew. Chem. Int. Ed.* **2008**, *47*, 9726–9729.

Appendix A: Qualifications of the Author

EDUCATION

University of Washington, Department of Chemical Engineering Seattle, WA
Ph.D., Chemical Engineering February 2015

University of Washington, Department of Chemical Engineering Seattle, WA
Master of Science, Chemical Engineering February 2012

University of Nevada, Department of Chemical Engineering Reno, NV
Bachelor of Science, Chemical Engineering, *Summa Cum Laude* May 2009

PUBLICATIONS

1) H. S. Sundaram; X. Han; **A. K. Nowinski**; N. D. Brault; Y. Li; J.-R. Ella-Menyé; K. A. Amoaka; K. E. Cook; P. Marek; K. Senecal; S. Jiang, Achieving One-Step Surface Coating of Highly Hydrophilic Poly(Carboxybetaine Methacrylate) Polymers on Hydrophobic and Hydrophilic Surfaces, *Adv. Mater. Interfaces*. 2014, *1400071*.

2) H. S. Sundaram; X. Han; **A. K. Nowinski**; J.-R. Ella-Menyé; C. Wimbish; P. Marek; K. Senecal; S. Jiang, One-Step Dip Coating of Zwitterionic Sulfobetaine Polymers on Hydrophobic and Hydrophilic Surfaces, *ACS Appl. Mater. Interfaces* 2014, *6 (9)*, 6664-6671.

3) **A. K. Nowinski**; A. D. White; A. J. Keefe; S. Jiang, Biologically Inspired Stealth Peptide-Capped Gold Nanoparticles, *Langmuir* 2014, *30 (7)*, 1864-1870.

4) F. Sun; T. Bai; L. Zhang; J.-R. Ella-Menyé; S. Liu; **A. K. Nowinski**; S. Jiang; Q. Yu, Sensitive and Fast Detection of Fructose in Complex Media via Symmetry Breaking and Signal Amplification Using Surface-Enhanced Raman Spectroscopy, *Anal. Chem.* 2014, *86 (5)*, 2387-2394.

5) A. J. Keefe; K. B. Caldwell; **A. K. Nowinski**; A. D. White; A. Thakkar; S. Jiang, Screening Nonspecific Interactions of Peptides Without Background Interference, *Biomaterials* 2013, *34*, 1871-1877.

6) A. D. White; A. J. Keefe; **A. K. Nowinski**; Q. Shao; K. B. Caldwell; S. Jiang, Standardizing and Simplifying Analysis of Peptide Library Data, *J. Chem. Inf. Model.* 2013, *53*, 493-499.

7) A. D. White; A. J. Keefe; J.-R. Ella-Menyé; **A. K. Nowinski**; Q. Shao; J. Pfaendtner; S. Jiang, Free Energy of Solvated Salt Bridges: A Simulation and Experimental Study, *J. Phys. Chem. B* 2013, *117*, 7254-7259.

8) **A. K. Nowinski**; F. Sun; A. D. White; A. J. Keefe; S. Jiang, Sequence, Structure, and Function of Peptide Self-Assembled Monolayers, *J. Am. Chem. Soc.* 2012, *134***,** 6000-6005.

9) A. D. White; **A. K. Nowinski**; W. Huang; A. J. Keefe; F. Sun; S. Jiang, Decoding Nonspecific Interactions from Nature, *Chem. Sci.* 2012, *3,* 3488.

PRESENTATIONS

1) **A. K. Nowinski**; A. D. White; A. J. Keefe; S. Jiang, Biologically Inspired Stealth Peptide-Coated Gold Nanoparticles, American Institute of Chemical Engineers Annual Conference, San Francisco, CA, November 7, 2013.

2) **A. K. Nowinski**; A. D. White; A. J. Keefe; S. Jiang, Biologically Inspired Stealth Peptide-Coated Gold Nanoparticles, University of Washington Graduate Student Symposium, Seattle, WA, September 19, 2013. **Best speaker 1st**

3) **A. K. Nowinski**; A. D. White; F. Sun; A. J. Keefe; S. Jiang, All-in-One Peptide Biomaterial: Biomolecular Recognition, Ultra-Low Fouling, and Surface Anchoring, American Institute of Chemical Engineers Annual Conference, Pittsburgh, PA, October 28, 2012.

4) **A. K. Nowinski**; A. D. White; L. Zhang; W. Yang; S. Jiang, Specific Targeting Stealth Nanoparticles Coated with Ultra-Low Fouling Peptides, American Institute of Chemical Engineers Annual Conference, Pittsburgh, PA, October 29, 2012.

5) **A. K. Nowinski**; S. Jiang, Ultra-Low Fouling Surfaces Derived from Peptide Self Assembling Monolayers, Society for Biomaterials Annual Conference, Orlando, FL, April 13, 2011.

POSTERS

1) **A. K. Nowinski**; A. D. White; A. J. Keefe; F. Sun; S. Jiang, Peptides as Stealth Biomaterials, University of Washington Graduate Student Symposium, Seattle, WA, September 18, 2014. **Best Poster 1st**

2) **A. K. Nowinski**; A. D. White; A. J. Keefe; F. Sun; S. Jiang**,** Peptides as Stealth Biomaterials: Biomimetic, Rational, and Combinatorial Design, Biomaterials Day, University of Washington, April 11, 2014. **Best Poster (4 awarded)**

3) **A. K. Nowinski**; A. D. White; F. Sun; A. J. Keefe; S. Jiang, All-In-One Peptide Biomaterial: Surface Anchoring, Ultra-Low Fouling, and Biomolecular Recognition, American Institute of Chemical Engineers Annual Conference, San Francisco, CA, November 4, 2013.

4) **A. K. Nowinski**; A. D. White; F. Sun; A. J. Keefe; S. Jiang, All-In-One Peptide Biomaterial: Surface Anchoring, Ultra-Low Fouling, and Biomolecular Recognition, University of Washington Graduate Student Symposium, Seattle, WA, September 20, 2012. **Best Poster 1st**

5) **A. K. Nowinski**; S. Jiang, Molecular Engineering of Surfaces for Sensing and Diagnostics, Advanced Sensors and Bio-Inspired Technology Conference, Shanghai, China, November 7, 2010.

6) **A. K. Nowinski**; D. P. Herman; D. G. Burrows; K. L. Tilbury, Assessing the Feeding Ecology of Beluga Whales in Cook Inlet, Alaska, Using Chemical Tracers, NOAA Conference, Silver Spring, MD, July 30, 2008. **Best Poster 1st**

HONORS AND AWARDS

Society of Women Engineers Outstanding Female Engineer Award, 2013
National Science Foundation Graduate Research Fellowship, 2010
Phi Kappa Phi Graduate Fellowship, 2009
American Institute of Chemical Engineers NorCal Graduate Scholarship, 2009
Clairmont L. Egtvedt Fellowship, University of Washington, 2009
Department of Chemical Engineering Outstanding Senior Student, 2009
NOAA Hollings Scholar, 2008